URBAN INFLUENCES ON CONVECTION AND LIGHTNING OVER HOUSTON

by

MICHAEL L. GAUTHIER

A DISSERTATION

Submitted in partial fulfillment of the requirements
for the degree of Doctor of Philosophy
in
The Department of Atmospheric Science
to
The School of Graduate Studies
of
The University of Alabama in Huntsville

HUNTSVILLE, ALABAMA

2006

REPORT DOCUMENTATION PAGE	Form Approved OMB No. 0704-0188

Public reporting burden for this collection of information is estimated to average 1 hour per response, including the time for reviewing instructions, searching existing data sources, gathering and maintaining the data needed, and completing and reviewing the collection of information. Send comments regarding this burden estimate or any other aspect of this collection of information, including suggestions for reducing this burden, to Washington Headquarters Services, Directorate for Information Operations and Reports, 1215 Jefferson Davis Highway, Suite 1204, Arlington, VA 22202-4302, and to the Office of Management and Budget, Paperwork Reduction Project (0704-0188), Washington, DC 20503.

1. AGENCY USE ONLY (Leave blank)	2. REPORT DATE 2.Aug.06	3. REPORT TYPE AND DATES COVERED DISSERTATION

4. TITLE AND SUBTITLE URBAN INFLUENCES ON CONVECTION AND LIGHTNING OVER HOUSTON	5. FUNDING NUMBERS

6. AUTHOR(S)
MAJ GAUTHIER MICHAEL L

7. PERFORMING ORGANIZATION NAME(S) AND ADDRESS(ES) UNIVERSITY OF ALABAMA HUNTSVILLE	8. PERFORMING ORGANIZATION REPORT NUMBER CI04-1834

9. SPONSORING/MONITORING AGENCY NAME(S) AND ADDRESS(ES) THE DEPARTMENT OF THE AIR FORCE AFIT/CIA, BLDG 125 2950 P STREET WPAFB OH 45433	10. SPONSORING/MONITORING AGENCY REPORT NUMBER

11. SUPPLEMENTARY NOTES

12a. DISTRIBUTION AVAILABILITY STATEMENT Unlimited distribution In Accordance With AFI 35-205/AFIT Sup 1	12b. DISTRIBUTION CODE

13. ABSTRACT (Maximum 200 words)

14. SUBJECT TERMS	15. NUMBER OF PAGES 169
	16. PRICE CODE

17. SECURITY CLASSIFICATION OF REPORT	18. SECURITY CLASSIFICATION OF THIS PAGE	19. SECURITY CLASSIFICATION OF ABSTRACT	20. LIMITATION OF ABSTRACT

Standard Form 298 (Rev. 2-89) (EG)
Prescribed by ANSI Std. 239.18
Designed using Perform Pro, WHS/DIOR, Oct 94

In presenting this dissertation in partial fulfillment of the requirements for a doctoral degree from The University of Alabama in Huntsville, I agree that the Library of this University shall make it freely available for inspection. I further agree that permission for extensive copying for scholarly purposes may be granted by my advisor or, in his absence, by the Chair of the Department or the Dean of the School of Graduate Studies. It is also understood that due recognition shall be given to me and to The University of Alabama in Huntsville in any scholarly use which may be made of any material in this dissertation.

_____   6/26/0C
(student signature)   (date)

DISSERTATION APPROVAL FORM

Submitted by Michael L. Gauthier in partial fulfillment of the requirements for the degree of Doctor of Philosophy in Atmospheric Science and accepted on behalf of the Faculty of the School of Graduate Studies by the dissertation committee.

We, the undersigned members of the Graduate Faculty of The University of Alabama in Huntsville, certify that we have advised and/or supervised the candidate on the work described in this dissertation. We further certify that we have reviewed the dissertation manuscript and approve it in partial fulfillment of the requirements of the degree of Doctor of Philosophy in Atmospheric Science.

Kevin Knupp _7/7/06_ Committee Chair
                        Date

Walt Petersen

John R. Mecikalski

Hugh Christian

Larry Carey

_____ Department Chair

_____ College Dean

Debra M. Moriarity _7/11/06_ Graduate Dean

ABSTRACT
The School of Graduate Studies
The University of Alabama in Huntsville

Degree_____ Doctor of Philosophy____ College/Dept._Science / Atmospheric Science___

Name of Candidate____ Michael L. Gauthier_____

Title __ Urban Influence on Convection and Lightning over Houston_____

.

The research presented in this dissertation addresses a fundamental question

regarding urban, ultimately anthropogenic, influences on convection as it relates to

lightning production and precipitation structure. In general, inadvertent weather

modification hypotheses offered to explain lightning and rainfall anomalies rely on either

or both perturbations in the spatial distribution and intensity of convection (from whence

warm-season rainfall and lightning emanate), or modification to convective cloud

microphysics through aerosol loading over and downwind of polluted cities such as

Houston, Texas.

Using eight independent datasets, causative mechanisms to explain enhancements

in summer season cloud-to-ground (CG) lightning over the Houston area were examined

in an attempt to isolated the primary contributor. We quantify a three-step process by

which thunderstorm electrification may become enhanced over the Houston area relative

to its surroundings. Findings indicate that the spatial extent of the flash density features

are primarily the result of "typical" convective activity tied to the presence of a persistent

thermal anomaly situated over the city center. Coupled with the land surface

heterogeneity of the surrounding area, this urban heat island (UHI) gives rise to a

preferential location of low-level convergence and convective initiation and

enhancement. We find the primary causative mechanisms responsible for the *intensity* of the Houston CG lightning anomaly to be those associated with a mixture of urban and natural influences, specifically that ***UHI thermodynamics*** provide a more favorable environment for convective initiation and thunderstorm intensification as well as contributing to an area of preferred convergence over, downwind of the city, with associated ***mesoscale enhancements in sea breeze convergence***. Regarding the effects of anthropogenic aerosols on enhanced flash densities, from the analyses presented here, it is unclear that enhanced aerosol (CCN) concentrations have any significant impact on the flash density enhancements under investigation leading us to the conclusion that *enhanced aerosol concentrations are the **least likely** (or at best, secondary) contributor* to the climatological enhancements in ground flash density over and around Houston. Complementing these results, we found the convective structure on days in which an enhanced UHI was in place to be much more vigorous than high pollution days.

Abstract Approval: Committee Chair   _Kevin Knupp_ 7/7/06

                                                          (Date)

                     Department Chair   _____

                     Graduate Dean   _Debra M. Moriarity_ 7/11/06

ACKNOWLEDGMENTS

Special thanks to my wife and son for their countless sacrifices and unending support throughout my entire career; it is from them that I derive my drive, inspiration and focus.

TABLE OF CONTENTS

Page

LIST OF FIGURES

LIST OF TABLES

CHAPTER 1

INTRODUCTION

1.1 Background and Motivation

Over the past two decades, studies of cloud-to-ground (CG) lightning have used data gathered from the National Lightning Detection Network (NLDN) to characterize spatial (and temporal) variations in CG lightning activity both regionally and throughout the continental United States (CONUS) [e.g., Orville et al., 1983; Orville and Huffines, 2001]. On sub-synoptic (20 – 50 km) scales, lightning "hot spots" have been noted in areas of complex and elevated terrain (such as the western United States) [Reap, 1986; Zajac and Rutlege, 2001], along mesoscale boundaries such as land/sea convergence zones along the Gulf Coast and in Florida, and even over the warm ocean waters of the Gulf Stream [Biswas and Hobbs, 1990]. Often embedded, and less often analyzed are more localized lightning enhancements documented to occur over and around several major US cities [e.g., Westcott, 1995; Orville et al., 2001; Steiger et al., 2002].

Anthropogenic influences such as the Urban Heat Island (UHI) and increased aerosol concentrations have been postulated for many years to have an effect on lower tropospheric chemistry, convection, lightning and rainfall [e.g., Huff and Changnon, 1973; Westcott, 1995; Jauregui and Romales, 1996;

1

Rosenfeld and Lensky, 1998; Bornstein and Lin, 2000; Shepherd et al., 2002; Rosenfeld and Woodley, 2003]. Moreover, these influences have been invoked as possible explanations for the CG lightning anomalies observed over metropolitan areas such as Houston, Texas. In particular, Orville et al. [2001] and Steiger et al. [2002] reported a 45% increase in annual CG lightning flash densities over and downwind of the Houston urban corridor relative to rural surroundings citing anthropogenic influences as possible causative mechanisms. Interestingly, these particular types of urban signals in CG lightning activity have also been noted downwind of other cities in the U.S. and abroad [e.g., Westcott, 1995; Soriano and Pablo, 2002; Naccarato et al., 2003].

Though local "anomalies" are not unique to the Houston area, or even to urban areas in general, the primary hypotheses offered to explain the localized enhancement in summer-season CG lightning over Houston revolve around "urban" effects. Broadly stated, the hypotheses can be summarized as follows:

- *UHI thermodynamics* provide a more favorable environment for convective initiation and thunderstorm intensity/severity over the Houston urban area resulting in more lightning activity and heavier precipitation [Huff and Changnon, 1973].

- UHI-forced convergence and associated *mesoscale enhancements in sea breeze (SB) convergence*, simply cause more frequent convection, and associated precipitation and lightning activity over the city [Braham et al., 1981; Hjelmfelt, 1982].

- ***Urban aerosol loading*** [Braham et al., 1981] particularly enhanced cloud condensation nuclei (CCN) concentrations in polluted air masses may contribute to the suppression of mean droplet size, delaying the onset of the collision-coalescence process thereby making more cloud water available to colder cloud regions where it would be operative in the charge generation process resulting in enhancements in CG lightning [Rosenfeld and Lensky, 1998; Rosenfeld, 1999, 2000; Rosenfeld and Woodley, 2000; Williams et al., 2002].

Additionally, findings that surfaced during METROMEX (the Metropolitan Meteorological Experiment; [Changnon et al., 1971]) may also be applicable to the problem at hand. Specifically, radar studies from this early-1970s campaign noted an enhancement in the merging and associated intensification of convective cells over and downwind of the urban corridor [Changnon et al., 1976]. A more recent example of the impact of cell mergers on upscale growth and lightning production was presented by Carey and Rutledge [2000], who noted that once cold pool outflow boundaries associated with precipitating convective cells began to interact with the sea breeze front, the previously isolated cells began to merge, resulting in vigorous upscale growth, accompanied by significant production of mixed phase ice mass, significant electric fields, and lightning. Given the fact that merged systems generally yield more than an order of magnitude more precipitation than their unmerged counterparts [Simpson and Woodley, 1971; Simpson et al., 1980], and that these merged systems are also more vertically developed and more intense than those that are not [Houze and Cheng, 1977; Westcott, 1984], it is conceivable to extend the METROMEX observations of enhanced

storm mergers downwind of the St. Louis urban area as a plausible explanation for the enhanced lightning ground flash densities that were found in the same location, as noted by Westcott [1995]. Therefore, in addition to the three hypotheses outlined above, this study will also investigate the role that convective cell mergers may have in explaining the existence/persistence of the lightning anomaly.

1.2 Problem Statement and Significance of this Study

The research presented in this study addresses a fundamental question regarding urban, ultimately anthropogenic, influences on convection as it relates to lightning production and precipitation structure. The essential building block in this study is the convective cell without which, subsequent lightning generation would be inconsequential; therefore, the hypothesis offered as the basis for the proposed research is

> "Thermodynamic and kinematic controls driven by the interaction
>
> between Houston area topography and the troposphere ultimately control
>
> the organization, frequency, and location of convection, thereby
>
> explaining the Houston lightning anomaly"

That is to say that lightning occurs when and where convection occurs ... the greater the frequency and intensity of convection, the greater the expected lightning generation. With regards to the multitude of hypotheses offered to explain the presence of the Houston lightning anomaly (as will be detailed in Chapter 2), the words of the medieval English philosopher and Franciscan monk William of Ockham (ca. 1285-1349),

"*Pluralitas non est ponenda sine neccesitate*" or "*plurality should not be posited without necessity,*" may prove to be quite applicable. Specifically, *when faced with several possibilities what is the simplest or most obvious explanation for the facts*? Given the complexities of the problem at hand, it seems equally plausible that a "first order" explanation involves some combination of UHI convergence and thermodynamics, perhaps interacting with the sea breeze front, resulting in enhanced initiation, and likely merging, of convective cells over and downwind of Houston. As the lightning anomaly under scrutiny is manifested in the climatic mean, so too must be the associated cause. The aim of this study is therefore to ascertain which, if any, of the proposed hypotheses can be deemed the primary climatological causative mechanism, or more likely which if any can be eliminated as a predominant contributor.

As evidence to the significance of the investigation at hand, one need only examine the recommendations made by the U.S. Weather Research Program's (USWRP) 10th Prospectus Development Team (PDT-10), who recommended *"that research into understanding and predicting weather impacts in urban areas should receive increased emphasis by the atmospheric science community"* [Dabberdt et al., 2000]. In addition to contributing to a better understanding to three of the nine thematic recommendations offered in the PDT-10 report: (1) *"improved understanding and forecasting of convective storms,"* (2) *"improved forecasting of intense/severe lightning"* and (3) *"further research into the impacts of large urban areas on the location and intensity of urban convection,"* this research will provide additional data points that will confirm or refute the METROMEX hypotheses, and in doing so will contribute to the ongoing debates regarding the impact of human civilization on local climate.

1.3 Organization of the Dissertation

A summary of pertinent background information related to this research will be presented in Chapter 2; in addition to a discussion surrounding the physics of the problem (thunderstorm electrification), this chapter will provide an overview of the literary hypotheses relevant to the Houston lightning anomaly. Chapter 3 will explore the role that convective cell mergers have in explaining the existence of the Houston lightning anomaly, highlighting a preferential location of enhanced merger occurrence downwind of the city. Documenting the existence of possible climatological forcing-response relationships capable of explaining the observed enhancement in CG lightning activity over Houston, Chapter 4 will present a series of regional and local climatologies addressing each of the hypotheses under investigation; through a process of selective exclusion, this chapter then ascertains the relative role that each of the hypotheses under investigation plays in shaping the characteristics (spatial extent and magnitude) of the Houston lightning anomaly. Synthesizing the information contained in the previous chapters, Chapter 5 quantifies the effects that enhanced boundary layer convergence (physical forcing) has on a thunderstorms ability to ultimately produce CG lightning (atmospheric response). Concluding remarks, along with recommendations for future research will be presented in Chapter 6. Two appendices provide additional support to the problem at hand. Appendix A scrutinizes the statistical characteristics of the Houston lightning anomaly, performing an independent analysis on an extended subset of the CG lightning dataset referenced in the literature. Appendix B establishes a physical link between a storms ability to generate enhanced concentrations of precipitation sized ice particles in the mixed-phase region, and its capacity to become electrified.

CHAPTER 2

BACKGROUND AND THEORY

The problem at hand deals with an anomaly in CG lightning. Therefore, it is logical to first form a conceptual understanding of the thunderstorm electrification process. Once established, this model will form the foundation from which the lightning anomaly can be investigated, shaping the conceptual framework for this study.

2.1 Thunderstorm Electrification – The Physics of the Problem

Although the exact processes by which thunderstorms become electrified and ultimately lower charge to the surface of the Earth continues to be debated, it is generally accepted that significant electrification, and subsequent lightning generation in clouds is attained when sufficient numbers of ice crystals (diameter ~ 100 μm) collide with millimeter-sized graupel particles in the presence of super-cooled liquid water [e.g., Reynolds et al., 1957; Takahashi, 1978; Jayaratne et al., 1983; Saunders and Peck, 1998; Berdeklis and List, 2001]. This non-inductive charging (NIC) mechanism operates independent of ambient electric fields, and is thought to be the primary charging mechanism responsible for the electrification of thunderstorms. While the physical means of charge transfer between ice surfaces remains uncertain [Baker and Dash, 1994; Dash et al., 2001], it is in these rebounding collisions that the transfer of charge is

7

manifested, with the consensus being that particles growing (evaporating) faster (slower) by vapor deposition gain positive (negative) charge in the collision [e.g., Baker et al., 1987; Jayaratne, 1993]. Though the results from various laboratory experiments differ to some degree, the above referenced studies have established that the magnitude and sign of charge transferred to the larger riming ice particle in these collisions is a function of temperature, liquid water content (LWC) and relative impact velocity, or equivalently, on temperature and rime accretion rate (RAR, the product of LWC, collision efficiency [a function of droplet size] and relative impact velocity). Figure 2.1 shows an example of the dependence of the charge transferred to the rimer on temperature and LWC. Smoothed contours connect points of equal magnitude with the shaded area representing the LWC and temperature which produced a negative charge on the rimer; note that at temperatures warmer than approximately $-10°$ C, the rimer is positively charged, regardless of LWC.

In addition to the charge generation via NIC, the riming of ice particles can lead to a stochastic process resulting in the rapid generation of secondary ice particles within a developing thunderstorm (the so called Hallett-Mossop Ice Multiplication Process; [Hallett and Mossop, 1974; Mossop and Hallett, 1974; Mossop et al., 1974]). Riming occurs when a super-cooled drop freezes upon contact with an ice embryo; upon freezing, these super-cooled drops may eject splinters of ice providing additional ice nuclei capable of commencing the riming process, thereby leading to the generation of additional ice nuclei through splintering [Prupacher and Schlamp, 1975; Chisnell and Latham, 1976]. Laboratory experiments conducted by Hallett and Mossop [1974] and Mossop and Hallett [1974] found that copious splinter production due to riming occurred within a
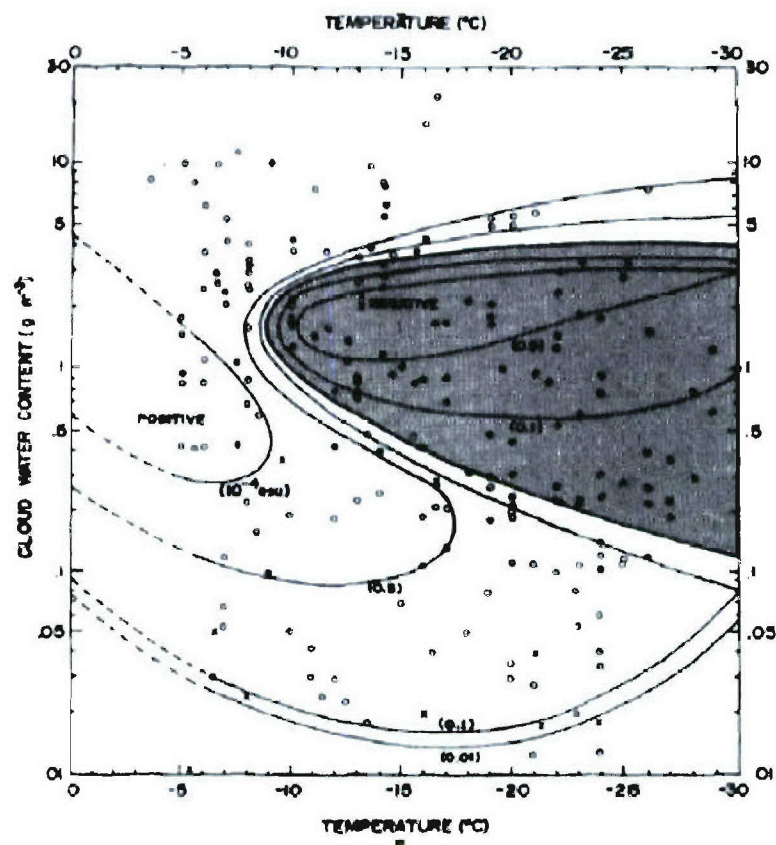
Figure 2.1 Sign and magnitude of charge imparted to riming particle in a collision as a function of temperature and liquid water content. Open circles show positive charge, solid circles show negative charge and crosses represent uncharged cases. The electric charge of rime per ice crystal collision is shown in units of 10^{-4} esu. Adapted from Figure 8 of Takahashi [1978].

temperature range of $-3°$ C to $-8°$ C for velocities in excess of about 0.9 m s^{-1}, with the presence of droplets of diameter greater than 24 μm being crucial to the occurrence of observed splintering. Given that this process is confined to relatively warm cloud temperatures, it is conceivable that smaller splinters (not yet of riming size) may be capable of participating in the NIC process as they are lofted into the upper (colder) portions of the storm. Although other secondary ice processes exist, the stochastic process just described is relevant to discussions surrounding the aerosol hypothesis to be discussed in Section 2.3.4.

Applying the above findings to a simplified model of a developing thunderstorm one can envision convective updrafts driving an ice process resulting in the suspension of large graupel particles within the mixed phase (0° C to $-40°$ C) region of the storm where they rime (grow), and interact with smaller ice crystals (likely generated through secondary ice particle production) being lofted into the upper portions of the storm. At temperatures cooler than the charge reversal temperature (some threshold between $-10°$ C and $-20°$ C dependent on LWC), these rebounding collisions result in positive charge being transferred to the smaller (ascending) ice crystals, with a net negative charge residing on the heavier graupel particles. These interactions can ultimately lead to the development of an electrical dipole, with positive charge situated over negative charge. Once the graupel's terminal velocity exceeds the storm updraft speed, it begins its descent towards the surface of the Earth. Graupel-ice crystal collisions occurring below the charge reversal temperature (i.e., at warmer temperatures), result in the falling graupel particle becoming positively charged and the ascending ice crystals negatively charged. The rising ice crystals can then contribute to the elevated negative charge region, while

the descending graupel can produce a small positive charge region below the main negative charge center. The result is the development of an electrical tripole, with the negative charge region sandwiched between two positive charge regions [Williams, 1989; 2001].

While the tripole model is conceptually simple, it is important to note that there remains considerable complexity in the microphysical charge separation process, and not all thunderstorms ascribe to this simple model. However, the particle-cloud scale physics associated with the NIC mechanism are still valid in the most general sense, with *three key requirements for thunderstorm electrification and subsequent lightning production being*: (1) the existence of convective updrafts, capable of (2) driving robust mixed-phase precipitation ice processes (i.e., production of graupel/hail and smaller ice crystals/splinters); and the occurrence of resultant (3) rebounding graupel-ice crystal collisions in the presence of super cooled cloud water. Although these three ingredients are critical to the thunderstorm electrification process, it is clear that (2) and (3) cannot proceed without the presence of a significant convective updraft. Indeed from an energetics standpoint, stronger updrafts should be capable of producing more lightning.

2.2 Houston and the Houston Lightning Anomaly

A city of 2.01 million people (Wikipedia; http://en.wikipedia.org/wiki/Houston,_Texas), the city of Houston has seen a period of significant growth over the last decade and a half, including a 23% increase in inhabitants over the 1990 population of 1.63 million [U. S. Bureau of Census, 1996], making it the fourth most populous city in the United States. Economically, Houston is

world-renowned for its energy industries (supplying over 40% of the nations oil refining capabilities) and its deep water port and shipping channel. Located on the upper Texas Gulf Coast (see Figure 2.2), Houston has an area of approximately 1,550 km^2. An area lacking significant orographic features, Houston sits adjacent to the complex coastline of Galveston Bay (to the southeast) with over 50 km^2 of winding and stationary waterways dispersed throughout. In addition to the Houston shipping channel, a heavily industrialized link between the city and the Gulf of Mexico, there are four major bayous that transect the city, with Lake Houston, a significant ground-level water source located approximately 30 km to the northeast of city center. The climate of Houston is classified as humid subtropical, with its proximity to Galveston Bay and the Gulf of Mexico causing winters to be quite mild, while the summers are rather hot and humid. Summer air temperatures average 33° C (92° F) during the day and 23° C (73° F) at night with mean daily dewpoint temperatures of 22° C (72° F). Southerly winds prevail during the summer months with wind speeds averaging 4 m s^{-1}, with an average of 19 lightning days per summer [Gauthier et al., 2005].

Using 12-years of CG lightning data (1989-2000) gathered by the NLDN, Orville et al. [2001] documented a persistent, year-round, enhancement in CG lightning activity downwind of the Houston metropolitan area. Steiger et al. [2002], using the same data set (5 km spatial resolution), quantified the enhancement observed by Orville et al., reporting a 45% increase in annual CG lightning flash densities over and downwind of the Houston urban corridor relative to rural surroundings (see Figure 2.3). Their findings are generally consistent with previous studies [i.e., Westcott, 1995], indicating
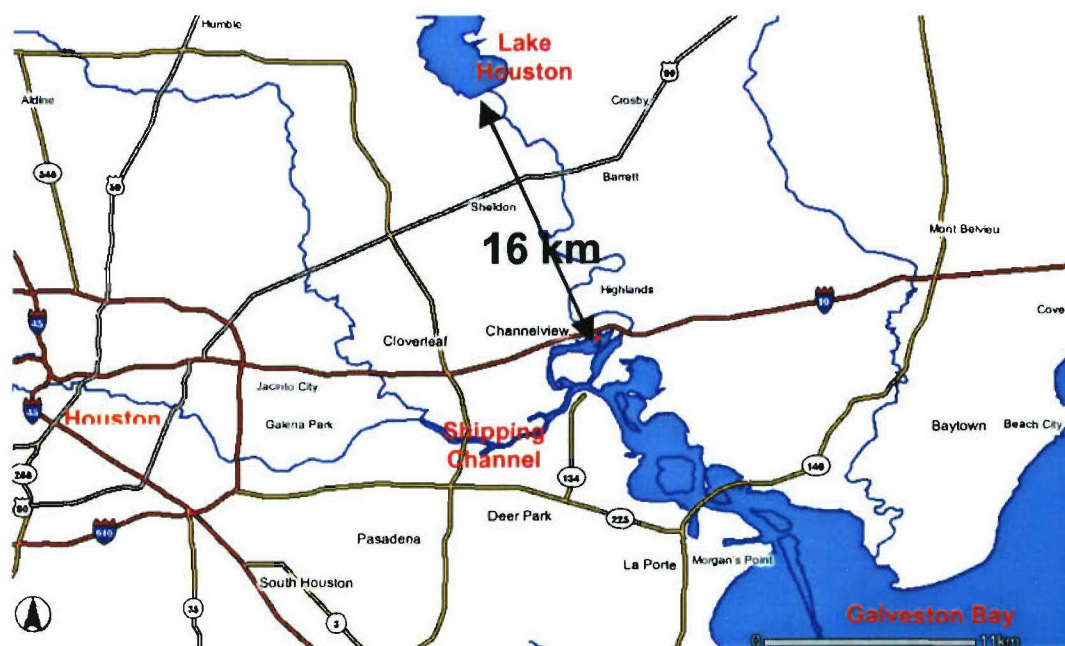
Figure 2.2 Base map depicting Houston area waterways (blue) and roadways (yellow and red). Geographical references in text are labeled in red.
(SOURCE: http://www.mapquest.com).

that observed enhancements in CG flash densities can occur over, and downwind of urban corridors.

Scrutinized in Appendix A [see also Gauthier et al., 2005], we performed an independent analysis as part of this dissertation research on an extended subset of the CG lightning dataset (1995 – 2003) referenced in the literature [Orville et al., 2001; Steiger et al., 2002] to further study the previously documented lightning anomaly. These findings indicate that the local Houston CG lightning anomaly is a persistent summer-season feature (even when large lightning events are excluded from the analysis), with flash densities over and downwind of the Houston metropolitan area approaching 1.5-2 times that of immediate surroundings. However, when examined more

1989-2000 (JJA 0900-1800 CST) Mean Flash Density (Flashes km-2)

0   0.5   1   1.5   2   2.5   3   3.5 >

0   50   100 km
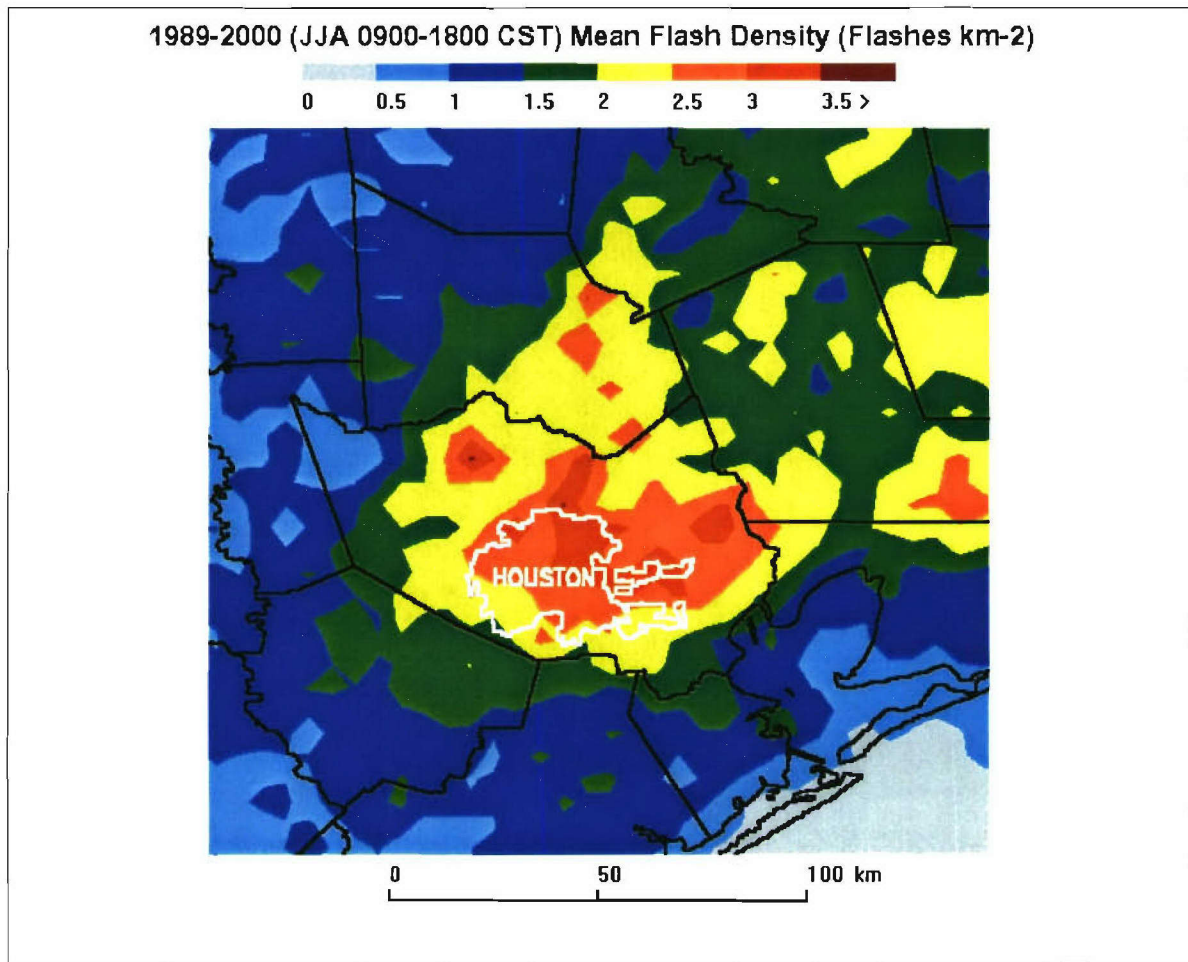
Figure 2.3 The twelve-year summer (June, July, and August) flash density in flashes km^{-2} summer^{-1} is plotted, from 1989 through 2000 for Houston, Texas. Galveston Bay is located to the southeast of the Houston city limits, shown in white. Adapted from Figure 1 of Orville et al. [2001].

regionally, we find the feature to be statistically non-unique, embedded with "anomalies" of similar scale within the more general enhancement of CG lightning along the Texas and Louisiana Gulf Coast. In fact, examination of annual lightning flash densities (flashes km^{-2} year^{-1}; Figure 2.4) observed by NASA's Optical Transient Detector (OTD) reveals a broad region of coastal enhancements, situated along the central Gulf of Mexico (including the Houston area), in *total*, not just CG lightning activity. This indicates that the Houston area likely falls victim to enhanced intra-cloud lightning activity as well; however, this study will focus on the CG component of the total lightning signal.
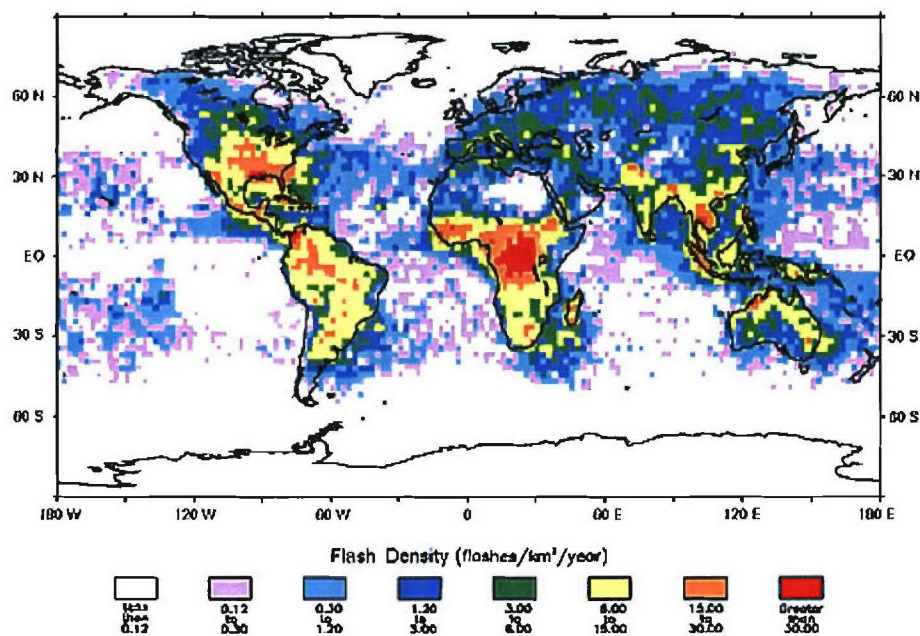
Figure 2.4 Spatial distribution of annual global lightning activity between September 1, 1995 and August 31, 1996 as observed by NASA's OTD. Lightning flash densities (flashes km^{-2} year^{-1}) were calculated statistically using OTD data from more than 400 separate 3-minute observations of each location on the earth (SOURCE: http://thunder.msfc.nasa.gov/otd/).

As it pertains to the NIC theory discussed above, the apparent climatological lightning anomaly over and around Houston (whether it be CG or total lightning) is ultimately the integrated effect of cloud-scale mixed phase ($0°$ C to $-40°$ C) microphysical interactions driven by deep, strong convective up and down drafts. Hence, one would expect a local maximum in precipitation ice mass (i.e., graupel and hail in the mixed phase zone) to accompany any peak in the CG flash density over Houston [e.g., Petersen et al., 2005]. As a simple test of this hypothesis (detailed in Appendix B), over 46,000 daytime volumes of convective WSR-88D (Weather Service Radar – 1998 Doppler) radar data, were used to investigated the relationship between radar derived precipitation ice mass and NLDN CG lightning over the period of seven summer seasons (1997 – 2003). As expected, local maximums in CG lightning over and around the greater Houston metropolitan area were indeed accompanied by peaks in precipitation ice mass, with linear correlation coefficients in excess of 0.97 regardless of analysis method. Whether examining observations of CG lightning and derived ice mass in a climatological (*Eulerian*) fashion, or doing so on a cell-by-cell basis, our findings corroborate those of previous investigators [e.g., Workman and Reynolds, 1949; Larsen and Stansbury, 1974; Goodman et al. 1988; Carey and Rutledge 1996, 2000, Petersen and Rutledge 2001 and Petersen et al. 2005, among others], firmly establishing a link between enhanced concentrations of precipitation sized ice particles in the mixed-phase regions of convection, and the presence/amount of lightning. Based on solid physical arguments and the synthesis of this and numerous previous observational studies (referenced above), we have every reason to believe that this strong correlation is also causal. Therefore, relative to the documented anomaly in summer season ground flash

densities over and around Houston, this implies that the unique aspects of the Houston urban area must first generate an anomaly in convective intensity and precipitation ice, which then generates an anomaly in lightning. *Hence, hypotheses offered to explain such an anomaly must be capable of (a) explaining either increased frequency and/or intensity of convection, and (b) relating (a) to the enhancement of ice mass and lightning production.*

2.3 Conceptual Framework

Although it is relatively easy to construct a number of concepts as to how urban areas influence precipitation and lightning, isolating the causative factor(s) is not trivial [Shepherd, 2005]. As outlined in Chapter 1, four primary hypotheses will be investigated in this study in an attempt to attribute causation, as it applies to the Houston CG lightning anomaly. The ensuing discussion is intended to provide a solid understanding of each of the pieces (hypotheses) to this complex puzzle, concluding with a presentation of the conceptual framework from which this study will be conducted.

2.3.1   The Urban Heat Island

Urban areas modify boundary layer processes in several ways. One of the primary mechanisms is through the development of an urban heat island (UHI), characterized by a temperature difference between the city and its outskirts [e.g., Oke, 1982]. Here, the urbanization of the landscape leads to the replacement of natural surfaces by artificial ones with different thermal properties (e.g., heat capacity and thermal inertia). These artificial surfaces are typically more capable of storing solar

energy and converting it to sensible heat.

In a recent review article, Arnfield [2003] summarized extensive studies of urban heat islands made during the previous 20 years, confirming empirical generalizations offered by Oke [1982]. These include that the UHI (intensity) 1) decreases with increasing wind speed, 2) decreases with increasing cloud cover, 3) is most well developed in summer or in the warm half of the year, 4) tends to increase with increasing city size and/or population, 5) is greatest at night (due mostly to differences in land surface characteristics) and 6) may disappear by day or the city may be cooler than the rural environs. Anthropogenically generated heat (i.e., additional heating associated with industrial sources) can also affect UHI intensity, enabling the UHI circulation to be more clearly observed during the daytime (contrary to summary points 5 and 6, above; [Shreffler, 1978; Fujibe and Asai, 1980]). This latter point illustrates why urban-forced convection is not simply a night-early morning phenomenon.

The UHI is known to alter the thermodynamic stability in metropolitan areas, which could lead to initiation or intensification of convection. Changnon [1978], using data obtained from METROMEX, determined that urban effects leading to increased thunderstorm activity were generally thermodynamic in nature, as opposed to microphysical (or mechanical). Braham et al. [1981] showed that a definite higher thermal instability (higher temperatures) existed over St. Louis compared to nearby rural areas during the METROMEX field campaign. In addition to these observational studies, several recent modeling and experimental studies have also provided relevant insights into UHI-dynamics. Through a set of extensive numerical experiments, Baik et al. [2001] investigated UHI forced convection. Given favorable thermodynamic conditions, their

moist simulations yielded a downwind (urban induced) updraft cell capable of initiating convection and downstream precipitation with cell intensity proportional to UHI intensity and inversely proportional to prevailing wind speeds. It was further shown that the time required for the first cloud water formation decreases as the intensity of the heat island increases, drawing its horizontal location nearer the urban heat source. Using a 2D mesoscale model with detailed urban surface exchange parameterizations, Martilli [2002] studied urban influences on boundary layer structure taking into account both thermal (i.e., differential heating) and mechanical (i.e., building induced drag and friction) effects. His findings show an increase in the convective (daytime) boundary layer (CBL) height above the city relative to surrounding rural values, strongly linked with wind speed and rural soil moisture. He also found that thermal factors play the most important role in modulating the CBL height evolution above the city mainly because the thermal effects reduce the destruction of the mechanically produced total kinetic energy (TKE) by buoyancy; the greater amount of TKE available resulted in a higher CBL depths. Mechanical factors became important in the evening, serving to delay the onset of the nocturnal boundary layer. Using a storm-resolving version of RAMS (the Regional Atmospheric Modeling System, [Cotton et al., 2003]) with sophisticated surface boundary conditions, Rozoff et al. [2003] investigated surface-driven low-level convergence mechanisms, and their role in initiating deep, moist convection over the St. Louis, Missouri area. Consistent with the previous cited findings, their representative simulations indicate that the UHI circulation (i.e., thermal factor) plays the dominant role in initiating thunderstorms, relative to the momentum flux generated over the city (i.e., mechanical factors) with the formation of a downwind convergence zone capable of

initiating storm development. Consistent with the downwind shifting of the convergence zone, advected boundary layer doming (on the order of 300 m) was observed lee of the city with enhanced precipitation totals also co-located in the downwind region. Attesting to the importance of land use and land cover (LULC), Cheng et al. [2005] coupled an updated high resolution LULC dataset with a high resolution mesoscale model to investigate the effects of land surface on resultant output. Regarding PBL height distributions, their updated simulations produced boundary layers depths over, and downwind of the Houston industrial area (i.e., to the east-northeast) on the order of 250 – 600 m greater than in control runs, clearly identifying Lake Houston as a water body land use type resulting in lower PBL heights (on the order of 700 m less than the control).

Without a doubt, an abundance of evidence exists supporting the ability of the UHI to focus areas of enhanced convergence, particularly downstream of the thermal source, capable of initiating and/or enhancing convective activity and (likely) lightning. Boundary layer doming, which is also a common theme associated with UHIs, may also serve to enhance the electrification process, following Williams and Stanfill [2002] and Williams et al. [2005]. In considering ways in which differences in updraft speed between land and ocean could be achieved with essential the same Convective Available Potential Energy (CAPE), Williams and Stanfill [2002] re-examined the idea that both the width of boundary layer thermals and the width of the ensuing moist convection scale with cloud base height (CBH; [Lucas et al., 1994]), with broader updrafts experiencing less entrainment, thereby enhancing the conversion efficiency of CAPE to updraft kinetic energy. Results comparing mean lightning flash rates with CBH [Williams et al., 2005]

show a quasi-exponential increase in lightning activity as a function of CBH with an order-of-magnitude increase from the 500 m typical of tropical oceanic convection to the 3000 m typical of strongly continental convection, despite considerable scatter. The implication here is that if CBH scales with CBL depth [Wilde et al., 1985; Stull, 1988; Karan and Knupp, 2005], boundary layer doming *may* result in broader, more vigorous updrafts capable of further enhancing updraft strength thereby enhancing the charge generation/separation process, with small changes in CBL depth potentially realizing large enhancements in resultant lightning activity. The validity of the CBH – flash rate relationship just described however is not universal. In fact, Williams et al. [2005], further investigating this relationship, elude to the existence of a delicate mix between CBH and instability, where one variable may dominate over the other in determining the intensity of resultant convection. Particularly, within the U.S., we note that the most intense convection (both electrically and in severity) tends to occur along a "*key*" north-south corridor situated over the central plain states where a combination of enhanced instability, fed by warm moist air originating over the Gulf of Mexico, and *moderate* CBHs coexist. We note that the extreme CBH values in the U.S. are climatologically found over the dessert regions of Nevada where the air is much drier, such that the LCL is extremely high, supportive of enhanced CBHs yet devoid of significant electrification (see Williams et al., [2005], Figures 4a – 4c).

2.3.2   The Sea Breeze Circulation

Relative to Houston, the complexities of the UHI are further compounded by the fact that the geography of the Houston area places it in the proximity of the Gulf of

Mexico, adjacent to a complex coastline and Galveston Bay with numerous inland waterways (i.e., the Houston "shipping channel," smaller rivers and lakes, see Figure 2.2) where it routinely falls victim to complex interactions between thermally driven circulations manifested in the sea breeze, and similar small scale circulations associated with LULC. Such interactions can constructively "interfere," leading to areas of low-level convergence capable of initiating and/or intensifying convection [e.g., Watson et al., 1991].

Estoque [1962] is one of the earliest studies to accurately model the sea breeze (SB) circulation, since then numerous investigators [see Miller et al., 2003 for extensive review] have contributed to our conceptual understanding of this diurnal phenomenon. Under ideal conditions, the sea breeze generally develops when the mean boundary layer temperature difference between adjacent air masses overlying coastal waters and coastal land is sufficient enough to create a density (and therefore pressure) gradient. This gradient in turn creates a thermally driven circulation favoring a low-level onshore flow of relatively cool air that intensifies throughout the day, eventually transitioning to an offshore flow during the evening hours. The leading edge of this low-level onshore flow is often referred to as the sea breeze front (SBF).

With inland penetrations on the order of 30-60 km, many studies have shown that convective thunderstorms frequently form near *and ahead of* the SBF [Gentry and Moore, 1954; Fovell, 2005], with coastline shape, synoptic scale winds and the proximity of water bodies to the coastline all influencing SB frontal morphology. Both numerical modeling [McPherson, 1970] and observational [Gibson and Vonder Haar, 1990] studies have shown that the sea breeze influenced by a complex coastline

develops convection in preferred locations. McPherson [1970] performed a numerical study of the effect of a complex coastline on the sea breeze circulation. The irregular coastline, crudely shaped like that southeast of Houston, TX (i.e., Galveston Bay), caused localized areas of enhanced mesoscale convergence and upward motion along the SBF. According to these model results, the preferred location for convective showers is in the vicinity of Houston. Observationally, Gibson and Vonder Haar [1990] noted enhanced SB convergence over convex portions of the coastline (outward bowing, from the coast), over the southeastern United States with a significant portion of the cloudiness resulting from the convergent sea breeze being classified as "deep convective." Several studies have also shown that areas of convergence are enhanced by interactions between the SB and synoptic winds [Gentry and Moore, 1954; Watson et al., 1991; Reap, 1994; Smith et al., 2005]. Reap [1994] provided results indicating a direct dependence of the magnitude of lightning activity over Florida on the direction of the synoptic-scale low-level flow, with a synoptic wind that directly opposes the low-level branch of the SB circulation resulting in maximum convergence and lightning over land. Examining warm season lightning distributions over the northern Gulf of Mexico, Smith et al. [2005] further highlighted the importance that the low-level flow regime had on regulating the strength and movement of the SB, with enhanced lightning activity occurring on days in which the prevailing low-level flow opposed the SB. Additionally, as discussed in Section 2.2 (see Figure 2.2), the Houston area (particularly the eastern portion, extending east-northeast) is host to numerous inland lakes, reservoirs and rivers. It has been documented that water bodies as small as rivers and inland lakes [Zhong et al., 1991; Laird et al., 1995] can develop local circulations of their own, capable of interacting with

an encroaching SB. The modeling efforts of Zhong et al. [1991] illuminated the presence of complex areas of convergence associated with the interactions between sea, river and lagoon breezes in the vicinity of the Cape Canaveral region of Florida. Using observational data (radar, sounding, and surface), Laird et al. [1995] confirmed the results of Zhong et al., finding preferential convective initiation zones to be located at intersection points between the sea and river breezes, indicating that low-level convergence is enhanced where these thermally driven circulations interact.

As eluded to in the beginning of this section, the interaction of the SB with the UHI circulation further compounds the problems associated with attribution of cause, as anthropogenic heating associated with the UHI will likely influence the encroaching sea breeze. Interactions between these two thermally driven circulations have been successfully modeled [Yoshikado, 1992; Yoshikado, 1994; Nielsen-Gammon, 2000] and recreated in the laboratory [Cenedese and Monti, 2003]; however, detailed observational studies of this process were lacking in the literature. The daytime UHI can persist under the influence of the sea breeze in the absence of significant synoptic-scale flows [Yoshikado, 1994], with the SBF having been found to linger over the city due to UHI effects; this may cause convergent flow patterns to appear more frequently and clearly over coastal cities. Further, Yoshikado [1994] shows maximum vertical motion occurred in his model simulation in the convergence zone of the sea breeze and the urban heat island circulation growing over the inland side of Tokyo, Japan around 1200 L. He also found that when heavily urbanized regions exceed 10 km in width (as Houston does), the interaction between the UHI and SB was *"significant and clearly influenced the local climate."* Yoshikado's (1992) results indicate that the effect of the Tokyo UHI can

increase the wind speed 2.3 m s^{-1} relative to the pure SB. Relative to the Houston area, Nielsen-Gammon's [2000] model simulation revealed similar results just southeast of the city with a convergence zone in the vicinity of the documented lightning enhancements. Subsequent simulations performed with the removal of the city, through the modification of LULC, conducted by Nielsen-Gammon, were devoid of the simulated convergence zone and did not develop convection over the Houston area, as in the control simulation. Extending modeling efforts to the laboratory, Cenedese and Monti [2003], used experimental data taken from a temperature-controlled water tank, to investigate the basic features of the circulations associated with an inland UHI and its interaction with a sea-breeze current. Absent a sea-breeze, their experiment generated a city centered thermal plume with peak upward vertical velocities directly over the thermal source. Corroborating the modeling efforts of Yoshikado [1994], the inclusion of a sea-breeze circulation resulted in a general leeward shift of the thermal plume, with the magnitude of the shift being inversely proportional to the speed of the encroaching sea-breeze.

2.3.3   The Convective Cell Merger

As suggested in Chapter 1, a relatively straight-forward explanation of urban maximums in convectively generated phenomenon was born out of the results of METROMEX. In addition to the observed increase in spatial distribution of convective initiation, Changnon [1976] observed that the frequency of convective storm mergers was maximized just downwind of the St. Louis metropolitan area. Unsurprisingly, the preferred location of storm mergers was also collocated with local maximums in urban rainfall, hail and general storm severity.

The merger of convective cells is a complex, non-linear process in which two previously separated convective cells tend to merge into a single entity. These merged systems generally yield more than an order of magnitude more precipitation than their unmerged counterparts [Simpson and Woodley, 1971; Simpson et al., 1980]. Further, it has been well documented that these merged systems are also more vertically developed and more intense than those that are not [Houze and Cheng, 1977; Westcott, 1984]. Coupling these observations with thunderstorm electrification theory, we find that many aspects of the merger process favor increased lightning production:

- Longer, more widespread, and more intense low-level forcing associated with interactions between downdrafts, cold pools and gust fronts create stronger, more organized updrafts capable of producing more mixed phase ice mass and subsequent charging [Simpson, 1980; Simpson et al., 1980; Tao and Simpson 1984].

- Subsequent cell mergers increase storm updraft area, decrease entrainment, and hence increase updraft strength and the efficiency of energy conversions [Lopez, 1978; Williams and Stanfill, 2002].

- Ice seeding of new convection from mature cells in a merged system increases charging [Carey and Rutledge, 2000].

Coupling the above discussions with the favorable environment, and focused convergence associated with the UHI, it is then conceivable to extend the METROMEX observations of enhanced storm mergers downwind of the St. Louis urban area as a

plausible explanation for the enhanced lightning ground flash densities that were found in the same location, as noted by Westcott [1995].

Therefore, there is every reason to believe that a link may exist between the convective merger process and increased lightning flash densities. A recent observational example of the impact of cell mergers on upscale growth and the electrification process was presented by Carey and Rutledge [2000]. Using a C-band polarimetric radar to infer precipitation rain and ice masses for tropical island convection, Carey and Rutledge found that lightning and the surface electric-field were strongly correlated to mixed phase ice mass and rainfall. During the pre-merger phase precipitation was dominated by warm rain processes, with little or no mixed phase ice mass, significant electrification, or lightning generation. Once cold pools began to interact with the sea breeze front, the previously isolated cells began to merge, resulting in vigorous upscale growth, accompanied by significant production of mixed phase ice mass, significant electric fields, and lightning. Further, their findings indicated that *merged convective cells, which resulted from gust front forcing, produced 97% of the rainfall and mixed-phase ice mass and 100% of the CG lightning.*

Clearly, the link between intensifying updrafts (leading to upscale convective growth, enhanced mixed phase interactions, and ultimately enhanced lightning flash densities) and convective mergers has been established. Application of this hypothesis to the Houston area further compounds the problem at hand as complexities of converging low-level flow associated with the interacting UHI and SB circulations may indeed interact favorably with gust fronts and cold pool outflow boundaries generated by the

downdrafts of dissipating convection to trigger new cells, which can then merge with older cells to further invigorate convection, thus linking all three hypotheses.

2.3.4   The Aerosol Hypothesis

The final hypothesis to be investigated in this study is referred to as the "Aerosol Hypothesis," and is primarily focused on impacts to cloud microphysics, although portions of the hypothesis have thermodynamic and kinematic implications. Here, urban aerosol loading [Braham et al., 1981], in particular enhanced CCN contents in polluted air masses, is believed to increase the cloud-droplet number concentration (i.e., so-called Twomey-effect, [Twomey, 1977]) leading to a decrease in mean cloud droplet sizes [Albrecht, 1989]. Hence, the number of droplets growing large enough to initiate the collision-coalescence processes is reduced, precipitation initiation is delayed, and precipitation rates may be reduced [Rosenfeld and Lensky, 1998; Rosenfeld, 1999, 2000; Rosenfeld and Woodley, 2000]. Following this line of reasoning, Williams et al. [2002] put forth a conceptual model broadly linking increased (decreased) CCN concentrations with increased (decreased) cloud electrification and lightning. According to their hypothesis, the increased concentrations of smaller aerosols, such as in polluted urban areas, lead to a narrowing of the cloud droplet spectra with fewer large drops available to initiate the collision-coalescence process. Consequently, increased super-cooled water contents are present at colder temperatures in the cloud, leading to increased buoyancy and updraft strength via release of the latent heat of fusion, while contributing to the growth of graupel particles through riming, ultimately enhancing cloud electrification and lightning through the collision of ice crystals in the presence of super-cooled water [e.g.,

Takahashi, 1978].

Importantly, the deceptively straight forward aerosol hypothesis as presented above can be difficult to support as conceded by Williams et al. [2002] in their discussion of ambiguities observed over the southwest Amazon. For example, Williams et al. found little difference in lightning production over the southwest Amazon between aerosol-rich October and aerosol-poor November in the pre-monsoon regime, casting doubt on a primary role for the aerosol in enhancing cloud electrification. During the following less active wet season, the distinction between aerosol and thermodynamic contributions is less clear-cut finding a positive correlation between a single point measurement of aerosol concentration and daily maximum lightning flash rates measured by a single flat plate antenna, but also noting a similar correlation between thermodynamic parameters (i.e., CAPE) and lightning.

Further, some observations suggest that in clouds with very large concentrations of small CCN, the formation of the ice phase can be delayed to very high altitudes and low temperatures [Rosenfeld and Lensky, 1998; Rosenfeld, 2000; Rosenfeld and Woodley, 2002]. Recall from Figure 2.1 that peak charge transfer occurs somewhere in the neighborhood of $-10°$ C to $-20°$ C (depending on LWC; [Takahashi, 1978]), thus a delay in the formation of ice to temperatures colder than $-20°$ C could actually decrease the charging efficiency, thereby resulting a suppression of cloud electrification, especially for the most intense storms. Rosenfeld [1999] himself, although not in the context of thunderstorm electrification, highlighted the fact that deep tropical clouds with temperatures extending well below freezing may be affected because of the less efficient accretion of smaller, super-cooled, cloud drops by the growing ice precipitation particles.

Following Saunders and Peck [1998], application of the NIC theory to the aerosol

hypothesis implies that the decreased collision efficiencies associated with reducing the

mean droplet size serve to lower the effective liquid water content (EW), thereby

decreasing the RAR (the product of EW and the graupel/ice collision velocity). A

decrease in RAR translates directly into a decreased efficiency with which charge can be

generated in the storm (i.e., less charge per collision is separated). The aerosol

hypothesis also appears to be flawed regarding the generation of ice particles, so critical

for NIC. Recall that the results of Hallett and Mossop [1974] and Mossop and Hallett

[1974] indicated three key ingredients for optimization of the ice multiplication process

responsible for the observed glaciation of some developing cumulus, specifically the

coexistence of (1) graupel particles with (2) super-cooled drops with diameters > 24 μm

allowing for (3) riming to occur, with optimum splintering occurring within a

temperature range of -3° C to -8° C. This process would not only lead to the development

of graupel particles, but also to the generation of copious amounts of smaller ice crystals

capable of being lofted into the upper portions of the storm, interacting with graupel aloft

allowing for the generation / separation of charge. As argued, the aerosol hypotheses

would actually serve to inhibit storm glaciation as smaller cloud droplets present at colder

temperatures could decrease the efficiency in which riming and splinter would occur,

further depriving the storm of the necessary ingredients to allow for NIC to ensue. As a

result, Williams et al. [2002] suggest that there is some optimum yet ill-defined level of

CCN concentration for maximum enhancement of electrification and lightning.

Adding further confusion to the general interpretation of "aerosol influences" on

precipitation (i.e., decreased precipitation associated with enhanced aerosol

concentrations), the aerosol hypothesis appears to contradict urban rainfall studies which find *increases*, not decreases, in rainfall in the vicinity of several cities [e.g., Changnon, 1968; Huff and Changnon, 1973; Changnon, 1979; Shepherd et al., 2002, among others] to include Houston [Shepherd and Burian, 2003; Burian and Shepherd, 2004]. Indeed, one hypothesis advanced as a result of METROMEX suggests that the microphysical influence of urban environments may *enhance* rainfall due to the presence of an increased concentration of ultra-giant (UG) CCN [Changnon et al., 1976], where a few UGCCN greatly enhances the efficiency of the stochastic coalescence process. Relative to the Houston area, Burian and Shepherd [2004] reported a 30-60% *increase* in rain volume and an 80% *increase* in rain frequency over the Houston urban area relative to its surroundings. Another complication not considered by the aerosol hypothesis, but advanced by Braham et al. [1981], is the potential importance of ice nuclei in the *modification* of cloud microphysical and rainfall processes. Since the production of large concentrations of small ice is fundamental to significant electrification of clouds, any urban influences on (primary) ice nucleation may also affect lightning production, especially in the water saturated environment that would exist if more cloud droplets existed at heights above the freezing level.

In summary, hypothesized urban influences of aerosols on cloud microphysics and electrification are complex and because they rely on the presence of convection to operate, do not function exclusive of the other hypotheses under investigation in this study.

2.3.5   Synthesis

In general, inadvertent weather modification hypotheses offered to explain lightning and rainfall anomalies rely on either or both perturbations in the spatial distribution and intensity of convection (from whence warm-season rainfall and lightning emanate), or modification to convective cloud microphysics through aerosol loading over and downwind of polluted cities such as Houston. Although each of the hypotheses under investigation posses their own strengths and weaknesses relative to the problem at hand, they all must be scrutinized with respect to the basic physics associated with thunderstorm electrification. Further, from the above discussion it is clear that the proximity of this highly industrialized urban area adjacent to the Gulf of Mexico (adjoined by a complex coastline) enables these causative hypotheses to operate in a simultaneous, sometimes complementary fashion, compounding isolation of the cause. To summarize, primary hypotheses offered to explain the documented enhancement in summer-season CG lightning revolve around "urban" effects. Specifically 1) enhanced convergence, thermodynamic instability, or dynamical influences associated with the urban heat island; 2) mesoscale enhancements in sea breeze convergence; 3) enhancements in the location, frequency and intensity of convective system mergers, and resultant thunderstorm intensification, which may be related to (1) and/or (2), and 4), altered microphysical processes associated with anthropogenic pollution.

As described in the previous sections of this chapter, application of the physics of the NIC theory of thunderstorm electrification to the problem at hand serves to form the foundation from which the lightning anomaly can be investigated. To that end, as a final synthesis of the above discussion, Figure 2.5 outlines the conceptual framework of this

study, showing the physical link between the thunderstorm electrification process and the lightning anomaly (bottom), while highlighting each of the causative hypotheses to be investigated (light gray filled boxes), along with their likely pathways (arrows and unfilled boxes) leading to the climological enhancement in ground flash densities over the Houston area. Note that the complex terrain and topography (black box) associated with the complex coastline of Galveston Bay and the numerous winding and stationary waterways exert an ever present influence on convective activity, regardless of causative hypothesis (dark gray shading encompassing all local processes). Also note that, as previously discussed, aside from the lightning anomaly itself, which represents the ultimate atmospheric response to the forcing hypotheses, the tractable portion of the thunderstorm electrification process in this study is precipitation ice mass. Additionally, with the exception of the aerosol hypothesis, the primary pathway to enhancing precipitation sized ice mass in the charging zone is by way of enhancements in storm inflow and boundary layer convergence, ultimately leading to enhancements in updraft characteristics (i.e., intensity, diameter and location), invigorating the NIC process within lightning producing storms that are responsible for the spatial extent and magnitude of the lightning anomaly.

In the context of this framework, we then pose the question: "*Which of these hypothesized mechanisms, if removed, would result in the disappearance of the lightning anomaly?*" The answer to this seemingly simple question would provide significant insights into the relative importance of each of the causative hypotheses in explaining the climatological lightning anomaly.
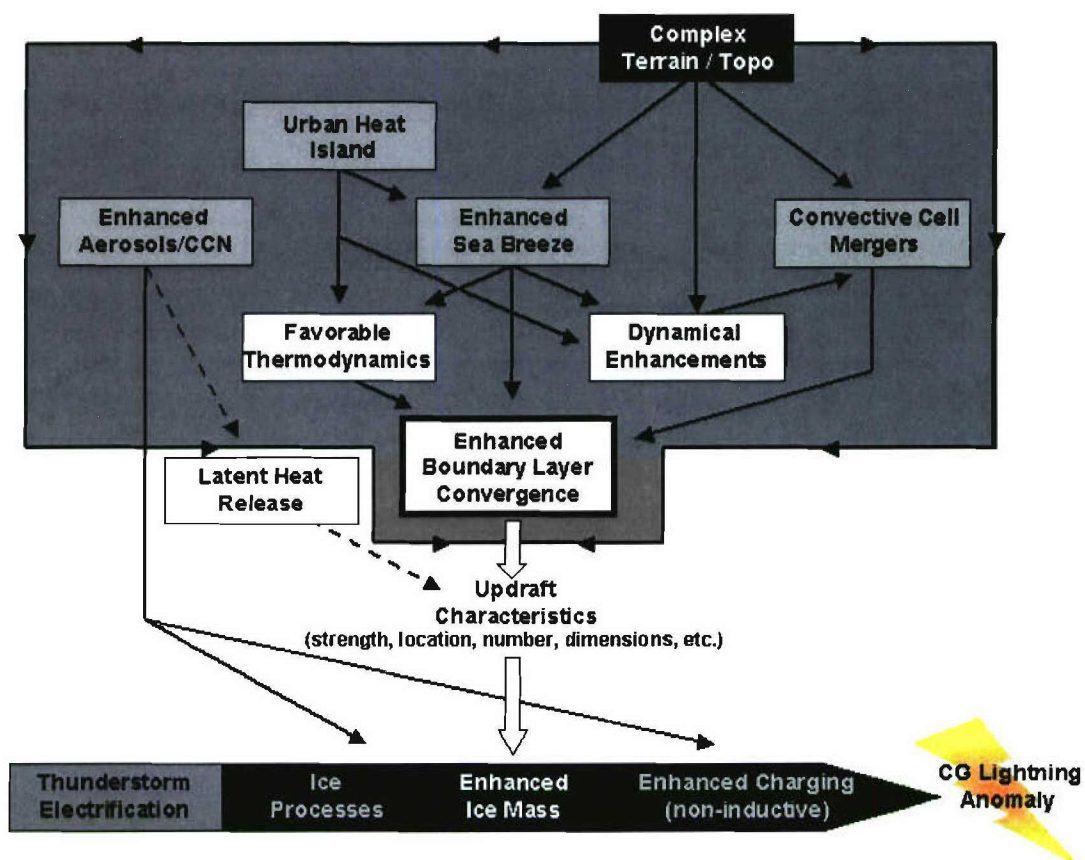
Figure 2.5 Conceptual framework associated with the Houston CG lightning anomaly, see text for complete description.

CHAPTER 3

CELL MERGERS AND THEIR IMPACT ON THE HOUSTON LIGHTNING ANOMALY

3.1 Introduction

As discussed in Chapter 2, numerous interacting factors exert influences on Houston area convection, each with its own possible pathway towards enhancing ground flash densities over and downwind of the city (see Figure 2.4). The overarching question becomes, can any of these factors be identified as the primary contributor, responsible for the existence of the lightning anomaly? Being that the problem at hand is quite complex, we have chosen first to investigate one of the more fundamental hypotheses offered to explain the anomaly (recall *Ockham's Razor*), that of convective cell mergers [Changnon, 1976]. Indeed an important result born out of METROMEX was the observation that the preferred location of storm mergers was also collocated with local maximums in urban rainfall, hail and general storm severity downwind of the St. Louis metropolitan area. However, the merger of convective cells does not operate independent of the other hypotheses under investigation, thus isolation becomes problematic. Therefore, rather than adopting an exclusionary approach (as will be done with the remaining hypotheses in Chapter 4), this chapter explores the role that

convective cell mergers alone (discussed in Section 2.3.3), regardless of origin, have in explaining the existence of the Houston lightning anomaly.

3.2 Data and Method

The analysis conducted in this chapter relies on a fused dataset spanning 8 summer seasons (JJA, 1996 – 2003) to create a regional, two-dimensional (2D) cell merger climatology for portions of eastern Texas and Louisiana (see Figure 3.1). Having a horizontal resolution of 2 km × 2 km, the 2D composite radar reflectivity data collected by the National Weather Service (NWS) Weather Surveillance Radar –1988 Doppler (WSR-88D) network is digitized every 15 minutes with peak columnar reflectivity values available for each grid point. The radar data, comprised of 16 levels of reflectivity (Z_{comp}), every 5 dBZ, beginning at level-0 (0 – 5 dBZ), was used as a primary input into a cell tracking algorithm (described below) along with corresponding CG lightning data. Here, NLDN detected ground strikes [Cummins et al., 1998] were gridded to match the horizontal dimensions of the Cartesian composite reflectivity grid for each of 80,000+ time steps (15-minute temporal resolution). Consistent with the methodology outlined in Appendices A and B, we have chosen to disregard flashes with positive peak currents less than 10 kA following the recommendations of Cummins et al. [1998] and Wacker and Orville [1999a,b]. The fused composite reflectivity and CG lightning datasets were used as input parameters to an Interactive Data Language (IDL) variant of the Thunderstorm Identification, Tracking, Analysis and Nowcasting (TITAN) software [Dixon and Wiener, 1993] where individual cells were identified and tracked throughout the domain over the entire period of record (POR; JJA, 1996 – 2003).

Before further discussion of the methodology employed within the cell-tracking algorithm, it is prudent to define the fundamental building block of a merger – the convective cell (or "composite cell" in this case). For the purposes of this climatology, a convective cell was defined as a contiguous region of composite reflectivity with values greater than or equal to $30 - 34$ dBZ (Z_{comp} = level-6) with minimum and maximum areas of 8 km^2 (2 pixels) and 5,988 km^2 (1,497 pixels), respectively. Although somewhat arbitrary, these thresholds were determined via experimental and statistical means. To investigate the sensitivity of the cell-tracking algorithm to the composite reflectivity threshold, Z_{comp} was set to levels-5, 6, and 7 (25-29, 30-34 and 35-39 dBZ, respectively). For all three cases, the identification and tracking technique worked well. The level-7 storms were smaller and more intense (on average) than the level-5 and level-6 storm echo areas. The lower the Z_{thresh} threshold, the greater the number of apparent mergers. Conversely, increasing Z_{thresh} resulted in a greater number of tracked cells. Based on the results of sensitivity testing, Z_{comp} was set to level-6 (30-35 dBZ, a reasonable threshold for the partitioning of convective activity, [Dixon and Wiener, 1993; Demott and Rutledge, 1998] for the final development of the cell-merger climatology. The use of area thresholds was necessary to eliminate ground clutter at the individual radar locations (lower threshold) as well as to minimize the impact of geo-location errors (discussed below) associated with larger tracked composite cells (upper threshold). Specifically, an examination of the merged cell area statistics revealed a positively skewed, non-Gaussian distribution with an upper-outer fence (defined as $Q_3 + 3IQR$, where IQR is the inter-quartile range and Q3 represents the 75th percentile of the cumulative distribution function [CDF] associated with cell areas) of 5,988 km^2. As the upper-outer fence of the

data distribution typically represents the upper threshold of the usable dataset, with values in excess deemed extreme outliers [Wilkes, 1995], the maximum area threshold was set to equal this value.

Using geometric logic regarding "composite cell" positions and shapes, the cell-tracking algorithm first identified cells that occurred within the domain. The following properties were then computed for each identified "composite cell":

- Mean composite reflectivity enclosed within the Z_{thresh} contour.

- Area enclosed within the Z_{thresh} contour.

- The size and shape of the storm projected onto a horizontal plane approximated by a best fit ellipse; ellipse properties included: latitude and longitude of centroid, major and minor axes, and orientation of major axis. Note that all cell properties were geo-located with the cell centroid (further detailed below).

- Flash Count (FC) – as the time interval between images was 15 minutes (unless data was missing), cell total flash counts were taken as the sum of flashes occurring ± 7.5 minutes of the composite reflectivity valid time, geo-located with pixels whose values were $\geq Z_{thresh}$. Note, this constraint eliminated flashes that may have been associated with the cell of interest, but did not come to ground within the confines of the Z_{thresh} contour; at the same time this methodology may have included ground strikes that originated in one cell and terminated within the cell of interest.

- Flash Density (FD) - together, cell FC and area were used to compute the FD for each cell (flashes km^{-2} $hour^{-1}$).

The algorithm then tracked identified cells, and determined if and when mergers occurred. Tracking was accomplished by matching cells at some time (t_1) with their corresponding counterparts in a subsequent time frame (t_2). Done successively, the cells were able to be tracked for their entire duration. Mergers were identified to have occurred when the region between two or more separated cells at t_1 exceeded Z_{comp} at t_2 (i.e., the best-fit ellipses overlap), at which point a new best-fit ellipse was created with the cell properties described above being *geo-located with the centroid* of the new merger ellipse. This means that, in the case of flash counts, all flashes associated with the pixels comprising the merged cell (i.e., flashes occurring $\pm$ 7.5 minutes of the valid time that were located within a pixel whose value is $\geq Z_{thresh}$) were geo-located with the merger centroid, hence losing their spatial identity, relative to this location.

Spatial distributions of cell properties (both individual and only those identified as merged cells) were then generated and examined in an effort to determine the statistical differences between the location, timing and properties of merged and individual cells.

3.3 Results and Discussion

Application of the cell-tracking algorithm to the 80,000+ time-steps contained within the fused composite reflectivity – lightning dataset resulted in the tracking and analysis of 3.8 million individual cells, 627,569 of which were classified as parents to 190,477 merged cells (summary statistics are presented in Table 3.1). We begin our discussion with an examination of the spatial distributions of cell and cell merger occurrences throughout the domain (Figures 3.1a and 3.1b, respectively). Spatially, there appears to be excellent agreement between the results of the independent analysis of

Table 3.1 Composite cell summary statistics for all, parent and merged cells generated from the tracking and analysis of 3.8 × 10⁶ cells over 8-summer seasons. Bold un-shaded values are statistically different than the corresponding IAH value for each cell type (at p-values < 0.05); statistical significance based on a nonparametric one-sided Wilcoxon Rank-Sum test.

Analysis Box	ALL CELLS	PARENT CELLS				MERGED CELLS			
	Count	Count	Mean Flash Count per	Mean Area [km²]	Mean Flash Density per [flashes km⁻²]	Count	Mean Flash Count per	Mean Area [km²]	Mean Flash Density per [flashes km⁻²]
DOMAIN	3,808,068	627,569	1.11	107	0.0014	190,477	12.5	798	0.0100
IAH	28,919	4,189	2.49	89	0.0048	1,567	21.47	663	0.0220
A	25,225	2,881	0.25	72	0.0003	1,316	10.13	792	0.0070
B	23,571	3,817	0.89	108	0.0018	1,319	15.74	840	0.0130
C	39,180	5,188	0.89	58	0.0013	1,638	10.46	529	0.0110
D	31,442	5,212	0.62	105	0.0016	1,715	17.57	742	0.0140
E	36,426	5,303	0.88	96	0.0012	1,750	12.2	698	0.0120
F	38,161	6,564	2.76	168	0.0024	2,016	12.35	653	0.0140
G	15,282	2,262	0.03	44	0.0005	777	17	840	0.0140
H	12,447	1,927	1.18	86	0.0024	572	12.35	672	0.0110
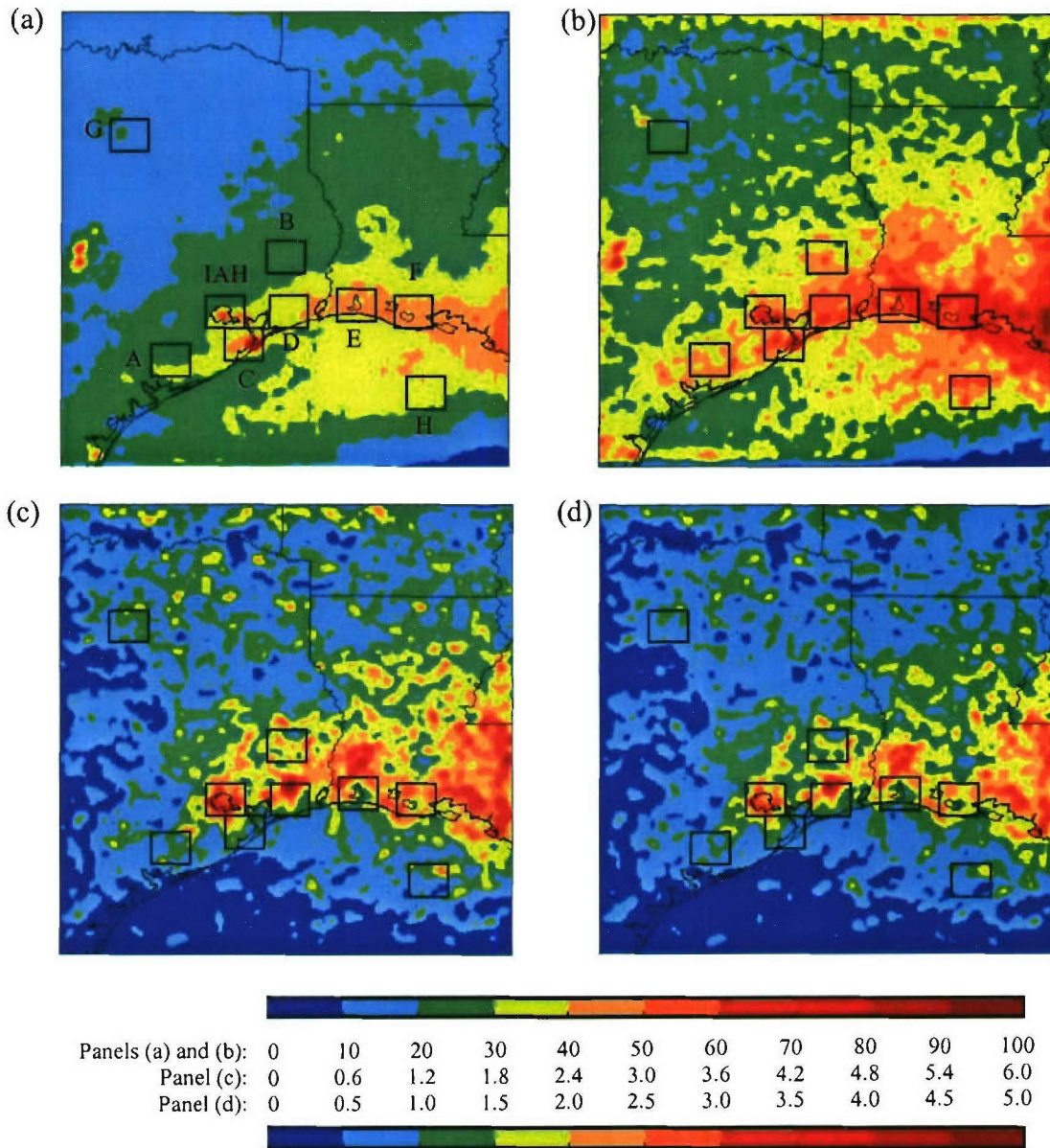
Figure 3.1 Eight-year (1996 – 2003) summer season spatial distribution of (a) relative frequency of occurrence [%] of 3.8×10^6 composite cell centroid locations, (b) spatial variations of the relative frequency of occurrence [%] of 3.9×10^5 composite cell merger centroids, (c) "Tracker produced" CG lightning climatology depicting the distribution of CG flashes associated with all cells in panel [flashes km_{-2} summer^{-1}] (a), scaled to match Figure A.1a, and (d) spatial distribution of flash density anomalies [dimensionless] created by normalization of mean flash densities of each pixel in panel (c) by the domain mean of panel (c). Appropriate scales for the color bar associated with each panel are as indicated. Black boxes represent sub-domains referenced in text.

CG lightning data performed in Appendix A, and the geo-location of cell and cell merger centroids. That is to say that convective cells tend to occur more frequently along the coast, with increasing frequency from west to east, in excellent agreement with the spatial distribution of lightning days presented in Appendix A (compare Figures 3.1a and A.1a). Regarding cell mergers, Figure 3.1b shows that there appears to be a preferred location of cell merger occurrence not only coinciding with locations of enhanced cell counts (Figure 3.1a), but more importantly, coinciding with climatological enhancements in CG lightning activity throughout the domain (compare Figure 3.1b with Figure A.1b). Additionally, enhanced flash counts gathered through the tracking of all 3.8 million cells appear to be consistent with the flash density patterns identified in Appendix A. Here, flash counts associated with each cell occurring within a given pixel were used to construct the spatial distribution of "tracker produced" mean summer flash densities (Figure 3.1c), scaled to match the independent lightning analysis conducted in Appendix A (Figure A.1b). Given the slight mismatch in PORs between the lightning climatology presented in Appendix A (1995 – 2003) and the analysis conducted herein (1996 – 2003, with intermittent gaps) and the limitations inherent within the cell-tracking algorithm and its associated geo-location assumptions (recall that all CGs coming to ground within the confines of Z_{thresh} were geo-located with the cell centroid and associated with a single pixel), the qualitative agreement between the observed (Appendix A) and the tracker produced lightning climatologies is remarkable, providing a strong indicator that the cell tracking algorithm is functioning as designed. Given the fidelity of the tracker-produced climatology (Figure 3.1c), we then created a flash density "anomaly" map (Figure 3.1d), as in Appendix A (see Figure A.2a), by normalizing the

mean flash density of each pixel ($\hat{x}$) by the mean flash density of the entire domain ($\bar{x}$), thereby creating flash density "anomalies" (i.e., $\hat{x}/\bar{x}$); for this parameter, values >1 (<1) are referred to as "positive" ("negative") anomalies.

Consistent with previous studies (detailed in Section 2.3.3) *this analysis confirms that merged cells are indeed larger and more intense than their unmerged counterparts.* Throughout the entire domain we find the average merger to be on the order of 8 times larger (horizontal extent) than the average parent cell, producing upwards of 11 times as much lightning with mean flash densities nearly an order of magnitude greater than the mean parent cell (see first row in Table 3.1). Further, findings indicate that CG lightning associated with merged cells contribute roughly 46% of the total lightning occurring throughout the domain.

To determine how parent cell and merged cell characteristics varied from location to location throughout the domain, 9 separate analysis boxes (each 4,080 km^2 in size) were qualitatively selected based upon the visual inspection of the spatial distribution of merger occurrences (Figure 3.1b). Throughout the entire POR, there were a total of 1,567 mergers whose centroids were geo-located over the Houston area (IAH box in Figure 3.1b). With the exception of analysis boxes G and H, the remaining boxes were chosen such that a similar number (±30% of IAH merger count) of mergers occurred within each. Boxes G (located in the vicinity of Dallas, TX) and H (located within Gulf of Mexico) were chosen for comparative purposes as the Dallas area is another major urban area within the domain that exits in a different meteorological regime, while the box located over the open Gulf waters (box H) contains a relative enhancement in merger activity (relative to other open water portions within the domain). Application of a

nonparametric one-sided Wilcoxon Rank-Sum test for statistical significance reveals that relative to the Houston area (IAH box in Figure 3.1a), cell mergers elsewhere in Texas (i.e., analysis boxes A, B, C, D, and G) have statistically larger areas (on the order of 10%; at p-values < 0.05), while those in analysis boxes E, F and H were found to be statistically similar. Additionally, with the exception of analysis boxes B (located to the northeast of Houston) and F (located along the central Louisiana Coast), cell mergers elsewhere produce, on average, 50% less lightning than mergers occurring over the Houston area. When comparing the mean flash densities of mergers occurring over the Houston area to those occurring elsewhere within the domain, we find the *mean Houston cell merger to have flash densities nearly double the mean flash density per merger elsewhere, all statistically significant (p < 0.05)*.

As previously mentioned, the degree of similarity between the observed and tracker-produced CG lightning climatologies provides a considerable degree of confidence in the performance of the cell-tracking algorithm. The total number of ground flashes contained within a given pixel (FC_{tot}) throughout the domain is equal to the sum of ground flashes associated with isolated convective cells (FC_i), parent cells (FC_p) and merged cells (FC_m) such that $FC_{tot} = FC_i + FC_p + FC_m$. Since the lightning contribution due to mergers at each pixel is known, it can be subtracted from FC_{tot} to determine if the flash density anomaly persists absent the influence of mergers. Figure 3.2a presents the spatial distribution of tracker-produced mean summer flash densities devoid of ground flashes associated with cells classified as mergers. Note the significant decrease in mean flash densities throughout the domain (on the order of 46%, domain wide, see Table 3.2). Despite the significant impact on the magnitude of flash densities, relative enhancements
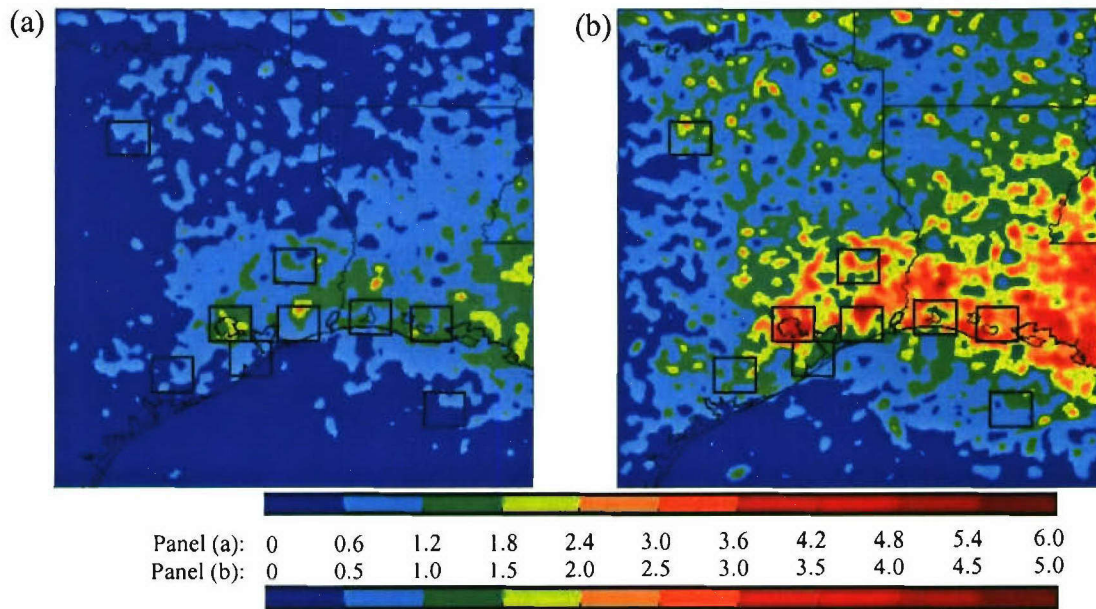
Figure 3.2 Eight-year (1996 – 2003) summer season spatial distribution of (a) ground flash densities and (b) anomalies (as presented in Figures 3.1c and 3.1d, respectively) excluding ground flashes associated with cells classified as mergers. Appropriate scales for the color bar associated with each panel are as indicated, scaled to match those in Figure 3.1c-d. Black boxes represent sub-domains referenced in text.

in flash densities remain apparent throughout the domain, particularly over the Houston

area. To further investigate the impact of the exclusion of ground strikes associated with

cell mergers on the lightning anomaly, a flash density anomaly map (similar to

Figure 3.1d) was created for the "merger removed" lightning climatology, the result of

which (Figure 3.2b) yields a very interesting result. Despite the significant decrease in

the magnitude of pixel mean flash densities associated with the removal of the lightning

strikes attributed to mergers, we find little change in the spatial distribution of flash

density anomalies (compare Figure 3.1d [with mergers] to Figure 3.2b [mergers

removed]), thus indicating that mergers contribute roughly the same percentage of the

total lightning signal, regardless of geographic location (see first column in Table 3.2).

In fact, the mean flash density anomaly over the Houston area (i.e., the IAH box) actually

increased from 2.64 to 2.84 time the domain mean when merger related ground strikes were excluded (Table 3.2). These findings have significant implications pertaining to the applicability of the cell-merger hypothesis under investigation; clearly *cell-mergers are not the predominant causative mechanism behind the Houston CG lightning anomaly.*

Table 3.2 The effect of excluding CG lightning associated with cells identified as merged cells.

Analysis Box	Lightning Contribution due to Mergers [%]	Mean Flash Density Anomaly	Mean Flash Density Anomaly, Mergers Removed	Percent Change [%]
DOMAIN	46%	1.00	1.00	0%
IAH	42%	2.64	2.84	8%
A	45%	1.08	1.09	1%
B	43%	1.73	1.81	5%
C	47%	1.24	1.22	-2%
D	48%	2.12	2.04	-4%
E	40%	1.90	2.00	5%
F	40%	2.19	2.42	11%
G	42%	1.00	0.90	-10%
H	53%	1.08	1.15	6%

3.4 Conclusions

Using 8 summer seasons (JJA, 1996 – 2003) of peak columnar radar reflectivity and associated CG lightning data coupled with an IDL variant of the TITAN cell tracking software, a two-dimensional cell merger climatology was created for portions of eastern Texas and Louisiana. Through the tracking and analysis of over 3.8 million "composite" cells, the impact of convective cell mergers on the Houston CG lightning anomaly was investigated. Results highlight the importance of cell-mergers on the upscale growth of convection, leading to significant enhancements (on the order of 46%) in the magnitude

of ground flash densities throughout the domain with areas of enhanced ground flash densities typically being co-located with areas of enhanced merger activity. Further, although mergers over the Houston area (relative to elsewhere in the domain) result in more vigorous convective cells that produce more lightning with larger flash densities, findings suggest that CG lightning contributions due to mergers are distributed similarly throughout the domain. The end result of this analysis lead us to ***reject the cell-merger hypothesis as a predominant causative mechanism*** in explaining the Houston CG lightning anomaly. What remains, and will be presented in Chapter 4, is to explore the remaining 3 hypotheses in an attempt to attribute causation.

CHAPTER 4

ANTHROPOGENIC ("URBAN") EFFECTS ON THE HOUSTON LIGHTNING ANOMALY

4.1 Introduction

The results of the cell-merger climatology presented in Chapter 3 highlighted the importance of cell-mergers on the magnitude of regional ground flash densities, with areas of enhanced ground flash densities typically co-located with areas of enhanced merger activity. As it pertains to the determination of cause, however, we found that cell-mergers alone were incapable of explaining the Houston lightning anomaly. CG lightning contributions due to mergers were similar throughout the analysis domain leading us to *reject the cell-merger hypothesis as a predominant causative mechanism.* In this chapter we isolate and address the feasibility of each of the remaining hypotheses (hence forth referred to as climatologically "forcing-functions") in explaining the *climatological* summer-season lightning anomaly over the Houston area by examining how flash density characteristics change through the selective exclusion of relevant subsets of the data (i.e., days in which a strong UHI is observed, high pollutant days, etc.) from subsequent calculations. We also investigate the climatological differences in convective structure utilizing a gridded radar dataset.

4.2 Data and Method

To investigate the feasibility of each of the outlined hypotheses, this study utilized data from three separate archived datasets spanning the summer months (JJA) of 1996 - 2003: (1) CG lightning data from the NLDN, (2) surface wind and temperature data and (3) sulfur-dioxide (SO_2) measurements, a proxy for CCN concentrations [i.e., Westcott, 1995]; the gridded radar dataset mentioned in Section 4.1 is detailed in Appendix B, the analysis of which will be discussed separately in Section 4.3.3.

Each dataset was used to establish long-term spatial and temporal variations (i.e., climatologies) for each of the respective observables. Further, the individual datasets were quantitatively filtered and merged into a single composite in which four specific classifiers could be assigned to each day within the dataset. Specifically, of the 736 summer days, there were 527 ("common") days in which each of the following could be established / calculated:

(1) Hourly and daily flash counts over the Houston area (large box in Figure 4.1).

(2) Sea-breeze classification (active 'SB' or not 'noSB').

(3) The intensity of the urban heat island index (UHI; defined in Section 4.2.3.3).

(4) The intensity of aerosol index (AI; defined in Section 4.2.3.4).

Following daily classifications, we examined how flash density characteristics over the Houston area changed through the selective exclusion of relevant subsets of the data (i.e., enhanced UHI days, enhanced AI days, etc.) from subsequent flash density calculations.
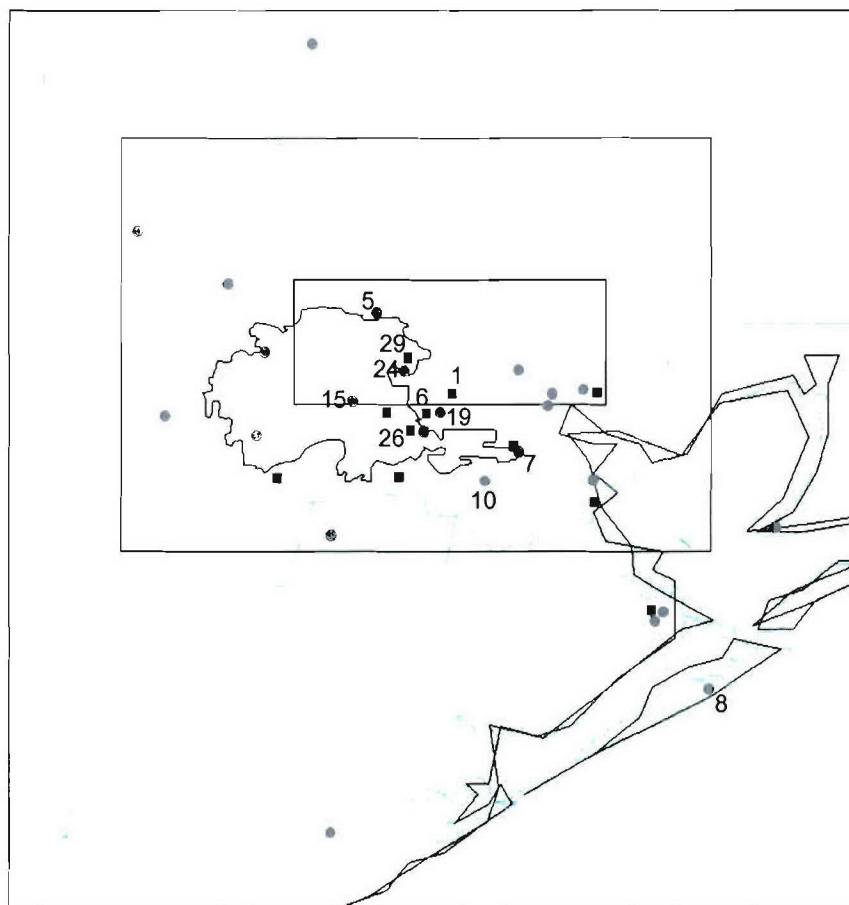
Figure 4.1 Location of 35 Continuous Ambient Monitoring Stations (CAMS; http://www.tceq.state.tx.us/compliance/monitoring/cams.html) operated by the Texas Commission on Environmental Quality (TCEQ) providing mean hourly surface measurements of temperature and winds (gray circles); sites denoted with black squares also provide mean hourly measurements of SO_2 concentrations; site numbers correspond to references in the text. Note that the Houston metropolitan area is outlined in black with the "Houston area" referenced in the text being encompassed by the black box, and the Houston "anomaly" box encompassed by the small inner box.

4.2.1   Cloud-to-Ground Lightning Dataset

As the premise for this study is the existence of a persistent summer-season anomaly in ground flash densities over the Houston metropolitan area, we will use NLDN CG lightning data [Cummins et al., 1998] as our primary dataset. Through a process of selective exclusion we will ascertain, and control for, the relative contributions of each of the proposed hypotheses on the flash density characteristics over and around the Houston area using as metrics the change in the mean flash densities over (1) the Houston urban area, and (2) the Houston "anomaly" box (see Figure 4.1, large and inner boxes, respectively).

In constructing these climatologies we have chosen to focus our attention on ground flashes occurring during daylight hours as it is during this timeframe in which each of the hypothesized forcing mechanisms are expected to have their greatest impacts, further it was during these hours that greater than 70% of the CG lightning occurred over the Houston area. To that end, a series of regional total ground flash density climatologies, each valid 0900-1859 CST (horizontal resolution of $0.05°$ latitude $\times$ $0.05°$ longitude) were generated with periods of record (PORs) ranging from 736 days (8 summer-seasons $\times$ 92 days per summer) to a final baseline of 202, non-contiguous, days in which synoptic conditions were quantitatively determined to be favorable for the formation of a sea breeze circulation (described in the Section 4.2.3.2). Note that, in all climatologies, we have disregarded flashes with positive peak currents less than 10 kA following the recommendations of Cummins et al. [1998] and Wacker and Orville [1999a, b].

4.2.2   Meteorological and Pollutant Datasets

Each day within the merged dataset was quantitatively classified as either a "Sea Breeze" (SB) or "Non-Sea Breeze" (noSB) day, with representative urban heat island and aerosol indices (UHI and AI, respectively) also being assigned. Hourly surface measurements of temperature, winds (speed and direction), and pollutant concentrations (i.e., SO_2, explained later) for these classifications came primarily from a network of Continuous Ambient Monitoring Stations (CAMS) operated by the Texas Commission on Environmental Quality (TCEQ), with supplementary upper air data extracted from NCEP/NCAR Reanalysis [Kalnay et al., 1996]. Figure 4.1 depicts the locations of the 35 CAMS meteorological monitoring sites (11 of which also provide mean hourly measurements of SO_2; black squares) used in this study.

It is important to note that there are times during the period of record (POR) in which various sites were inactive. Although we expect the long term climatological means of the thermal and surface wind fields to be minimally impacted as the hourly mean at each data point was taken over a minimum of 30 hourly observations (i.e., at least 30 days worth of data were available for all observing sites), the lack of data at some locations can prove problematic when trying to establish a composite dataset for each requisite parameter, as will be described in Sections 4.2.3.2 – 4.2.3.4. Therefore, the number of days included in the "common" dataset was reduced to 527 days in which there were sufficient hourly observations at specific CAMS sites (discussed below), each of which were selected based on predominant features present in the various component climatologies (to be discussed in Section 4.3.1), as well as to maximize the period of

overlapping observations (i.e., maximize the number of "common" days for inclusion in the final dataset).

4.2.2.1 Meteorological Analysis

In constructing the spatial climatologies for each of the meteorological variables (surface temperatures and horizontal wind components), mean hourly climatologies were first generated for each individual site. Once site-specific hourly climatologies were generated, the analysis area (depicted in Figure 4.1) was divided into a 29 × 36 Cartesian grid with a horizontal resolution of 4.5 km × 4.5 km, with the mean hourly data interpolated onto the grid using a Cressman-Barnes objective analysis method [Barnes, 1964]. This analysis resulted in a series of hourly maps depicting the spatial variations of mean temperatures and component wind vectors; for further comparison, mean hourly divergence fields were calculated from the gridded component wind vectors.

4.2.2.2 Pollutant Analysis

Past studies attempting to correlate enhancements in CG lightning activity to anthropogenic effects have used measurements of different aerosol tracers as gross indicators of pollutant levels and CCN concentrations. Most notably, researchers have attempted to use measurements of annual means of PM_{10} (particulate matter with aerodynamic diameters smaller than 10 microns) and SO_2 as the tracers of choice in their analyses [i.e., Westcott, 1995, Steiger et al., 2002, Soriano and Pablo, 2002 and Naccarato et al., 2003].

Although archived data is available from the Environmental Protection Agency (EPA) for county mean PM_{10} and SO_2 concentrations, temporal resolutions are insufficient for use in this study (only daily means, available every eighth day, for PM_{10} measurements); therefore, we chose to use available mean hourly measurements gathered by CAMS sites, a component of the daily EPA county means, to form the complementary pollutant analysis. Specifically, we used SO_2 vice $PM_{2.5}$, particulate matter with aerodynamic diameters smaller than 2.5 microns, as our tracer of choice as hourly SO_2 measurements were available throughout the entire POR ($PM_{2.5}$ data was only available from 2001-2003). As further justification for this choice, we noted a positive correlation between the time-averaged mean $PM_{2.5}$ and SO_2 observations at a common site with a correlation coefficient (R) of 0.70, indicating that approximately 50% of the variance in mean $PM_{2.5}$ measurements could be explained by the variance in mean SO_2 measurements.

The methodology applied to the gridding of the temperature and wind fields described in Section 4.2.2.1 was also applied to the pollutant analysis, resulting in hourly maps depicting the spatial distribution of mean SO_2 concentrations.

4.2.3 Data Filtration – the Use of Selective Exclusion (SE) Filters

To explore the aforementioned hypotheses, the merged dataset was filtered so as to isolate each of the three forcing-functions (sea breeze, enhanced UHI, and enhanced AI) from the other two, thereby allowing a direct assessment of the contribution of each to the long-term CG lightning climatology. Specifically, using the statistical distributions of each variable within the merged dataset, four quantitative filters (discussed herein)

were developed to statistically reduce the dataset from 527 common days to 202 distinct days for inter-comparison.

4.2.3.1 Selective Exclusion Filter #1 (SE1) – Large Lightning Event Days

As previously established, the Houston lightning anomaly is a persistent, non-unique feature along the Gulf Coast; therefore, our baseline climatology must be one in which the lightning anomaly persists with the selective exclusion of large events. Here, we have chosen, as in Gauthier et al. [2005], to include a larger domain (see Figure 4.2a) for the first portions of our selective exclusion analysis. Using the sum of daily flash counts in each of four coastal grid boxes within the domain (see solid white boxes Figure 4.2a) we used statistics of the summed daily flash count distribution to guide the classification of large event days within our dataset. Due to the skewed, non-Gaussian nature of the flash density distribution, we chose thresholds appropriate to the nature of the flash density histogram based on the cumulative flash density distribution to identify large events. Specifically, large event days were chosen as those days whose 4-box flash count total exceeded 1,930 flashes - the outer fence of the data distribution (defined as $Q3 + 1.5 \cdot IQR$; [Wilkes, 1995], note that this threshold is different than the upper-outer fence used in Chapter 3). Equivalent to the 90th percentile of the cumulative conditional flash density distribution (conditioned on the presence of lightning in at least one of the four coastal boxes), this method allowed for the objective classification of the tail of the distribution as large (coastal) "event days," of which there were 41.

Application of this first selective exclusion filter (SE1) reduced the dataset from 527 to 486 days with large events excluded, from which we note the presence of a
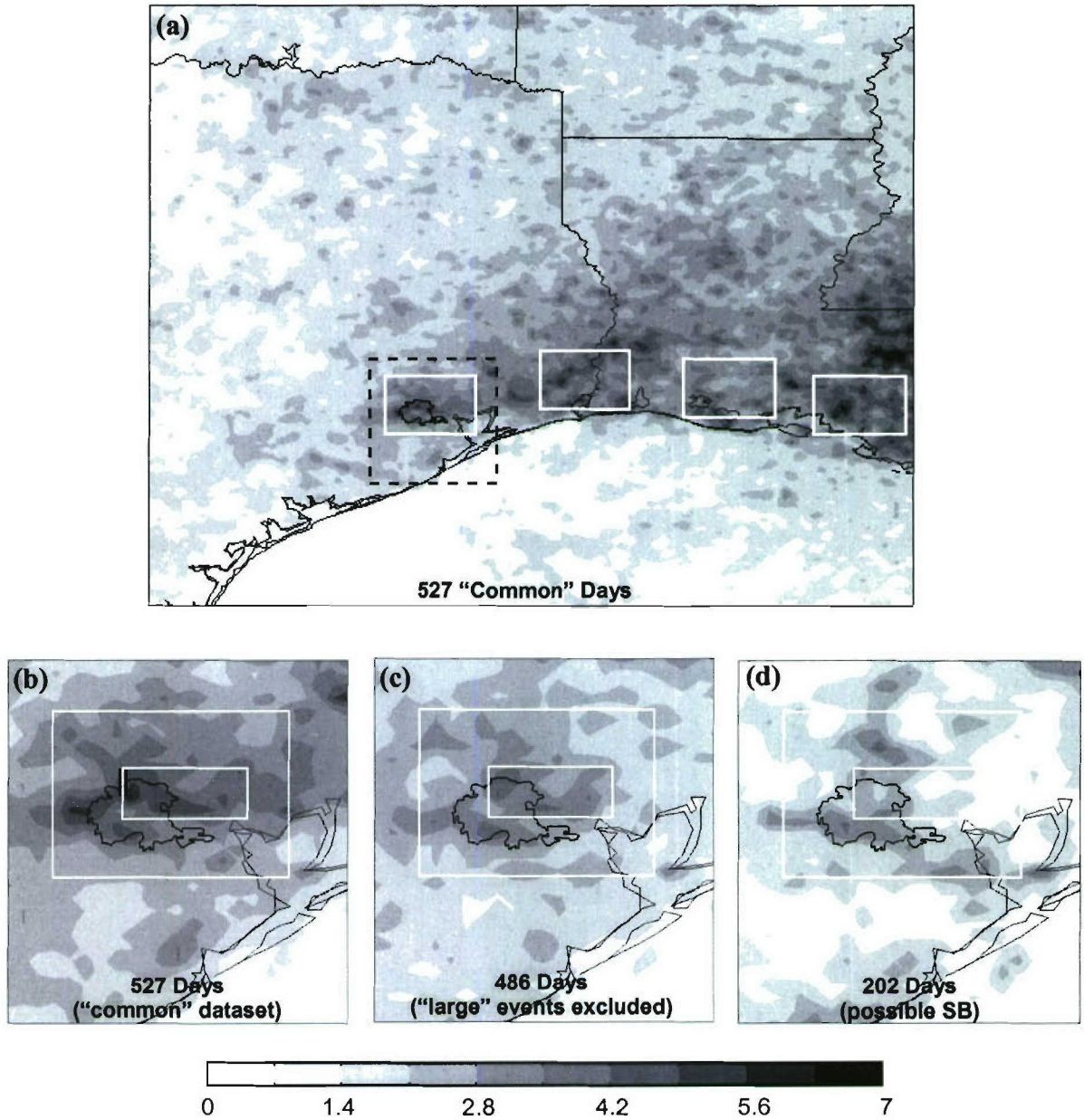
Figure 4.2 Spatial distribution of mean summer season flash density [flashes km^{-2} summer^{-1}] valid 0900-1859 CST for (a) 527 "Common" days presented over the larger domain utilized by Gauthier et al. [2005]; daily flash counts contained within white boxes were used in the "large event" classification algorithm while the dashed black box represents the CAMS sub-domain presented in Figure 4.1; (b) as in panel (a), only focused on CAMS sub-domain; (c) 486 days with "large events" excluded following application of SE1; and (d) 202 days in which background conditions were favorable for the formation of a sea-breeze, following application of SE1 and SE2 (F1-F4). Outer white box in panels b-d depict the "Houston area," while the inner white box depicts the Houston "anomaly" box, both referenced in the text.

persistent flash density anomaly located over the Houston metropolitan area with a finger of enhanced flash densities extending to the east-northeast (i.e., downwind) of the urban corridor (compare Figures 4.2b and 4.2c).

4.2.3.2 Selective Exclusion Filter #2 (SE2) – Sea Breeze Day Classification

As a mesoscale feature, the sea breeze can be important in the organization, initiation and/or intensification of coastal convection; therefore, knowledge of its occurrence within the dataset is critical. The magnitude of the remaining dataset (486 days following application of SE1) prohibits manual classification of this phenomenon; further, doing so would be subjective with the results not easily reproducible. However, quantitatively determining the historical incidence of this observable is not trivial. In this study, we have chosen to use a modified version of the classification algorithm outlined by Borne et al. [1998] who used six observational filters leading to the objective classification of sea breeze days within their dataset.

The filters were developed from empirical studies of the characteristic features of the sea breeze using data from field stations and radiosondes. In the present study, mean hourly wind and temperature data from various CAMS sites (Figure 4.1) were used to monitor the diurnal evolution of the surface wind and thermal fields, while 700 mb data from the NCEP/NCAR Reanalysis [Kalnay et al., 1996] was used as a measure of the general synoptic conditions. The first two filters (F1 and F2) were constructed to exclude days with probable large changes in synoptic conditions, while the third filter (F3) excluded days in which synoptic winds were too strong:

F1: change in 700 mb wind direction of less than 90° in the previous 12 hours

F2: change in 700 mb wind speed less than 6 m s^{-1} in the previous 12 hours

F3: wind speed < 11 m s^{-1} at 18Z (13L)

As the sea breeze is a thermally driven circulation, filter 4 (F4) ensured the presence of a reasonably large temperature difference between coastal (CAMS site 8; $T_{coast\,(8)}$) and inland temperatures (CAMS site 1; $T_{land\,(1)}$) for at least 1 hour during the diurnal heating cycle (0700-1800L).

F4: $T_{land(1)} - T_{coast\,(8)} \geq 3°\,C$

Applied to the dataset, F1 through F4 ensured that background conditions were favorable for the development of a sea breeze circulation yielding a total of 239 possible SB days. Passage of the remaining two filters (F5 and F6, described below) is what resulted in the classification of these remaining days as SB or noSB days.

Given appropriate background conditions (i.e., passage of F1 through F4), evaluating the behavior of the surface winds during (and following) sea breeze onset is what comprised the final two filters. Specifically, the sea breeze was characterized by a distinct change in surface wind direction of at least 30° resulting in an increased onshore wind component (F5), followed by 5 hours of relatively stable conditions in wind direction (F6). Based on manual inspection, we applied the final two filters as follows: CAMS sites 7 and/or 10 **and** CAMS sites 1 and/or 6 must pass the two filters (see Figure 4.1 for sensor locations). Although this approach proves to be rather stringent,

requiring a wind shift to occur at two separate locations (along the eastern edge of the metropolitan boundary, as well as further inland – note two sites in the vicinity of each location are used to allow for instances of missing data at one of the sites), the results provided a high degree of confidence that the algorithm was correctly classifying SB days.

To evaluate the accuracy of the filter method, 66 of 239 possible SB days (i.e., only considered days in which F1 through F4 had passed) were manually classified as either SB or noSB days prior to the application of the final two filters (F5 and F6). The filter method selected 40 days as SB days, while the manual classification selected 46 days as SB days out of a total 66 days. Of the 40 days selected by the filter method as SB days, the manual method gave the following results: 35 SB and 5 noSB. These statistics yield a false alarm rate (FAR) of 0.125 indicating that *the constructed selection method has an accuracy of greater than 85% in the process of selecting sea breeze days.*

Given the accuracy associated with the established methodology, we further filtered the dataset through the application of SE2 from 486 days (large lightning events excluded) to 215 possible SB days (i.e., 215 days that passed F1 through F4), with 124 days ultimately classified as SB and 91 as noSB.

4.2.3.3 Selective Exclusion Filter #3 (SE3) – Urban Heat Island Classification

Among the many differences between urban and rural areas that have emerged due to urbanization and industrialization, the most notable and well documented is the increase in air temperature over urban areas, the UHI. The classical definition of a UHI

is that of a temperature difference between the urban city and its surrounding rural background [Oke, 1982].

Using hourly temperature data from CAMS sensors, each day within the dataset was classified with an index proportional to the intensity of the UHI on that given day. Here, the UHI for a given hour was defined as

$$UHI = T_{urban(15,24,29)} - T_{rural(1,5,19)} \,, \quad (4.1)$$

where $T_{urban(15,24,29)}$ was the average hourly mean temperature of CAMS sites 15, 24, and 29 and $T_{rural(1,5,19)}$ the average hourly mean temperature of surrounding CAMS sites 1, 5 and 19 (see Figure 4.1 for sensor locations). The CAMS sites chosen for use in this index were based on the results of the thermal climatology (to be discussed in Section 4.3.1.2). Since each of the hypotheses under investigation invoke "forcing-response" relationships (i.e., enhanced UHI forcing resulting in the atmospheric response of enhanced CG lightning activity), the final UHI associated with each day was taken as the maximum UHI that occurred during the 6 hours preceding the peak in hourly flash counts over the Houston area (taken as the area encompassed by the larger box in Figure 4.1), or 08-14L on non-lightning days.

As with SE1, the statistics of the daily cumulative UHI distribution guided the objective classification of "large" (enhanced) UHI days (SE3). Specifically, enhanced UHI days were taken to be those days whose UHI fell within the upper quartile of the cumulative UHI distribution, equivalent to a daily UHI $\geq 2.58°$ C, of which there were 116 of the 486 days (excluding large lightning days).

4.2.3.4 Selective Exclusion Filter #4 (SE4) – Aerosol Classification

As previously discussed, SO_2 was chosen as the aerosol (CCN) tracer for use in this study, with all days in the dataset receiving an Aerosol Index (AI) proportional to the mean SO_2 concentrations over the industrial center of the Houston metropolitan area. As was the case with the development of the UHI, the SO_2 climatology (to be discussed in Section 4.3.1.4) was used to determine the location and diurnal timing of peak SO_2 concentrations (a proxy for the location of peak pollution). Here the AI for a given hour was defined as

$$AI = SO_{2(1,6,26)}, \qquad (4.2)$$

where $SO_{2(1,6,26)}$ was the average of the hourly mean SO_2 concentration measured at CAMS sites 1, 6 and 26 (Figure 4.1). Similar to the UHI, a "forcing-response" relationship was applied, with the final AI associated with each day taken as the average (vice maximum) of the aerosol indices during the 6 hours preceding the peak in hourly flash counts within the Houston box (08-14L on non-lightning days).

Again, statistics of the daily cumulative distribution guided the objective classification of "large" (enhanced) event days. Here, enhanced AI days (SE4) were taken to be those days whose AI fell within the upper quartile of the cumulative AI distribution, equivalent to a daily AI of 7.1 ppb or greater, of which there were 121 of the 486 overlapping days (excluding large lightning days).

Eliminating overlapping large AI and UHI days (of which there were only 13) from the 215 possible SB days that emerged from application of SE2 resulted in a dataset

of 202 distinct, non-consecutive days (with background conditions favorable for the formation of a sea breeze circulation) for inter-comparison allowing us to investigate each of the three proposed hypotheses (see Figure 4.2d for spatial lightning distribution).

4.3   Results and Discussion

As previously outlined, this study has two primary components, (1) the establishment of component climatologies and (2) the filtering of the conditioned dataset through a process of selective exclusion, the results of both will be discussed herein.

4.3.1   Component Climatologies

The first portion of this study established separate eight-year (1996-2003), hourly climatologies for each of the respective observables: CG lightning, surface temperatures, surface winds and convergence, and SO_2 pollutant concentrations.

4.3.1.1 Cloud-to-Ground Lightning Climatology

We begin our discussion of the CG lightning climatology with a simple time-series depicting the diurnal lightning cycle over the Houston area for the entire POR (Figure 4.3a – solid line). Here we observe a dearth in lightning activity during the late evening and early morning hours, followed by a rapid increase in convective activity at around 1100L, peaking at 1600L. As previously discussed, our subsequent analyses focus on the onset and intensification of convective activity between the hours of 09-18L (14-23 UTC) as it is during this timeframe that the hypothesized forcing mechanisms are
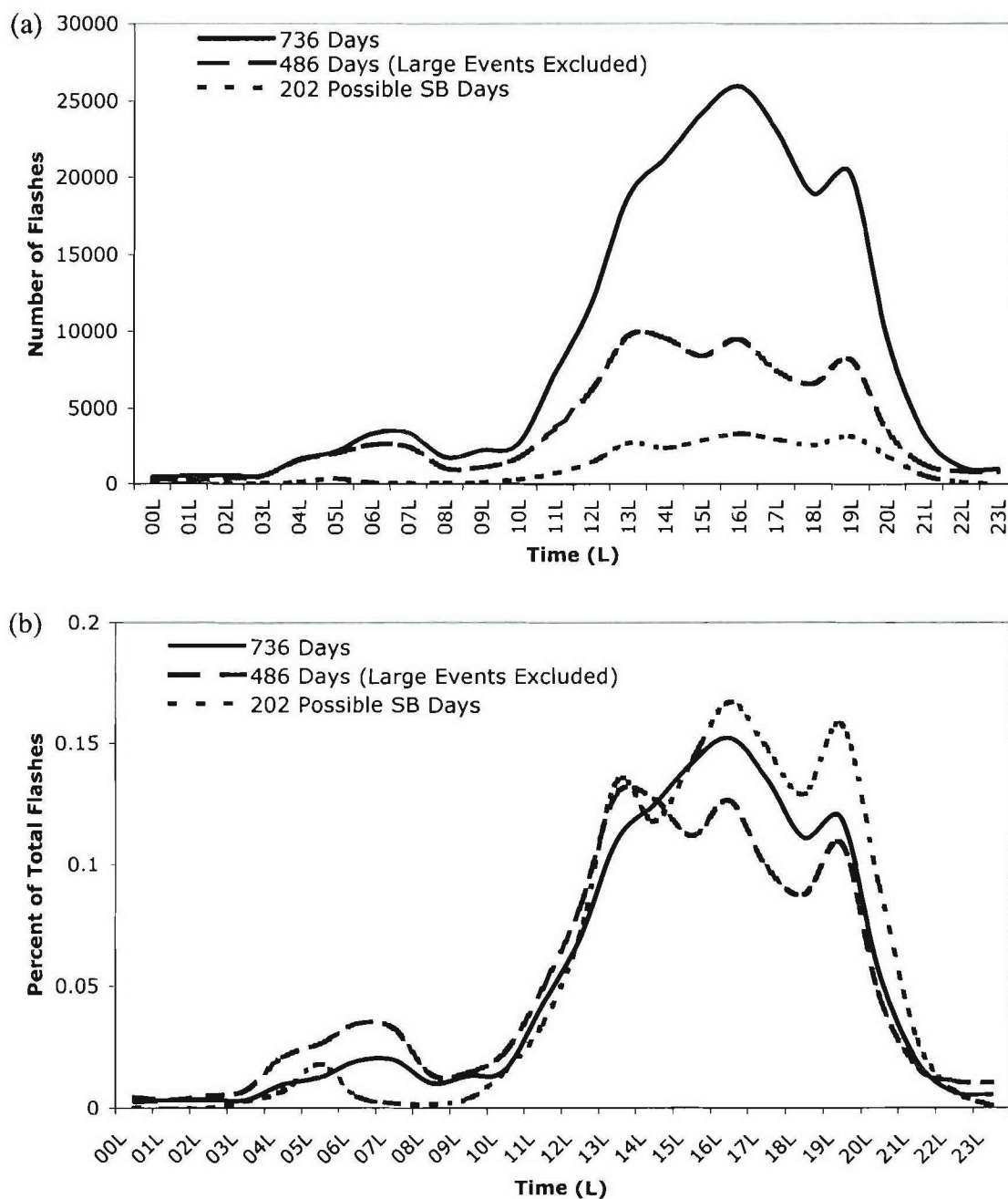
Figure 4.3 Diurnal time series of CG lightning over the Houston area for various subsets of the POR. Panel (a) presents the total number of CG flashes detected during each hour of the day for each subset, while (b) presents the normalized CG lightning activity for each hour, with each subset normalized by their relative total flash counts.
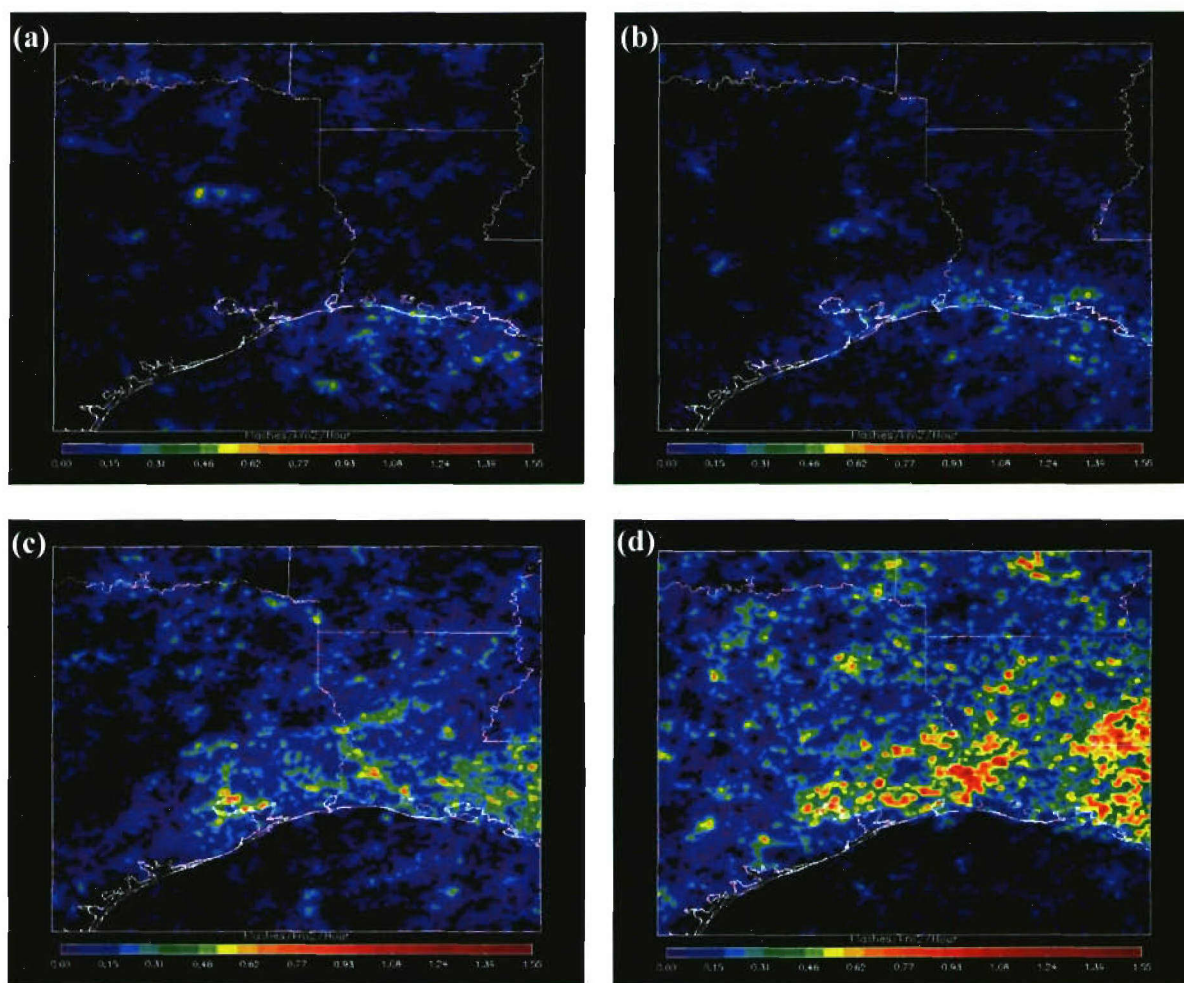
Figure 4.4 Spatial distribution of mean summer season flash density for various hours of the day based on the entire 736 day dataset; valid (a) 0600L, (b) 1100L, (c) 1300L and (d) 1600L.

observed to be dominant. Additionally, it is during this timeframe that approximately 75% of the climatological CG lightning activity occurs.

Significant insights into the characteristics behind the diurnal lightning cycle can be gained by examining the spatial characteristics of flash densities as well. Beginning at local midnight, with a regional inspection of the entire domain, we note minimal lightning activity over land between the hours of 00-09L (Figure 4.4a; valid 0600L) with predominantly offshore flow along the entire coastal region, evidenced by the appearance of coastal propagating lightning features (as opposed to onshore propagating). Likely tied to lags in local diurnal heating cycles, the beginning of organized onshore convection first becomes apparent along eastern portions of the coastline by 0800L with the Galveston Bay area falling victim to this organized convection within one to two hours of the eastern onset such that by 1100L (Figure 4.4b) a definite band of organized inland lightning activity is apparent from the Galveston Bay area eastward across the domain. This band, likely organized by the inland penetration of the sea breeze, continues forcing convection as it propagates inland such that significant enhancements in flash densities, particularly over the Houston area, become apparent by 1300L (Figure 4.4c). It is important to note that other areas of localized enhancements also become apparent at this time, primarily co-located in areas with complex coastal features and/or inland lakes. Beyond this timeframe convection becomes more widespread as the diurnal heating cycle nears its peak, with enhanced flash densities fanning eastward from the Houston area, increasing in latitudinal extent to the east (see Figure 4.4d; valid 1600L). Near the end of the daily heating cycle, convective activity begins to subside across the domain after 1700L, with lightning data indicating an apparent return to offshore flow by 1900L.

From the above discussion the following key points can be surmised:

- It is apparent that the sea breeze is acting to organize coastal convection throughout the domain, with the western extent in coastal enhancements terminating in the vicinity of the Houston area.

- Depending upon location in the diurnal cycle (i.e., 13-16L), significant coastal enhancements in ground flash density appear downwind of areas of complex coastline and/or inland lakes (assuming a SB flow perpendicular to local coastlines).

- Depending upon location within the diurnal cycle, enhancements further east of the Houston area appear more significant in both intensity and spatial extent.

Given the second and third points above, it is clear that the Houston lightning anomaly is a non-unique feature along the Gulf Coast; however, relative to its immediate surroundings, flash densities over the Houston area exhibit interesting/persistent spatial and temporal characteristics, that in and of themselves warrant closer examination. As previously mentioned, the apparent organization of inland propagating lightning activity begins mid-morning as the land surfaces heat up. At 0900L a finger of weak convective activity appears to impinge upon the eastern portion of the Houston metropolitan area off of the northwestern tip of Galveston Bay (Figure 4.5a). Over the next 2-3 hours the concave shape of this complex coastal feature appears to have a significant effect on localized lightning features, particularly their initiation. Principally, convective activity
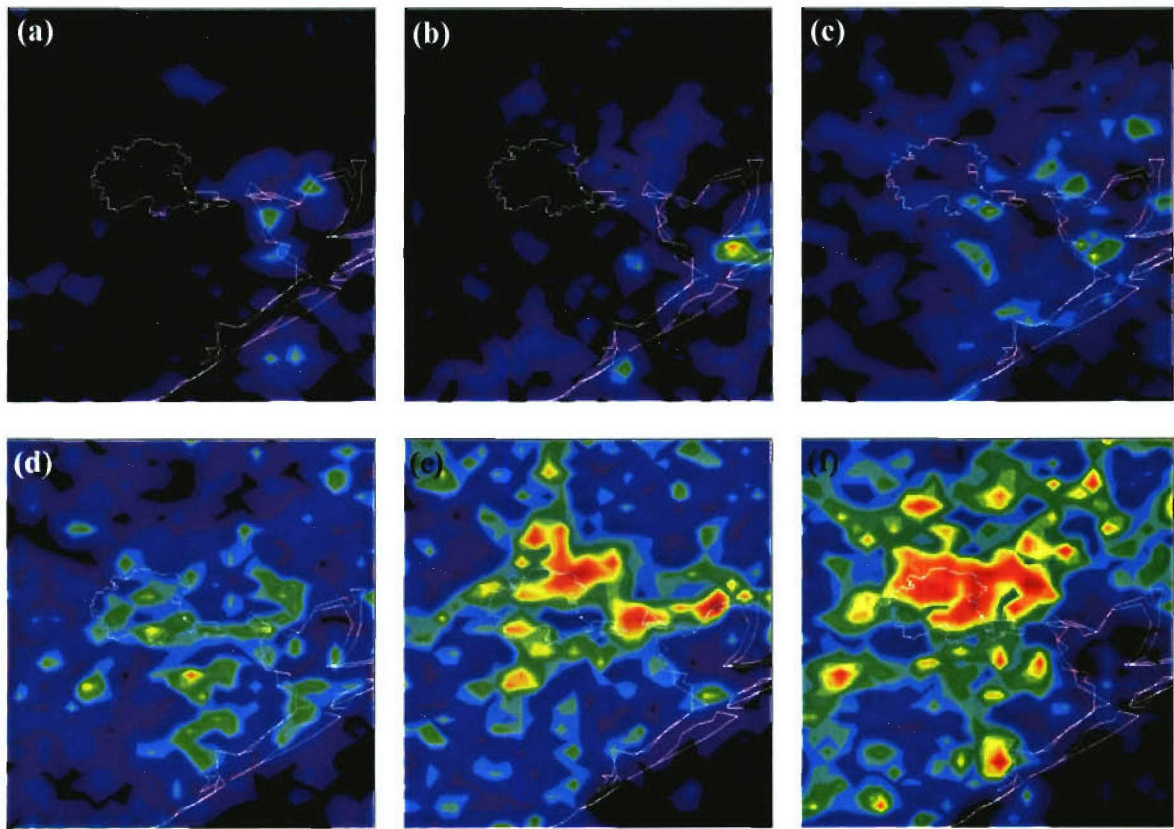
Figure 4.5 As in Figure 4.4 (including color scale), only focused on CAMS sub-domain presented in Figure 4.1; valid (a) 0900L, (b) 1000L, (c) 1100L, (d) 1200L, (e) 1300L and (f) 1500L.

appears to propagate onshore, perpendicular to the local coastline; here the previously mentioned finger penetrates further inland nearing the northeastern portion of the Houston domain with the appearance of initial convection to the north and southwest (SW) of the western edge of the Bay, emanating perpendicular to their adjacent coastlines (see Figure 4.5b; valid 1000L). Between 1000L and 1100L the northeasterly flow off of the SW shoreline of Galveston Bay appears to merge with the southeasterly flow perpendicular to the Gulf Coast forcing the first moderate enhancements (upwards of 0.5 flashes km^{-2} $hour^{-1}$) in flash densities to impinge upon the southeastern boundary of the city by 1100L (Figure 4.5c). Initial enhancements of this feature along the southern peripheries of the metropolitan outline at noon (Figure 4.5d) are shadowed by the explosive enhancements observed over the northeastern tip of the city one hour later (Figure 4.5e). Enhanced flash densities continue throughout the remainder of the afternoon with peak enhancements occurring between 1500L and 1600L over and to the northeast (i.e., over and downwind) of the city (Figure 4.5f; valid 1500L).

Further examination of Figure 4.3a (dashed and dotted lines) provides insight as to the effects of the application of SE1 and SE2 to the diurnal lightning cycle. Particularly, we note that exclusion of large lightning days (SE1; dashed line) results in dramatic reduction in hourly flash counts, particularly during the late afternoon, with the predominant peak in daily flash counts occurring at 1300L. The decrease in the diurnal peak in late afternoon activity indicates that "large" lightning events are likely associated with the subsequent intensification of initial convective activity forced earlier in the day (i.e., approximately 1300L). Further reduction, through the application of SE2 (F1-4), yields the diurnal lightning cycle associated with 239 possible sea breeze days (dotted

line). Here we see a continued decrease in hourly flash counts (Figure 4.3a); however, when normalized by the total daily flash counts (as in Figure 4.3b) we see that, with the exception of the eliminated peak in afternoon flash counts associated with the removal of large events, peak hourly flash counts are occurring at roughly the same time for each of the three datasets. Particularly, we note an initial ramp up in hourly flash counts around local noon, followed by a brief plateau, and then subsequent intensification during the later afternoon hours.

4.3.1.1 Surface Temperatures – Establishing the UHI Climatology

Simple time-series depictions of mean hourly temperatures, as presented in Figure 4.6, clearly show the influence that the urban environment has on temperatures recorded at urban sites (solid line), compared to surrounding rural (dashed line) and coastal (dotted line) sites. Here we see mean midday temperatures at urban sites located directly in the center of the Houston metropolitan area (CAMS sites 15, 24 and 29; solid line in Figure 4.6) to be as much as $2°$ C warmer than surrounding rural stations (CAMS sites 1, 5 and 19; dashed line). Additionally, note the modulating effect that the Gulf waters have on coastal temperatures (dotted line) with relatively warmer coastal temperatures during the nocturnal hours and cooler coastal temperatures during the heating portion of the diurnal cycle – foreshadowing support for a thermally driven circulation (i.e., the sea breeze). Using Equation 4.1 we have superimposed the diurnal evolution of the UHI (gray bars in Figure 4.6) noting that peak intensities occur at 1300L, preceding the diurnal temperature peak by 1 hour. Further insight into the spatial extent and timing of the UHI can be gained through examination of the gridded temperature
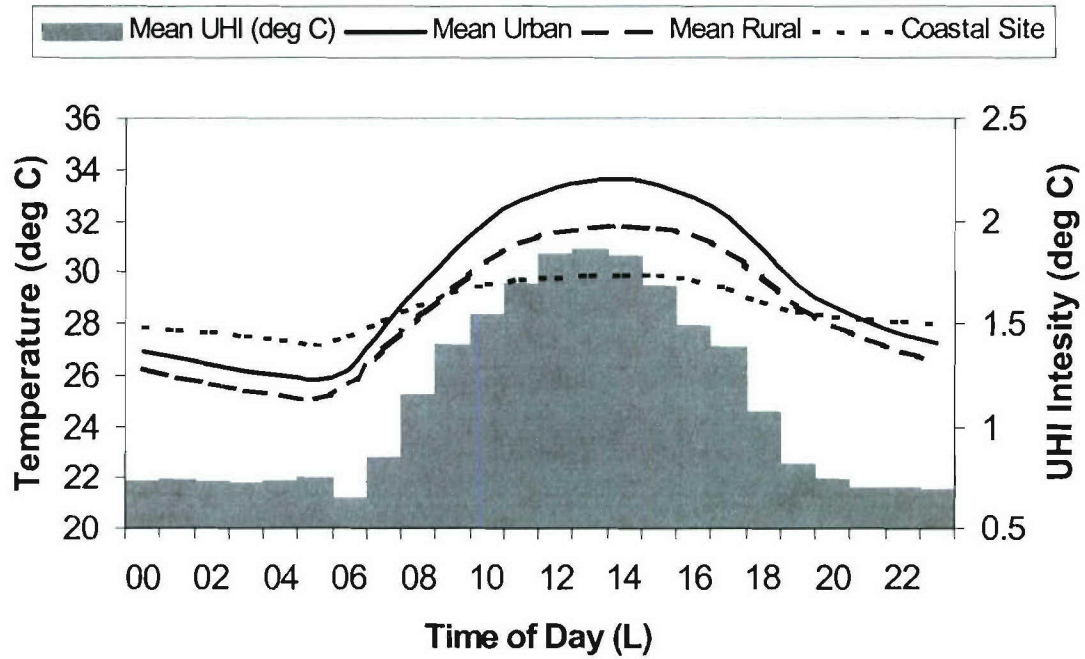
Figure 4.6 Diurnal time-series of mean hourly temperatures for urban (solid), rural (dashed) and coastal (dotted) sites, left ordinate superimposed upon the diurnal evolution of the UHI (gray bars, right ordinate) based on Equation 4.1.

fields described in Section 4.2.2.1. Here we have chosen to graphically represent the

UHI in terms of a thermal anomaly with the mean hourly temperatures at each pixel

(T_{pixel}) being reduced by the mean domain temperature (T_{domain}) for the same period

(i.e., $T_{pixel} - T_{domain}$). Figures 4.7a-d presents the diurnal evolution (00, 06, 12 and 18L,

respectively) of the gridded thermal anomaly field. At local midnight (Figure 9a) we see

that temperatures over the Houston area are centered on the domain mean, with cooler

temperatures (as much as 2.8° C) to north and south of the city. Here, we also see the

modulating influence of the warm Gulf waters, with temperatures at coastal locations

being the warmest throughout the domain. Nocturnal cooling continues, as evident in

Figure 4.7b where we see a general intensification in the features described during the

previous 6 hours. With the beginning of the diurnal heating cycle we see inland
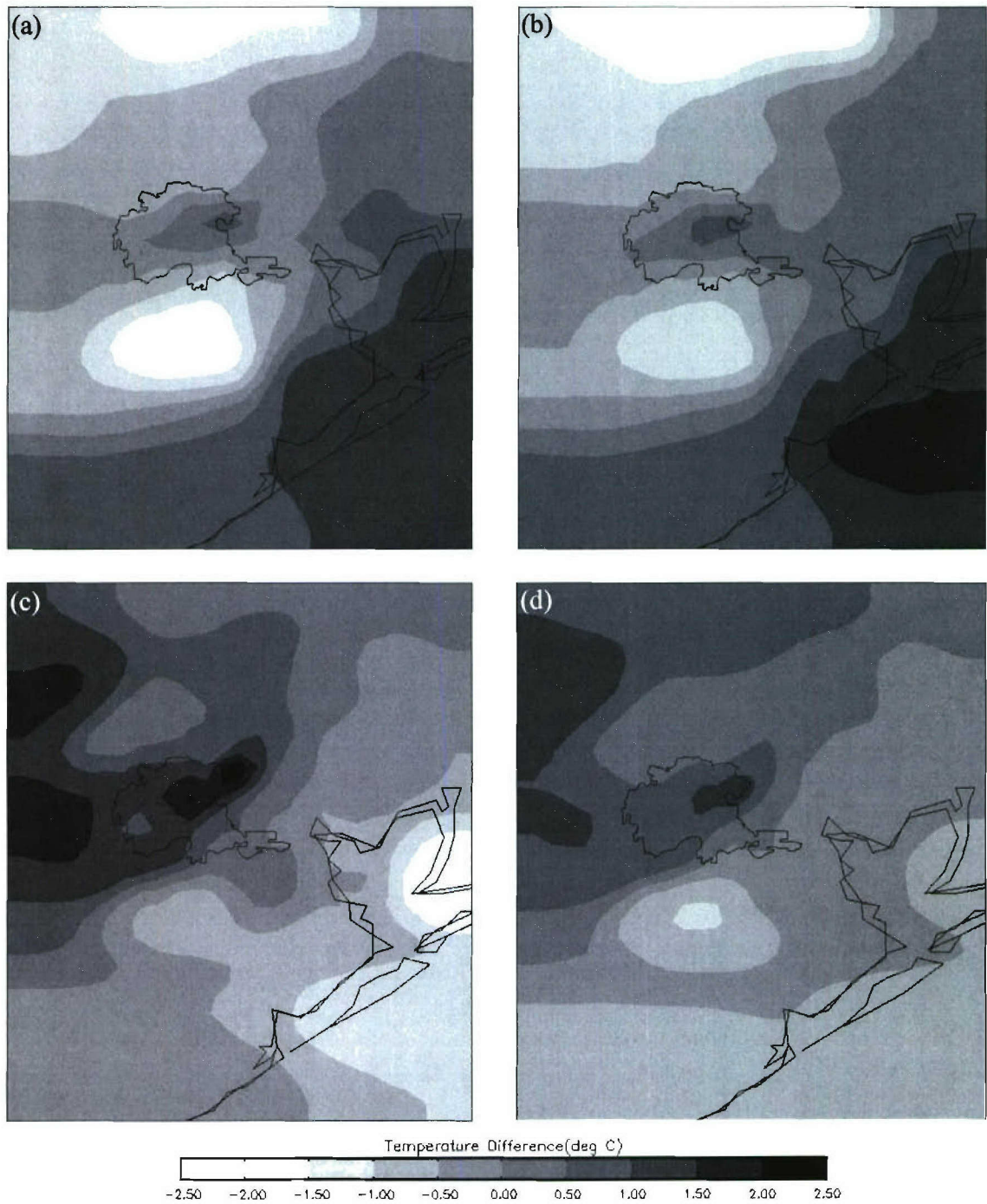
Figure 4.7 Spatial distribution of the mean hourly thermal anomaly fields valid
(a) 0000L, (b) 0600L, (c) 1200L and (d) 1800L.

temperatures quickly increase such that by local noon (Figure 4.7c) we see a definite warm thermal anomaly situated over the north central portions of the Houston domain, with modulated coastal temperatures to the southeast. The relative intensity of this strong thermal anomaly increases, with persistent spatial extent, until approximately 1500L at which time a gradual cooling begins to take place associated with the diurnal heating cycle. 1800L (Figure 4.7d) marks the transition to the nocturnal regime with inland temperatures decreasing much more rapidly than the more consistent water temperatures.

The results of this portion of the analysis clearly establish the presence of a persistent thermal anomaly (i.e., an urban heat island) situated over the northern central portions of the Houston metropolitan area. The fact that peak afternoon values of this thermal anomaly are nearly coincident, in both timing and spatial distribution, with the peak in hourly ground flash densities suggests, as hypothesized, that influences associated with UHI related forcing (in this case thermodynamics) may be related to the CG maximum, presumably through the destabilization of the atmosphere. These *observations suggest the existence of the climatological "forcing-response" relationship* previously hypothesized between these two parameters. Next we will establish a similar type of relationship between the diurnal evolution of the surface winds and these two parameters.

4.3.1.2 Surface Winds & Convergence – Establishing Sea Breeze/Convergence Climatologies

As with the previous two sections, we begin our look at the surface winds with diurnal time-series of both wind speed and wind direction (Figure 4.8). For clarity, we

have chosen to present the evolution of the mean wind vectors in the vicinity of those CAMS sites used in the sea breeze classification algorithm (i.e., those used in the quantification of F4, described in Section 4.2.3.2). Noteworthy features in this figure are as follows: (1) coastal winds (bottom) remain the strongest throughout the entire time period, with progressively decreasing intensities further inland (middle and upper) – at all sites weakest winds are observed just prior to sunrise; (2) a marked wind shift is evident during the mid-morning hours at all locations, with an increased cross-coastal component further inland (i.e., Inland-2; top) lagging those observed at more coastal locations (i.e., Inland-1; middle and Coastal; bottom) by 1-2 hours; (3) at all locations, peak winds appear to occur near the time of greatest (directional) onshore flow, relative to each location, indicative of the passage of the SBF – first at coastal locations followed by inland locations with an inland propagation speed of approximately 30 km hr^{-1}. When comparing the evolution of the diurnal winds (Figure 4.8) with the evolution of the UHI (Figure 4.6), the possibility of a secondary responsive relationship begins to emerge, with surface winds appearing to respond to the diurnal heating cycle. Most notably, the morning increase in wind speeds, and subsequent increase in cross-coastal flow coincide with the beginning of the daily heating cycle, with peak southerly flow at inland locations lagging peak UHI intensities by approximately 3-4 hours.

Spatially, the diurnal evolution of the mean gridded components of the wind field, are presented in Figures 4.9a-d in the form of scaled wind vectors overlaid upon contours of vector-based convergence; for clarity, the 3.5 m/s contour is outlined in pink – subsequent references to this contour will be as "stronger winds." We begin our discussion at local midnight (see Figure 4.9a), where we see predominantly southerly
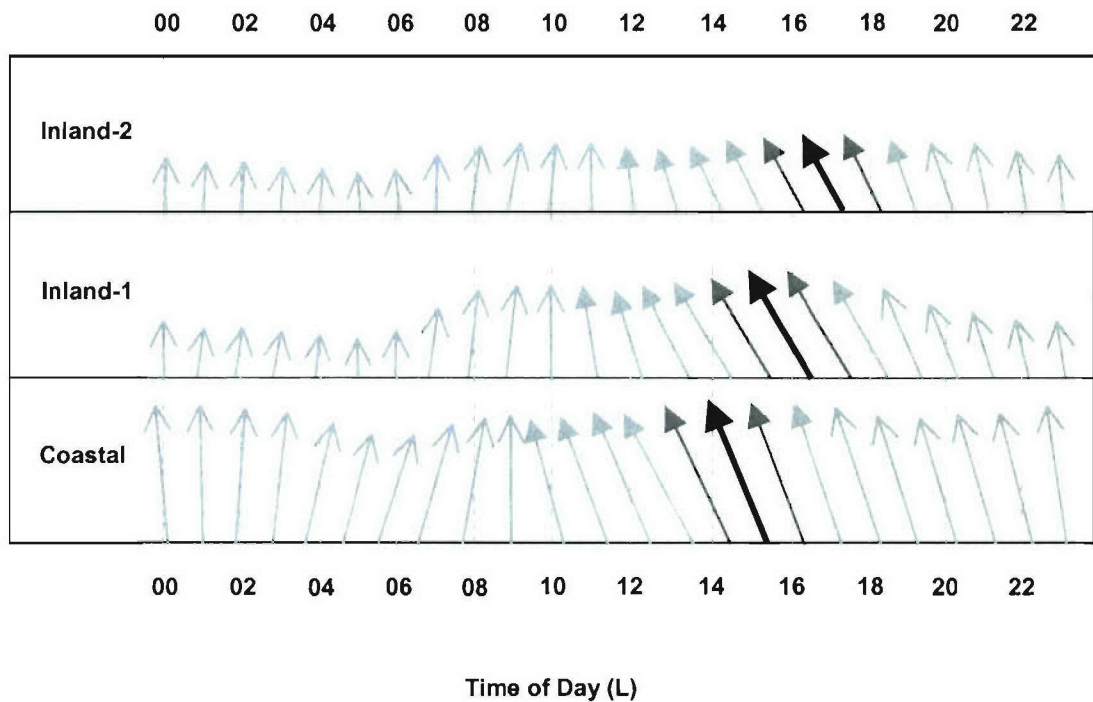
Figure 4.8 Diurnal evolution of mean wind vectors at coastal (CAMS site 8), and inland location (Inland-1: mean of CAMS sites 7 and 10; Inland-2: mean of CAMS sites 1 and 6). All wind vectors are scaled to the maximum mean wind occurring at these locations, corresponding to 5 m/s occurring at the coastal site at 1500L. Further, a change from open arrows to closed arrows indicates the onset of increasing cross-coastal wind flow with black arrows denoting peak onshore flow (both direction and magnitude); the directional transition from peak onshore component is denoted by a return to open arrows.
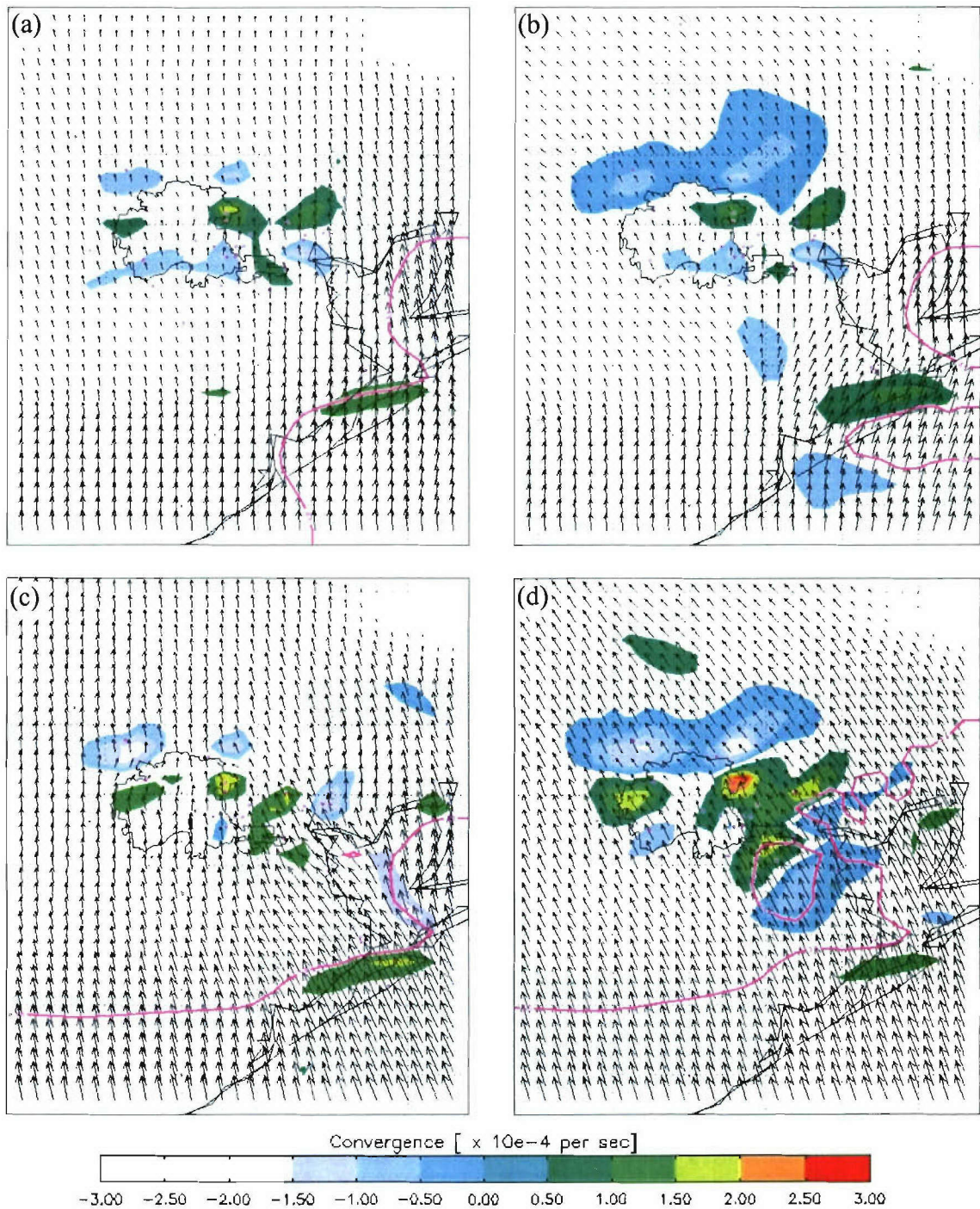
Figure 4.9 Spatial distribution of the mean components of the horizontal wind (vectors, scaled to panel maximum value) overlaid upon color filled contours of kinematically calculated convergence valid (a) 0000L, (b) 0600L, (c) 1200L and (d) 1800L; for clarity, "stronger winds" denoted by the location of the 3.5 m s^{-1} contour is outlined in pink.

flow throughout the domain with stronger winds confined to offshore coastal locations and an area of convergence located over the northern central portions of the Houston metropolitan area (coincident with the location of the peak thermal anomaly over Houston at this same time). Six hours later (Figure 4.9b), we see a clockwise rotation of the winds near the coast associated with the nocturnal portion of the sea breeze circulation, as surface winds respond to the warmer temperatures over the Gulf of Mexico. This clockwise progression ceases with the onset of the diurnal heating cycle (approximately 0700L), as flow returns to predominantly southerly by 0900L. We note that the presence of strong winds remain confined to coastal locations, with variable (weaker) inland winds continuing to create areas of localized convergence over northern Houston. By 1000L (not shown) a distinct (approximately $30°$) shift in the surface winds occurs over Galveston Bay with winds quickly backing southeasterly, likely in response to rapid warming occurring over the city at this time. By local noon (Figure 4.9c), strong evidence suggests a sea breeze type flow is in effect, coincident in timing with the warm thermal anomaly presented in Figure 4.7c. By this time, we begin to notice a finger of stronger winds beginning to encroach upon the eastern confines of the Houston metropolitan area with intensifying areas of convergence associated with the inland progression of the sea breeze front, nearly collocated with the area of enhanced flash densities shown in Figure 4.5e, 1 hour later. By 1400L (not shown) we see predominantly southeasterly flow throughout the majority of the domain with strong winds well inland, beginning to enter the extreme eastern boundaries of the Houston metropolitan area. Although widespread convergence appears to be present along the "strong wind" contour, we see a definite area of localized convergence downstream near

the area of localized heating presented in the UHI climatology. The maximum inland

extent of the strong winds (and associated convergence maximum) occurs at 1700L, with

a weakening of the flow evident one hour later at 1800L (Figure 4.9d). Beyond this

timeframe surface winds continue to weaken as they slowly transition to more of a

nighttime regime with a decrease in the onshore cross-coastal component of the wind.

Coupled with the results of the previous section, it appears that from a

climatological sense urban heat island thermodynamics not only provide a more

favorable environment for convection over the Houston area, but that the *UHI should act

to enhance the inland progression of the sea-breeze*. An enhancement of this nature may

possibly enhance the area of localized convergence over the northern central portion of

the city (to be further investigated in Chapter 5). These observations support hypotheses

dealing with the UHI and its favorable influence on (1) thermodynamics and (2) SB

convergence.

4.3.1.3 Sulfur-Dioxide (SO_2) – Establishing the Climatology of Area Pollutants

Mean hourly aerosol measurements for all CAMS sites falling within the confines

of Harris County are presented in Figure 4.10. Though not utilized as a tracer in this

study, we present the mean diurnal cycles of both $PM_{2.5}$ (dashed line) in addition to our

SO_2 tracer (solid line) for their common years of observation (2001 – 2003). Although

both aerosols peak in the early to mid-morning hours, a distinct time lag exists between

the peak in mean hourly $PM_{2.5}$ levels at 0600L and the subsequent peak in SO_2 levels

from 09-10L. The fact that both peaks occur during the early morning hours suggests the

possibility of localized enhancements over the Houston area being tied to increased
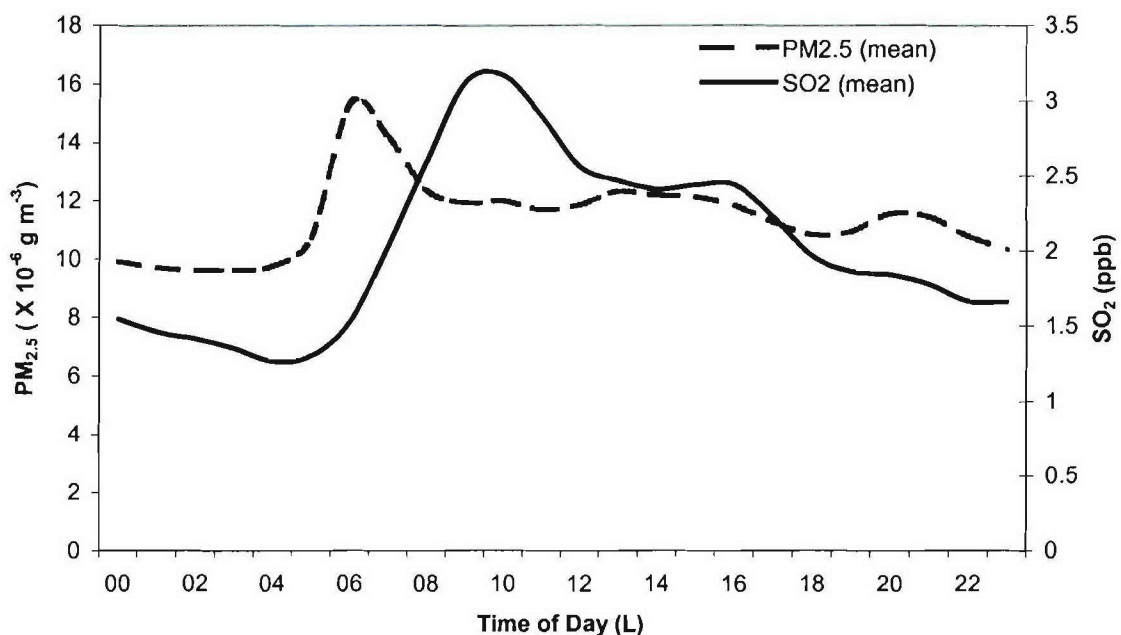
Figure 4.10 Diurnal time-series of mean hourly aerosol concentrations (SO_2, solid line – right ordinate; $PM_{2.5}$, dashed line – left ordinate) for all CAMS sensors located within the confines of Harris County, Texas.

automobile emissions associated with the morning commuter activity coupled with industrial emissions occurring during a time when the stable nocturnal boundary layer has yet to erode. Several processes can be offered to explain the diurnal modulation of climatological pollutant concentrations throughout the domain. First, as the depth of the CBL begins to increase throughout the day, area pollutant concentrations begin to dilute. These arguments are similar to those of Fan et al. [2005] who compared field measurements with simulations of fine particulate matter and its major components during an eight-day episode (24 to 31 August 2000) in Houston. Among their explanations for the high morning peak in pollutant concentrations, they cited high primary emissions and low PBL heights as primary factors, with diurnal evolutions similar to those found in this study. Second, we note SO_2 levels begin to fall off
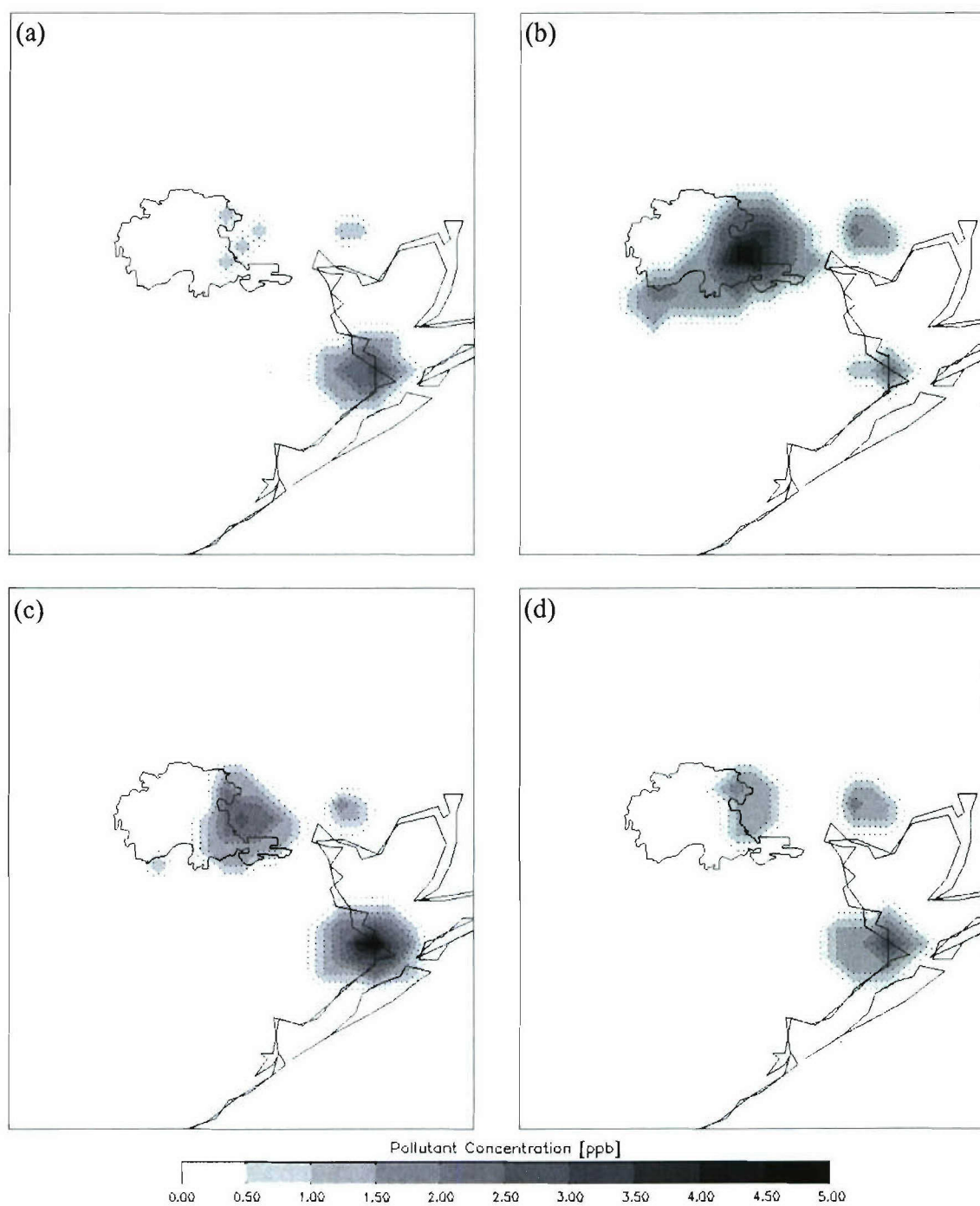
Figure 4.11 Spatial distribution of mean hourly SO$_2$ concentrations valid (a) 0300L, (b) 0900L, (c) 1500L, and (d) 2100L.

beginning at 1100L, around the time of initial sea breeze encroachment upon the city, helping to further dilute the pollutants via physical mixing, with a secondary drop evident in the early evening hours as the land breeze component of the circulation begins to sweep remaining pollutants towards the coast. Finally, precipitation scavenging and PBL venting associated with convective storms serve as aerosol sinks. As previously mentioned, the diurnal peaks in both pollutants, although lagged in time relative to one another, appear spatially consistent, with peak concentrations of both located near the Houston urban center; these results are also in good agreement with the modeling results of Fan et al. As SO_2 is our primary tracer, it is the spatial evolution of this variable that will be presented next.

Figures 4.11a-d present the results of the gridded SO_2 climatology over the entire period of record (1996 – 2003). Beginning at 0300L (Figure 4.11a) we note higher concentrations located near the coast. Nearing sunrise, the coastal enhancement begins to diminish as offshore flow clears the pollutants out of the area. A shallow nocturnal boundary layer, coupled with increased industrial and commuter emissions after sunrise result in enhancements beginning over the Houston metropolitan area with urban maxima evident by mid-morning (see Figure 4.11b; valid 0900L). Although pollutant emissions continue throughout the day, we note that urban concentrations decrease with increased concentrations appearing near the Gulf coast (see Figure 4.11c; valid 1500L). These observations are consistent with previous discussions surrounding the urban heat island. Specifically, that increasing temperatures, particularly over the urban area, lead to a deepening of the boundary layer resulting in a diluting effect on (urban) area pollutants. Cooler coastal temperatures would have a stabilizing effect at coastal locations, resulting

in a shallower CBL with associated increases in coastal pollutant concentrations due to the trapping of increased emissions. By late afternoon the CBL has reached its greatest vertical extent, this coupled with a coincident peak in surface winds (previously discussed) allows for continued mixing and dilution of area pollutant concentrations coupled with convective scavenging, such that by 2100L (Figure 4.11d) pollutant concentrations have been relatively homogenized throughout the domain.

4.3.1.5 Synthesis

Overlaying the various climatologies upon one another provides a useful tool for the identification of potential "forcing-response" relationships that may exist within the long-term mean (i.e., enhanced UHI forcing resulting in the atmospheric response of enhanced CG lightning activity). The results of this effort are presented in a series of spatial composites (Figures 4.12a-e), as well as in the form of a composite time series of mean values observed over the Houston urban area (Figure 4.13). For clarity, in Figure 4.12 we have contoured total hourly flash densities using a grayscale, and have chosen a color scale to represent areas of convergent flow only (i.e., divergence is not presented). Additionally, only wind vectors in excess of 2.5 m s^{-1} have been overlaid, with thermal anomalies contoured in red every 0.5° C beginning at 1.0° C, and mean hourly SO_2 concentrations in blue, every 1 ppb, beginning at 1 ppb.

Throughout the predawn hours, warmer surface temperatures reside over the water with predominantly southerly flow and stronger surface winds located at coastal locations. Additionally, various areas of enhanced convergence, particularly one over north-central Houston are also present, with nominal enhancements in mean SO_2
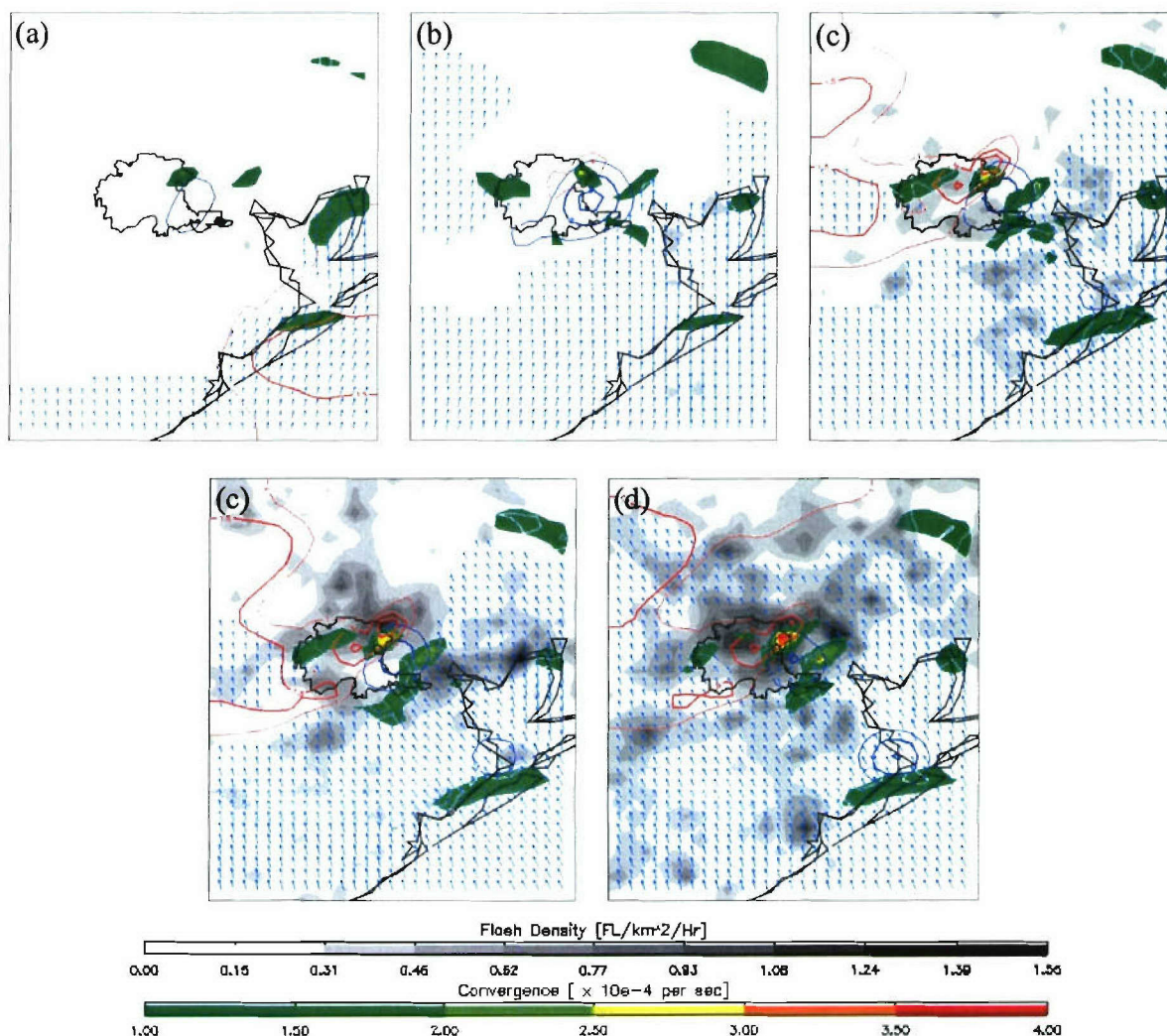
Figure 4.12 Spatial composites of hourly mean climatologies valid (a) 0600 CST, (b) 0900 CST, (c) 1200 CST, (d) 1300 CST and (e) 1500 CST. For clarity, contours of total hourly flash densities are in shades of gray, with a color scale to representing areas of convergent flow only (i.e., divergence is not presented). Additionally, only wind vectors in excess of 2.5 m/s have been overlaid, with thermal anomalies (i.e., mean hourly pixel temperature reduced by the mean hourly temperature of the entire domain) contoured in red every 0.5° C beginning at 1° C, and mean hourly SO_2 concentrations contoured in blue every 1 ppb, beginning at 1 ppb.
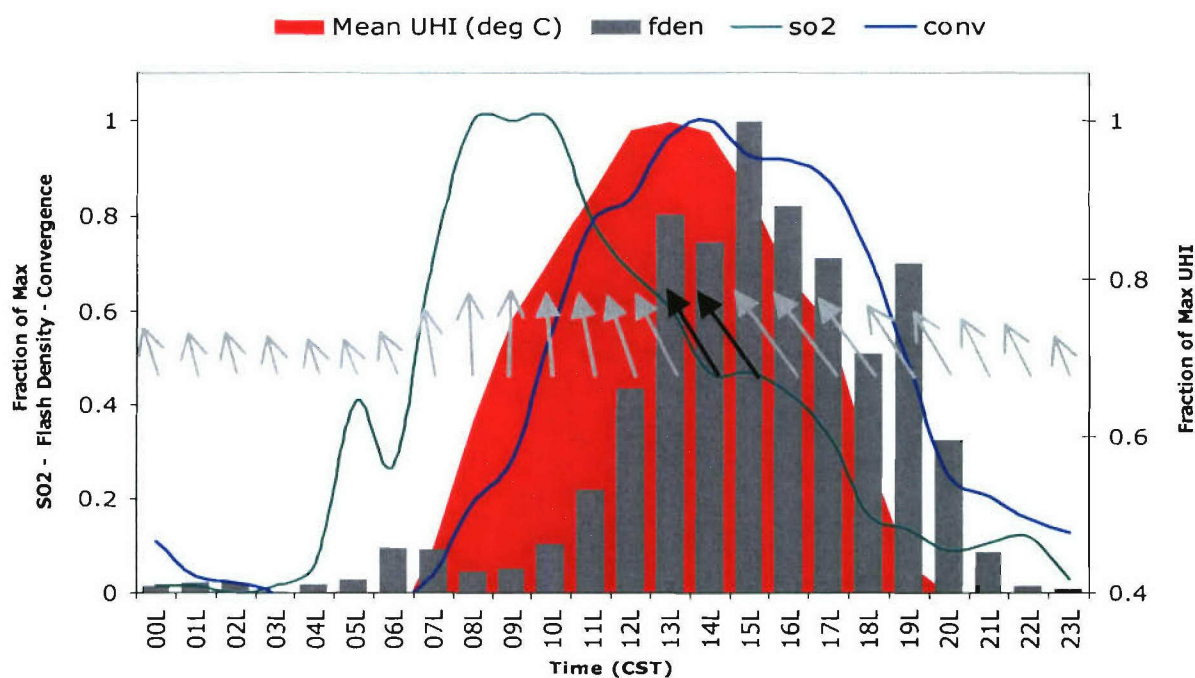
Figure 4.13 Diurnal time-series of the spatial hourly means for the following parameters, each computed over the Houston area and normalized by their respective maximum values: UHI intensity (red shading), scaled mean wind vectors (as in Figure 4.8, relative to the climatological maximum observed at 1500L), mean hourly convergence over the Houston area (blue line), mean hourly SO₂ concentrations (green line) and mean hourly flash densities (fden; gray bars).

concentrations near the mouth of Galveston Bay. As would be expected, climatological lightning activity appears insignificant over land, with only minimal enhancements located near the mouth of Galveston Bay. By 0600L (Figure 4.12a) surface winds have bottomed out throughout the domain, with only a minimal onshore component. At this point, warmer temperatures continue to persist over the water, with no apparent sign of organized lightning activity as of yet. Initial enhancement in pollutant concentrations also becomes apparent over the central portions of the city, likely associated with the onset of commuter activity coupled with industrial emissions occurring during a time when the stable (shallow) nocturnal boundary layer has yet to erode. Following sunrise, the next 3 hours see an increase in surface wind speeds, becoming predominantly southerly, with the beginnings of an enhanced UHI over north-eastern Houston along with peak SO_2 concentrations located over the industrialized portions of the city (see Figure 4.12b; valid 0900L). By local noon (Figure 4.12c) we see that the UHI has expanded over the central portion of the urban domain and has intensified significantly, further enhancing the area of low-level convergence located over the north-eastern portions of the city with aerosol concentrations decreasing, likely due to dilution associated with physical mixing (encroachment of the SB) along with rainout and a deepening of the convective boundary layer. Organized lightning activity becomes apparent along the leading edge of the sea breeze front, still predominantly outside the confines of the city. Figure 4.12d, one hour later, illustrates the atmospheric response to the localized forcing due to the enhanced UHI over the north-central portion of the city. Here the strong UHI contributes to intensifying surface wind convergence while at the same time destabilizing the PBL yielding a strong response in convective activity with

mean hourly flash densities nearing the maximum within the domain during this timeframe. Following this initial pulse in lightning activity at 1300L, convection appears to become more organized, propagating from the northwestern tip of Galveston Bay over the Houston area (particularly the area of the strongest UHI) where it intensifies, followed by a subsequent cessation in activity as it departs the favorable convergence zone (see Figure 4.12e; valid 1500L). By this time we note further decreases in aerosol concentrations over the city, with increases at coastal locations, a testament to our earlier statement where we speculated that continuous emissions throughout the day are diluted over the urban area likely due to precipitation scavenging and rainout processes coupled with a deeper CBL, compared to cooler coastal regions where we would expect a more stable, shallower boundary layer to exist. At this time, the increased surface roughness within the city, associated with the presence of buildings and other structures is also quite apparent, evidenced by the lack of wind vectors in excess of 2.5 m s^{-1} over the city in Figure 4.12e. Subsequent to this timeframe we begin to see a rapid weakening of the thermal forcing (i.e., UHI), with a lag in decreasing wind speeds. Following sunset the area of enhanced convergence over the northern portion of the city weakens rapidly as surface winds begin the transition to the nighttime leg of the sea breeze circulation resulting in a "clearing" of area pollutants.

Complementing this discussion, Figure 4.13 presents a general time series of hourly means of each variable taken over the Houston area. Presented this way, several interrelated relationships begin to emerge. Thermal forcing, manifested in the UHI, which peaks at local noon, occurs nearly coincident with increases in wind speeds, both intensity and onshore component, thereby leading to enhanced convergence over the

Houston metropolitan area (1400L) followed by peak mean hourly flash densities (1500L), the ultimate atmospheric response. The time lag between peaks for each of these variables is suggestive of a physical forcing-response relationship. Another, yet to be explored, relationship may exist between mean hourly SO_2 concentrations over the city and enhanced flash densities. Here, mean hourly flash densities appear to lag peaks in mean hourly SO_2 concentrations by about 5 hours. It is important to note, however, that some, all or none of these hypothesized relationships may prove to be predominant causative mechanisms in explaining the climatological lightning anomaly over the Houston area; these findings will serve as the focus of the selective exclusion analyses that follows.

4.3.2   Apportioning the Cause – Selective Exclusion Filtration

The results of the first portion of this study support the existence of possible climatological "forcing-functions" that may be capable of explaining the observed enhancement in CG lightning activity over the Houston area. What remains is to determine which, if any, of the proposed hypotheses can be deemed a primary causative mechanism, or more likely which, if any, can be eliminated as a predominant contributor. To that end, the second portion of this study focuses on determining the relative contributions that each of the proposed hypotheses have on the Houston CG lightning anomaly through the selective exclusion of relevant subsets of the data.

As previously discussed, SE1 and the first portion of SE2 (F1-4) were utilized to filter and condition the 786 day dataset into 202 distinct non-consecutive days for inter-comparison, each conditioned upon the existence of favorable conditions for the

formation of a sea breeze circulation. Here we examine the results of the application of the remainder of SE2 (identification of SB and noSB days, and subsequent exclusion of noSB days), SE3 (exclusion of enhanced UHI days) and SE4 (exclusion of enhanced AI days) to the conditioned dataset.

4.3.2.1. Initial Investigation - Application of Filters to Sea Breeze Days Only

Given that the FAR associated with the statistical classification of SB days is less than 15%, we have chosen to use the SB portion of the dataset, as classified by SE2, as our initial baseline from which to investigate each of the hypotheses. Eliminating overlapping large AI and UHI days (of which there were only 6) from the 124 days classified as SB days we are left with a dataset of 118 distinct non-consecutive days in which the sea breeze was statistically determined to have occurred. Relative to the 202 possible sea breeze days, the 118 SB days contribute 72% of the mean CG lightning signal over the Houston area.

Although not necessarily the case, our limiting assumption is that the three hypotheses under investigation are the only three forcing-functions under consideration (i.e., that 100% of the lightning can be explained by the sum of the contributions made by each of the three hypotheses). As our primary metric will be the change in mean flash densities over the Houston area, we will establish our comparative baseline as the mean flash density associated with SB days (averaged over the black box in Figure 4.14a), specifically, 1.51 flashes km^{-2} summer^{-1}.

Of the 118 SB days, there were 71 days in which the SB was isolated such that it was the only dominant "forcing function" present on those days (i.e., they were neither
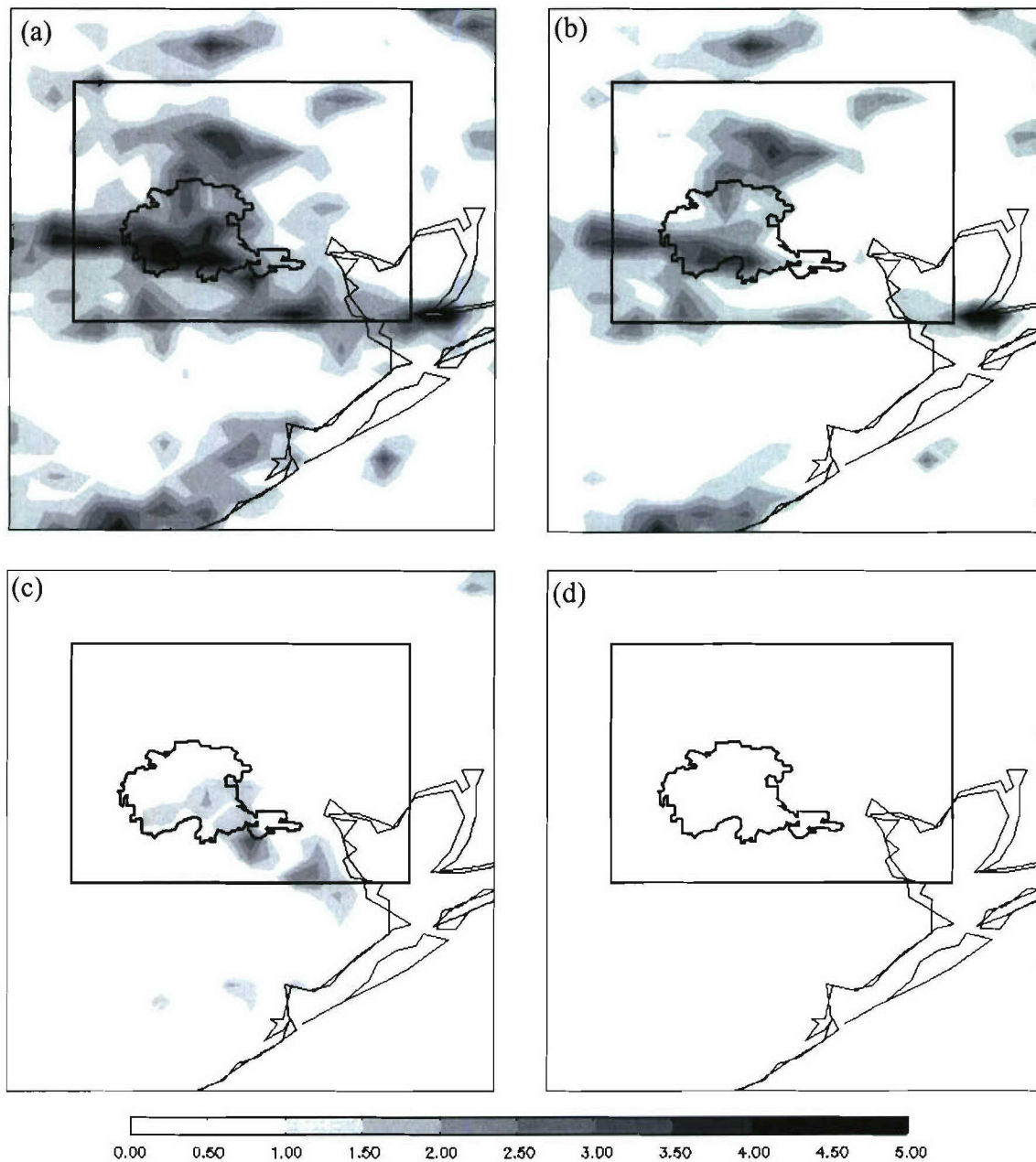
Figure 4.14 Spatial variations of mean flash density (valid 0900-1859 CST) for (a) 118 non-contiguous SB days resulting from the application of SE1 and SE2, (b) 71 days in which the SB was isolated as the dominant "forcing function", (c) 25 days in which an enhanced UHI was isolated as the dominant forcing and (d) 22 days in which enhanced aerosol concentrations were isolated as the dominant forcing. NOTE: contour shading in all panels are normalized to the 118 days presented in panel (a).

classified as enhanced UHI nor enhanced AI by SE3 and SE4, respectively). Reconstructing the lightning climatology for these days yields a mean decrease in flash densities over the Houston area of 32%, indicating that relative to the 118 SB days, *68% of the mean lightning signal over the Houston area occurs on these isolated SB days*; spatially, Figure 4.14b shows largest contributions just north of the northern periphery of the city as well as along the southern boundary.

Isolation of large UHI and AI days from this dataset was accomplished by subtracting the lightning contribution due to SB days from the lightning contributions due to large UHI days (93 days) and large AI days (96 days), respectively. Once isolated, *25 large UHI days contribute 27%* of the mean flash densities over the Houston area while 22 *large AI days contribute only 5%* (see Table 4.1 for summary; mean flash density metrics are all statistically significant, at p-values < 0.05). Spatially, enhanced UHI days exhibit their largest influence on CG lightning along the southeastern edge of the city (see Figure 4.14c), coincident with the area if initial convergence and convection discussed in Section 4.3.1.3 as well as in the vicinity of the warm thermal anomaly identified in Section 4.3.1.2. Relative to the Houston metropolitan area, CG flashes occurring on enhanced AI days appear to have a minimal influence on the predominant areas of enhancement present in Figure 4.14a. Here, Figure 4.14d shows largest contributions to be off of the northwestern tip of Galveston bay; however, overall mean flash densities associated with these contributions are on the low end, relative to other spatial maximums.

Given the limiting assumption that the three hypotheses under investigation are the only three "forcing functions" under consideration, it is clear that the primary forcing

associated with ground flash densities located over the Houston area (as constructed from

the 118 day climatology) is that of the sea breeze, and/or enhancements thereof.

Table 4.1 Mean flash densities associated with each set of isolated days, along with
their relative contributions to the total flash densities (percentages) for each metric box.

	Sea Breeze Days	Synoptically Conditioned Days	
	Houston Box	Houston Box	"Anomaly" Box
Total Days	118	336	336
Mean Flash Density (FDEN; flashes km^{-2} $summer^{-1}$)	1.51	1.88	2.49
Number of Isolated Non-Enhanced Days	N/A	169	169
Mean FDEN (flashes km^{-2} $summer^{-1}$)	N/A	0.98	1.52
Mean Contribution to FDEN over Houston	N/A	52%	61%
Number of Isolated Sea Breeze Days	71	62	62
Mean FDEN (flashes km^{-2} $summer^{-1}$)	1.02	0.33	0.31
Mean Contribution to FDEN over Houston	68%	18%	12%
Number of Isolated Enhanced UHI Days	25	57	57
Mean FDEN (flashes km^{-2} $summer^{-1}$)	0.41	0.46	0.49
Mean Contribution to FDEN over Houston	27%	25%	20%
Number of Isolated Enhanced AI Days	22	48	48
Mean FDEN (flashes km^{-2} $summer^{-1}$)	0.08	0.11	0.17
Mean Contribution to FDEN over Houston	5%	6%	7%

4.3.2.2. Expanding the Dataset - Application of Filters to Synoptically Conditioned Days

Although the metrics presented in the previous section are all statistically

significant, the sample size under consideration is arguably rather small, at least in the

case of isolated enhanced UHI and AI days (25 and 22 days, respectively). Additionally,

due to the exclusion of associated event days, several key spatial features present in the

486 day common dataset (with large event days removed, see Figure 4.2c) were missing

in the further conditioned 118 day dataset (Figure 4.14a): namely (1) the area of enhanced flash densities over, not just northward, of the northern periphery of the city, and (2) the finger of enhanced flash densities extending to the east-northeast from the urban center towards and north of Galveston Bay. In order to address both of these issues, an expanded analysis was performed using a slightly less restrictive initial conditioning. Particularly, the new baseline under investigation is that linked with the mean flash densities associated with non-overlapping days (i.e., days in which each of the hypothesized forcings were isolated from one another) in which synoptic conditions were favorable for the formation of a sea breeze circulation, disregarding the requirement for thermal support (F4) used in the previous analysis (i.e., SE1 and SE2, F1 through F3). The results of this less restrictive conditioning is a dataset consisting of 336 distinct, non-consecutive days in which synoptic conditions were favorable for the formation of a sea breeze circulation. Examination of Figure 4.15a, reveals the reemergence of key spatial features previously omitted from the 118 day dataset, indicating that our new starting point is more representative of the long term record. The increased size of this particular dataset enables us to perform a slightly different form of comparison; therefore, for this expanded dataset, Table 4.1 (see last two columns) will also track changes in the mean flash density over the Houston "anomaly" box, centered on the new features outlined above (smaller white box in Figure 4.15); our new baseline metrics then become 1.88 and 2.49 flashes km^{-2} $summer^{-1}$ for the Houston and "anomaly" boxes, respectively.

Examining the results of the application of the remainder of SE2 (identification of SB and noSB), SE3 (exclusion of enhanced UHI days) and SE4 (exclusion of enhanced AI days) to the conditioned dataset, there were a total of 169 days that were not
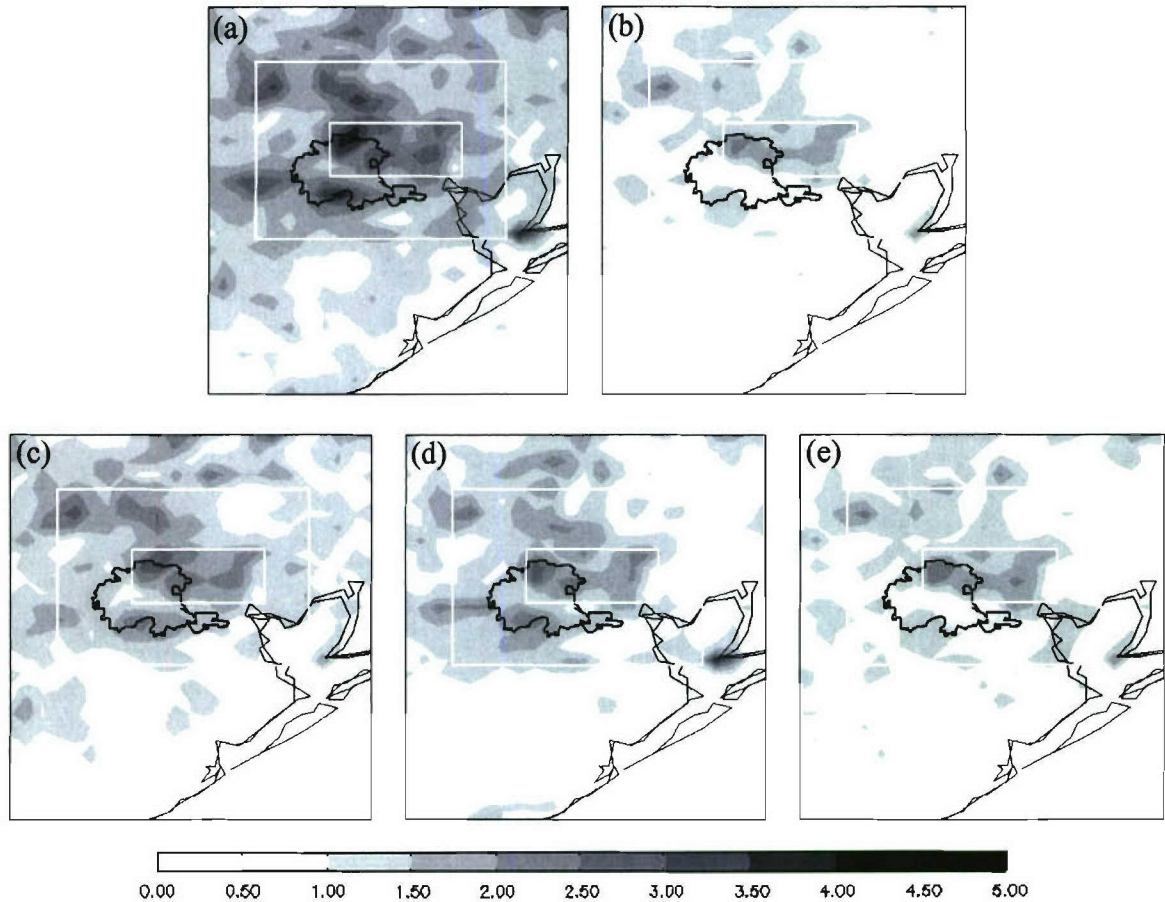
Figure 4.15 Spatial variations of mean flash density (valid 0900-1859 CST) for (a) 336 non-contiguous days resulting from the application of SE1 and the first half of SE2, (b) 169 non-enhanced days (following application of SE1-4, as is the case for panels c-e, (c) 169 non-enhanced days plus 57 enhanced UHI days, (d) 169 non-enhanced days plus 62 sea breeze days and (e) 169 non-enhanced days plus 48 enhanced AI days. NOTE: contour shading in all panels are normalized to the 336 days presented in panel (a).

dominantly influenced by any of the defined forcing-functions – these days comprise the background value, to which each of the isolated forcing-functions will be added to examine how they particularly enhance the spatial flash density distributions. The new dataset is comprised of the following isolated days with associated contributions to the mean flash density metrics just described (the sum of which construct the climatology presented in Figure 4.15a; summarized in Table 4.1), contributions to the "anomaly" box are presented in parentheses: 169 non-enhanced days contributing 52% of the total CG lightning over Houston (61% over the anomaly box), followed by 57 enhanced UHI days contributing 25% (20%) of the mean, 62 SB days contributing 18% (13%), with 48 enhanced AI day providing the remaining 6% (7%) of the mean flash densities over Houston.

Spatially, the 169 non-enhanced days comprising the background provide the foundation for areas of enhanced flash densities over the northern periphery of the city (on the order of 50-60% of the total mean), and a finger of enhanced flash densities extending ENE from northeastern boundaries of the urban area (60-70% of the mean) and to a lesser extent an area of activity along the central southern boundary of the city (Figure 4.15b). Absent the hypothesized forcing-functions, we conclude the presence of these features to be associated with "typical" convective storms driven by (1) normal diurnal forcing (i.e., the presence of a "typical" UHI over the north central portions of the city giving rise to an area of preferred convective initiation and/or enhancement) and (2) local topography, as opposed storms occurring on days in which enhanced forcing is present. That is not to say that the intensity of these features is not strengthened through enhanced forcing, rather *the presence of these key features cannot be directly attributed*

to the hypotheses under investigation. Regarding local topography, given a regional map, as in Figure 2.2, it is clear that the topography to the north and west of Galveston Bay is quite complex, with various fingers of Gulf water extending inland in differing directions. This coupled with the proximity of inland lakes and reservoirs, namely Lake Houston approximately 16 km north of the northwestern tip of Galveston Bay (and to a lesser extent Sheldon Reservoir 12 km to the northwest, not depicted in Figure 2.2) provides for a favorable environment of convergence associated with interacting bay and lake breezes consistent with the locations of the observed flash density enhancements to the east-northeast of the city center. Additionally, this area is primarily classified as that of forest and grassland allowing for a greater latent heat flux, relative to the asphalt coated urban areas.

Overall, enhanced UHI days contribute 25% of the mean flash density over the Houston area, with peak enhancements over the central northern and southern boundaries of the city (Figure 4.15c; background plus UHI). The result of allowing days in which the SB is active to be included in the analysis, is to primarily enhance the features identified in the background, while contributing upwards of 50% of the lightning surrounding the area of enhanced flash densities extending westward from the southwestern portion of the city (Figure 4.15d; background plus SB). Isolating enhanced aerosol days, we found that the *overall contributions of enhanced SO_2 days on the mean flash densities over Houston to be minimal at best* with mean enhancements over the "anomaly" area of approximately 7% (Figure 15e; background plus AI).

Based upon the analyses conducted herein, we present the following summary observations:

- Enhanced pollution levels do not appear to have a significant effect on flash densities over the Houston area (i.e., *the results do not support the aerosol hypothesis*).

- Devoid of additional forcing offered by the hypotheses under investigation, certain spatial features persist within the climatology suggesting that the *presence of the enhanced flash densities over and northeast (i.e., downwind) of Houston are the result of "normal" convective activity tied to areas of preferred convection and local topography, and not the result of extreme anthropogenic enhancements.*

- UHI and SB forcing contribute relatively the same amount to the mean flash densities over the Houston area, both tending to enhance the persistent features present in the background climatology on the northeast side of the city (i.e., *support for hypotheses dealing with the UHI and its favorable impacts on organizing and intensifying convection*).

4.3.3   Diagnosing Climatological Differences in Convective Structure

Thus far, the results of the component climatologies (Section 4.3.1) and selective exclusion analyses (Section 4.3.2) substantiate the existence of physical forcing-response relationships consistent with the observed CG lightning anomaly, with the Houston area typically being associated with an area of enhanced low-level convergence, particularly during days in which an enhanced UHI is present. As discussed in Appendix B, the intermediate requirement linking the forcing-functions investigated in this study to the lightning anomaly is the enhancement of precipitation sized ice particles within the

charging-zone (climatologically between 7 km and 11 km altitude, based on

NCEP/NCAR reanalysis). Therefore, we would expect to observe enhancements in

precipitation ice (manifested in radar reflectivity data) consistent with the climatological

lightning anomaly resulting from the enhancements attributed to each of the hypotheses

under investigation. Through the use of contoured frequency by altitude diagrams

(CFADs; [Yuter and Houze, 1995]), this section provides quantitative statements

pertaining to convective structure relative to each forcing-function, particularly regarding

differences in upper-level structure conducive to NIC. Using over 24,000 daytime

volumes (0900 – 1859 CST) of convective WSR-88D radar data (detailed in

Appendix B), we statistically examine the salient differences in vertical structure of

convection over the Houston area from both spatial (i.e., Houston relative to

surroundings; see Figure 4.16a for location of analysis areas) and forcing (i.e., UHI

relative to background, etc.) perspectives. Here, the hypothesis being that the

climatological forcing-function(s) having the greatest impact on the magnitude of the

lightning anomaly should also have the greatest enhancement in radar reflectivities within

the climatological charging zone.

The CFAD is a convenient way to display multiple histograms in a two-

dimensional format. At each height the CFAD displays the relative frequency of

occurrence of a given parameter, in this case radar reflectivity. As a basic illustration of

the utility, and interpretation of CFADs, Figures 4.16b-d present climatological CFADs

comparing 14,214 VCP-11 radar volumes gathered during 145 lightning days (LTG;

Figure 4.16b) and 9,819 VCP-11 volumes collected during 117 non-lightning days
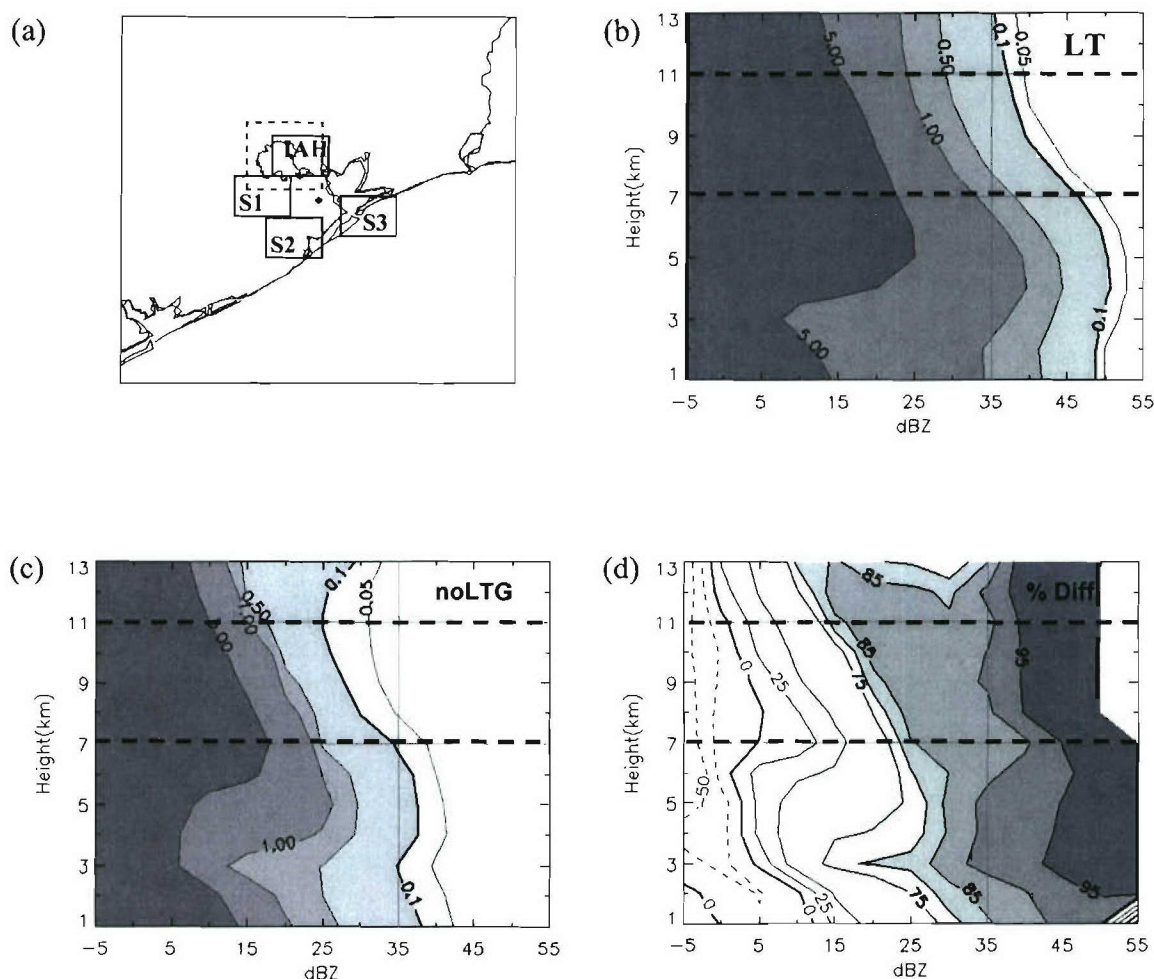
Figure 4.16 (a) Locations of analysis areas from which 24,033 individual radar volumes (valid 0900 – 1859 CST) were used to construct mean CFADS of radar reflectivity; solid boxes depict locations used in the spatial analysis (Section 4.3.3.1), while the dashed box represents the location used in the forcing analysis (Section 4.3.3.2). Mean CFADs of radar reflectivity associated with (b) 14,214 convective volumes gathered during 145 lightning days (LTG) and (c) 9,819 volumes gathered during 117 non-lightning days (noLTG), bother over the Houston area (dashed box) with shaded contours increasing in darkness at 0.05, 0.1, 0.5, 1.0 and 5.0% relative frequency of occurrence for each; for reference, the 0.1% relative frequency of occurrence contour is bold, with horizontal dashed lines denote the top and bottom of the climatological charging zone. Panel (d) presents the percent difference between the LTG and noLTG CFADS; bold contour denotes the transition from negative (dashed lines) percent differences to positive (solid lines) percent differences.

(noLTG; Figure 4.16c) over the Houston metropolitan area (see larger dashed box in Figure 4.16a), with Figure 4.16d, presenting the percent difference between the LTG and noLTG CFADs (i.e., [LTG-noLTG]/LTG). Comparison of LTG and noLTG CFAD's (Figures 4.16b and 4.16c) shows that LTG days have significantly higher frequencies of occurrence of intense echo features throughout the depth of the troposphere, particularly within the climatological charging zone (depicted by horizontal dashed lines). For example, in the convective region the height at which the probability of occurrence of 35 dBZ echo falls below 0.1% is above 11 km for the LTG days compared to 7 km (the base of the charging zone) for the noLTG days (compare bold contours in Figures 4.16b and 4.16c). These results are in excellent agreement with numerous observational studies [e.g., Workman and Reynolds, 1949; Shackford, 1960; Goodman et al., 1988; Williams et al., 1989; Carey and Rutledge, 1996, 2000; Vincent and Carey, 2003 among others] whose conclusive findings demonstrate the relationship between the presence of enhanced values of radar reflectivity in the mixed-phase (charging) zone (a proxy for the presence of graupel/hail) and subsequent electrification and lightning. Examining the percent difference between lightning and non-lightning day CFADs (Figure 4.16d), we see that the mean probability of a 35 dBZ radar echo being present between 7 and 11 km is roughly 90% greater on lightning days, compared to non-lightning days. This striking difference is consistent with the physical forcing-response relationship highlighted in Appendix B, where we identified a strong correlation between precipitation sized ice mass in the charging zone and the occurrence of CG lightning, consistent with NIC.

The appearance of enhanced reflectivities in the charging zone present in the LTG profile, preserved after extensive data processing and combining (all VCP-11 volumes

from 0900 – 1859 CST on each lightning day were used to create the composite) is a strong indicator that the CFAD is a reliable way to represent this structure in a summary fashion. When comparing multiple CFADs to one another (as will follow), the development of a comparative metric allows for the quantitative comparison of relevant features. As it pertains to the NIC mechanism, we have chosen to compare the mean probability of 35 dBZ occurring within the charging zone (P35) as our primary means of evaluating the convective vigor for each of the scenarios to be investigated, with larger P35 values indicative of enhanced probabilities of lightning; the fractional change of this metric will also be presented relative to various baselines.

4.3.3.1 Spatial Differences

As the Houston ground flash density anomaly is a spatially unique feature, relative to its *immediate surroundings*, we would expect to see spatial differences in convective structure as well, with the Houston area having enhanced P35 values, relative to its surroundings. Here, climatological CFADs encompassing four geographically similar sub-domains (all similar relative to the location of the radar) were generated using all 262 days described above (145 LTG + 117 noLTG; see boxes labeled IAH, S1, S2 and S3 in Figure 4.16a). Shown in Figure 4.17a-d (summarized in Table 4.2) are the radar reflectivity CFADs for each sub-domain; for ease of comparison, note that the 0.5% contour is bold in Figures 4.17a-d and that the 0.5% contour from Figure 4.17a associated with the IAH CFAD has been overlaid on Figures 4.17b-d in the form of a dashed white line. As expected, relative to the Houston area, radar echoes observed in other sub-domains have decreased probabilities of having reflectivities of 35 dBZ located

in the charging zone (P35 = 0.30, 0.22, 0.21 and 0.15% for IAH, S1, S2 and S3,

respectively) with echoes observed over the water (S3) having the greatest fractional

decrease in mean probabilities (54%). Although extensions of these metrics to the NIC

mechanism do not necessarily mean that the Houston area has a greater probability of

enhanced CG lightning activity that is equal to the fractional change presented in

Table 4.2 (i.e., 54% in comparison to S3), they do imply proportionally greater

probabilities of enhanced charging, possibly leading to enhancements in CG lightning;

that is to say that of the four sub-domains examined, the Houston area is most likely to

have enhanced flash densities, with areas S1 and S2 having greater probabilities of

enhancements relative to S3.

Table 4.2 CFAD summary statistics (spatial analysis), see Figure 4.16a for box locations.

Analysis Box	P35 [%]	% Difference in P35 Relative to IAH Box
IAH	0.30	
S1	0.22	34%
S2	0.21	32%
S3	0.18	54%

4.3.3.1 Forcing Differences

As the statistical algorithms used to partition each day into its appropriate forcing

type were unique to the Houston area, we are unable to compare differences between

forcing days for domains other than that of the primary Houston area (larger dashed box

in Figure 4.16a). As presented above, Figure 4.18a-d present the radar reflectivity

CFADs for each set of isolated forcing days taken over the primary Houston sub-domain,
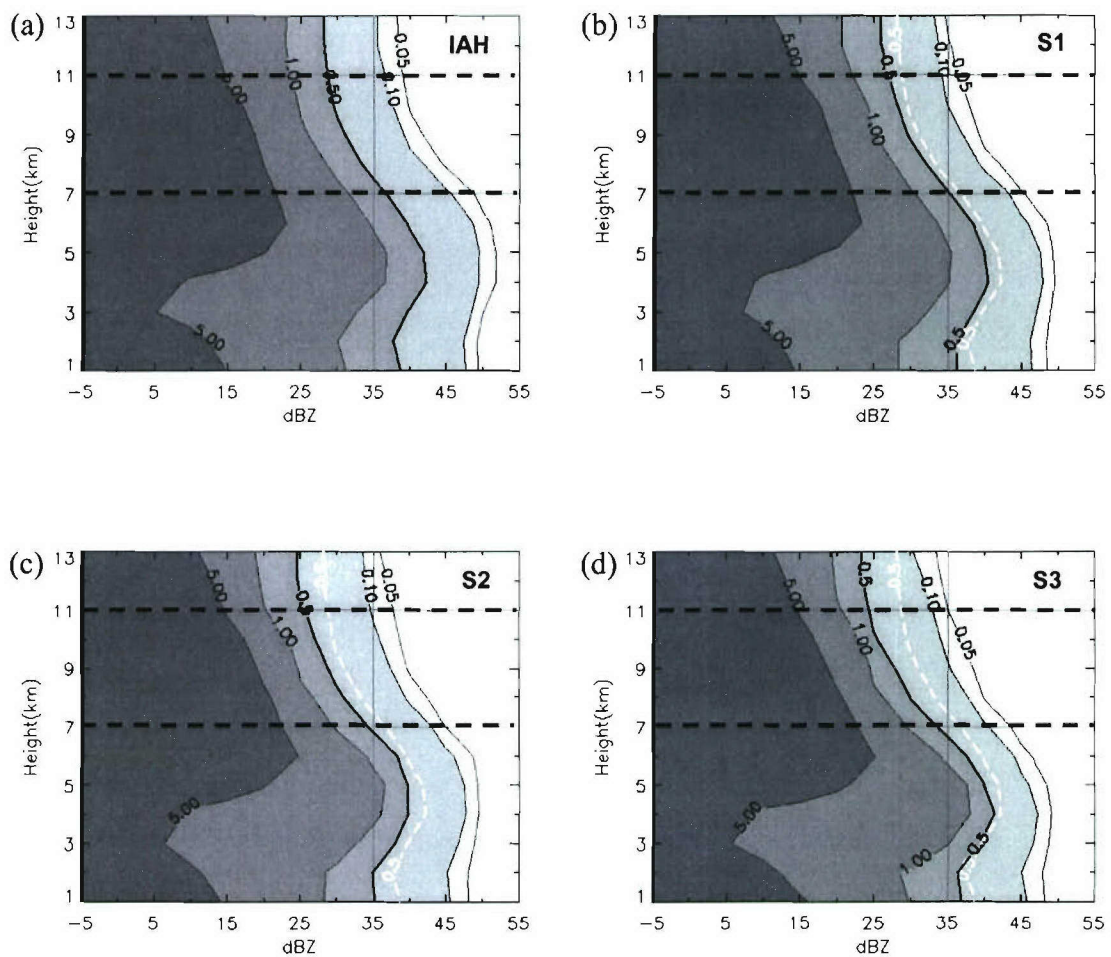
Figure 4.17 As in Figures 4.16b-c, mean CFADS of radar reflectivity for all 262 days (24,033 convective radar volumes; valid 0900 – 1859 CST) for the (a) IAH, (b) S1, (c) S2 and (d) S3 analysis areas depicted in Figure 4.16a; for reference, the 0.5% relative frequency of occurrence contour is bold, with the 0.5% contour in panel (a) overlaid in white (dashed) on panels b-d.

with Table 4.3 providing a summary of the metric statistics for each forcing-function; again for clarity the 0.5% contour has been highlighted in Figures 4.18a-d, with the 0.5% contour from Figure 4.18a being overlaid on Figures 4.18b-d in the form of a dashed white line. Comparison of the CFADs presented in Figure 4.18a-d reveals a great degree of similarity between the CFADs associated with non-enhanced ("background") days (Figure 4.18a) and isolated sea breeze days (Figure 4.18b), with P35 = 0.27% and 0.30%, respectively. Although not shown, it is noteworthy to mention that these CFADs are also very similar to the overall mean CFAD (i.e., all 262 days) with P35 = 0.31%. These similarities, however, do not hold when examining CFADs associated with enhanced UHI and aerosol days (Figures 4.18c and 4.18d, respectively). With a broader CFAD at higher altitudes, the mean probability of 35 dBZ in the charging zone is 196% greater on enhanced UHI days, relative to enhance aerosol days, with P35 = 0.51% and 0.21%, respectively.

Relative to the "background" (i.e., isolated non-enhanced days; Figure 4.18a) radar echoes observed on days in which an enhanced UHI was in place had a 94% greater probability of having reflectivities of 35 dBZ within the charging zone (see UHI CFAD in Figure 4.18c), with isolated sea-breeze days having a 20% greater probability (Figure 4.18b). As previously mentioned, extension of these metrics to the NIC mechanism are not linear, however they lead us to conclude that *days in which an enhanced UHI is in place have the greatest enhancement in lightning potential.* Contrary to these relative enhancements, enhanced AI days are 28% *less likely* to see enhanced reflecitivities in the charging zone relative to "background" days, implying that
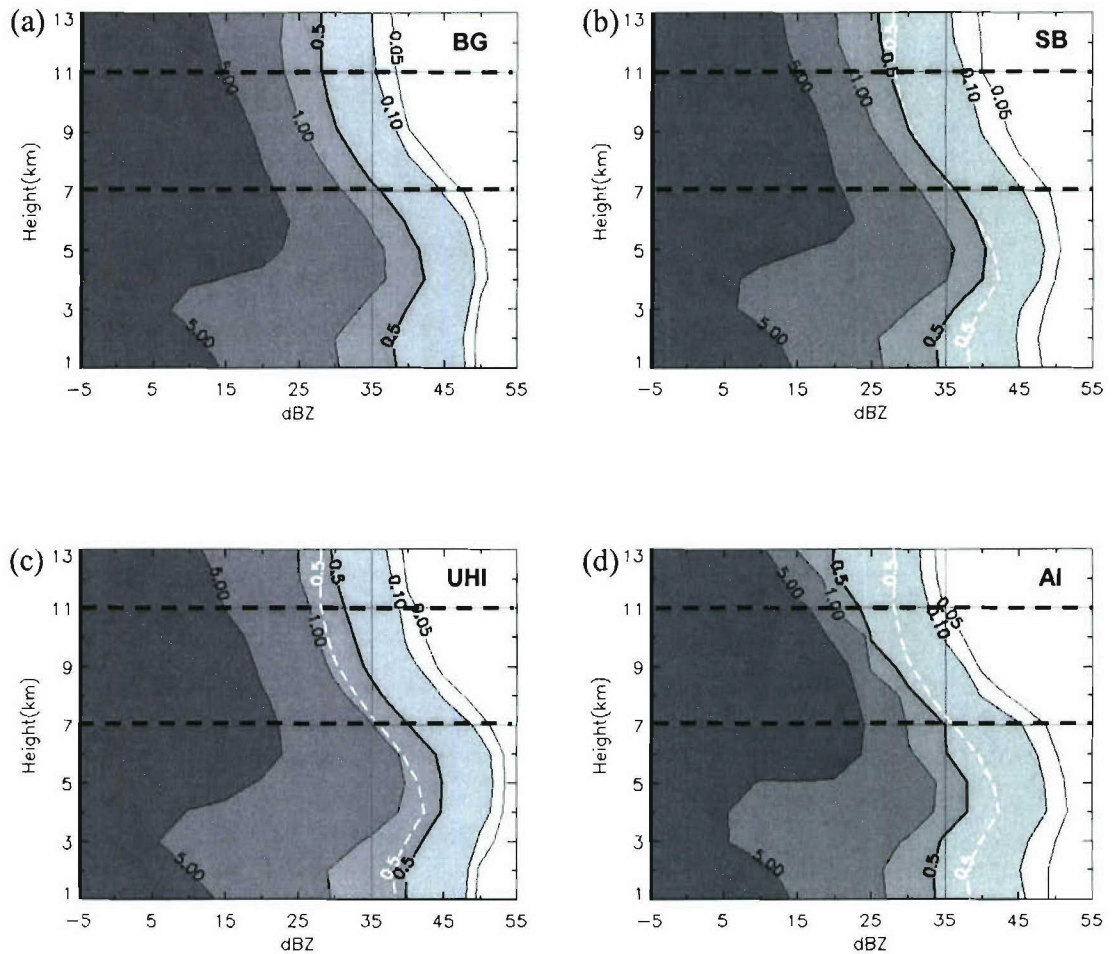
Figure 4.18 As in Figures 4.17, mean CFADS of radar reflectivity over the Houston area (dashed box in Figure 4.16a), associated with the following isolated days (a) 138 non-enhanced background (BG) days, (b) 62 sea breeze (SB) days, (c) 57 enhanced UHI days, and (d) 48 enhanced AI days; for reference, the 0.5% relative frequency of occurrence contour is bold, with the 0.5% contour in panel (a) overlaid in white (dashed) on panels b-d.

Table 4.3 CFAD Summary Statistics (Forcing Analysis) – negative % differences imply that the forcing-function being compared to (i.e., relative to columns) have a decreased probability of 35 dBZ in the charging zone compared to the forcing function in the first column.

Forcing Function	Total Days	Radar Days	Radar Volumes	P35 [%]	% Difference in P35, Relative to:				
					ALL	BG	SB	UHI	AI
ALL	336	262	24,033	0.31					
Non-Enhanced (BG)	169	138	12,899	0.27	13%		15%	49%	-50%
Isolated Sea Breeze (SB)	32	47	3,923	0.3	-4%	-20%		39%	-86%
Enhanced UHI (UHI)	57	42	3,882	0.51	-69%	-94%	-64%		-196%
Enhanced AI (AI)	48	35	3,329	0.21	37%	28%	39%	63%	

days having the largest concentrations of pre-convective aerosols (a tracer for CCN

concentrations) are the least likely to encounter enhancements in CG lightning activity.

4.4 Summary

Utilizing data from four separate archived datasets the hypothesized causative

mechanisms behind the documented enhancement in summer season ground flash

densities over the Houston area were examined, with differences in convective structure

documented. Findings indicate that the spatial extent of the flash density features are

primarily the result of "typical" convective activity tied to the presence of a persistent

thermal anomaly over the center of the city, giving rise to a preferential location of

low-level convergence and convective enhancement, coupled with the land surface

heterogeneity of the surrounding area. Further, through the analysis of over

24,000 volumes of radar data it was shown that there were greater probabilities of

enhanced radar reflecitivies being located within the charging zone over the Houston

area, relative to its surroundings indicating the potential for enhanced charging and

lightning generation, via NIC. That is not to say that the magnitudes of these features are

not enhanced through the hypotheses investigated in this study, rather that the presence of these *key features cannot be directly attributed to the hypotheses under investigation.*

Relating to the apportionment of cause, based on a climatic viewpoint, we conclude the primary causative mechanisms responsible for the *intensity* of the Houston CG lightning anomaly (i.e., *those responsible for the predominant enhancements to the background* features discussed above) to be those associated with a mixture of urban and natural influences, specifically that *UHI thermodynamics* provide a more favorable environment for convective initiation and thunderstorm intensification as well as contributing to an area of preferred convergence over, and to the east-northeast of the city, with associated *mesoscale enhancements in sea breeze convergence.* Acting together, these two enhancements cause more frequent convection over the Houston urban area resulting in more lightning activity over the city. However, the dominant of the two remains uncertain as they are both intimately tied to thermal forcing, the common denominator between the two. Regarding the effects of anthropogenic aerosols on enhanced flash densities, from the analyses presented here, it is unclear that enhanced aerosol (CCN) concentrations (in particular, SO_2) have any significant impact on the flash density enhancements under investigation leading us to the conclusion that *enhanced aerosol concentrations are the **least likely** contributor* to the climatological enhancements in ground flash density over and around the Houston metropolitan area during the summer season. Complementing these results, we found the convective structure associated with enhanced UHI days to be much more vigorous than that observed on enhanced AI days, with the mean probability of radar reflectivities of

35 dBZ located in the charging zone being 196% greater on enhanced UHI days than on enhanced AI days.

As mentioned in Section 4.3.1.3, where we discussed the results of the Sea Breeze/Convergence Climatology, Chapter 5 will further investigate the area of localized convergence over the northern central portion of the city, serving as a final synthesis for the research at hand.

CHAPTER 5

THE RELATIONSHIP BETWEEN BOUNDARY LAYER CONVERGENCE AND CLOUD-TO-GROUND LIGHTNING – A FINAL SYNTHESIS

5.1 Introduction

The results presented in the preceding chapters lead us to conclude that the Houston lightning anomaly is likely the result of "typical" convective activity tied to a persistent thermal anomaly that gives rise to a preferential low-level convergence zone situated over the city. As hypothesized, *factors significantly enhancing the magnitude of the anomaly are those that serve to enhance boundary layer (BL) convergence* (recall Figure 2.4). Constrained by mass continuity, updrafts leading to deep moist convection are necessarily associated with sub-cloud horizontal mass convergence. Given that the Earth's surface is impermeable with respect to the wind, it is clear that horizontal convergence of BL winds would result in compensating upward vertical motions with greater convergence over a given area resulting in greater vertical motions, possibly capable of initiating and/or intensifying convection. Given the physics of the problem, all else being equal (i.e., sufficient moisture and instability requisite for the development of deep moist convection), enhancements in boundary layer convergence (BLC) should deepen the PBL, thereby enhancing the instability, with the end result being an

enhancement in the number of updrafts capable of breaking the "cap" (capping inversion) allowing for more vigorous interactions between precipitation sized ice particles and ascending ice crystals within the charging zone, ultimately resulting in enhancements in thunderstorm electrification and lightning via NIC.

The effect of enhanced BLC, and the atmospheric response (i.e., rainfall and/or lightning) has been illustrated in previous observational studies from southern Florida [Ulanski and Garstang, 1978; Watson and Blanchard, 1984; Watson et al., 1987], highlighting the importance that boundary layer winds have on new thunderstorm growth and potential lightning production. In particular, Watson and Blanchard [1984], examined 121 convergence "events" during the 1975 Florida Area Cumulus Experiment (FACE) campaign and found a relationship between the change in total area divergence (the negative of which is used in this study; total area convergence (TAC), discussed below) and the amount of radar-derived rainfall. Watson et al. [1987] coupled these findings with those that documented a proportionality between thunderstorm precipitation output and the total number of flashes [i.e., Workman and Reynolds, 1949; Battan, 1965], by relating CG lightning with surface wind convergence (both spatially and temporally) for 42 summer days in 1983 over central Florida. Their examination of divergence and lightning time series during this period showed that CG lightning began near the time of strongest convergence, peak lightning activity typically occurred when the total area divergence was near zero in the transition from convergence to divergence, and CG lightning ended just after peak divergence over the area. Further, through a set of scaling arguments Banacos and Schultz [2005] showed that horizontal mass convergence associated with smaller mesoscale boundaries such as lake/sea breezes, and active or

remnant convective outflow boundaries, is at least an order of magnitude larger $[O(10^{-4}s^{-1})]$ than convergence associated with typical frontal boundaries.

Utilizing BL convergence fields generated by the National Center for Atmospheric Research's (NCAR) Variational Doppler Radar Assimilation System (VDRAS; [Sun and Crook, 1997]), this chapter complements the convergence climatology presented in Chapter 4 (Section 4.3.1.3), independently establishing the presence of an enhanced convergence zone located in the vicinity of the Houston metropolitan area. Area averaged, and cell-scale analyses link the BL convergence zone (forcing #1) with enhancements in radar derived precipitation ice mass (response #1, forcing #2) and ultimately enhanced ground flash densities (response #2; see Appendix B for details on the relationship between radar derived precipitation ice and CG lightning).

5.2 Background

As VDRAS is an analysis tool developed, maintained and operated by NCAR, and the intent of this chapter it to evaluate the relationship between boundary layer convergence (as diagnosed by VDRAS), radar derived precipitation ice mass, and lightning, this section provides the reader with a cursory overview of VDRAS. For a detailed description of the system the reader is referred to Sun and Crook [1997], Sun and Crook [2001] and Crook and Sun [2004].

It has long been recognized that the success of numerical weather prediction (NWP) models depends strongly on the accuracy with which the atmosphere is represented at the time of model initialization. Unfortunately, by themselves, traditional weather observations provide a less than complete dataset from which to describe the

initial state of the atmosphere in these models. Herein lies the need to incorporate, or assimilate, "unconventional" sources of weather information such as in-situ measurements and/or satellite observed/derived quantities into atmospheric NWP models to help "fill the gaps" in traditional observing networks, and provide a more complete (and hopefully more accurate) description of the atmosphere for use in the critical model initialization process. As its name implies, VDRAS utilizes a four-dimensional variational assimilation technique to incorporate a time series of radar observations (both radial velocity and reflectivity) from WSR-88D radars into a cloud-scale numerical model in order to better represent the evolution of flow (components of the horizontal wind) within the atmosphere. Through the minimization of a cost function, the model is fit to the observations over a specified period of time in order to develop a set of optimal initial conditions for use by the constraining numerical model.

VDRAS has been applied in both research and operational environments; the application of the system to different stages of convective development has demonstrated that the detailed structure of wind, thermodynamics and microphysics could be obtained with reasonable accuracy [Sun and Crook, 1998; Sun and Crook, 2004], thereby highlighting the utility of the system in diagnosing convergence within the boundary layer. Application of VDRAS generated fields to lightning studies such as this is a new endeavor; therefore, the work presented in this dissertation is a *"first of its kind"* (A. Crook, personal communications, 2005).

5.3 Data and Method

This study complements the previous datasets used throughout this dissertation (CG lightning, radar reflectivity, and precipitation ice mass) by incorporating BLC fields through the assimilation of radial velocity data contained within the radar reflectivity dataset (detailed in Appendix B) into VDRAS. Data gathered were used to construct a spatial climatology of convergence throughout the domain, with accompanying area and cell-scale analyses investigating the relationship between BLC, precipitation ice mass (IM) and CG flash densities and counts (FD and FC, respectively). As with the CFAD analysis conducted in the previous chapter (Section 4.3.3), we diagnose the climatological differences in boundary layer forcing and its impact on thunderstorm electrification over the Houston area from both spatial (i.e., Houston relative to surroundings; see Figure 4.16a for location of analysis areas) and forcing (i.e., enhanced UHI relative to background, etc.) perspectives.

Two separate analysis methods were used to compare warm-season statistics of VDRAS derived BLC, radar derived IM, and NLDN detected FDs and FCs, both of which mimic approaches taken in Appendix B where we performed similar analyses comparing IM with FDs and FCs. The first method compared time-integrated (TI) or cumulative means of BLC, IM and FD for each 4 km grid square within the domain yielding a total of 10,000 data points for comparison (one for each 16 km^2 pixel within the horizontal analysis domain). The second approach utilized the cell identification component of the IDL cell-tracking algorithm detailed in Chapter 3 to compare storm integrated BLC values with storm IMs, FCs and FDs on a cell-by-cell basis. Here, the software was modified to incorporate the VDRAS BLC dataset; we set the minimum

storm size area, and tracking altitude for identifying radar reflectivity cells as 32 km^2

(2 pixels) at Z = 2 km with a threshold reflectivity value of 30 dBZ. Since pixel relative

BLC, IM and FC measurements had previously been computed, cell totals of each

parameter were taken as the sum of positive BLCs (justified in Section 5.3.3), IMs and

FCs associated with each pixel comprising the cell; cell FDs were computed by

normalizing the cell FC by cell area. As pointed out in Appendix B, this approach

effectively treated each cell as a vertical entity, accounting for neither vertical tilt, nor

ground flashes coming to ground in regions of reflectivity less than 30 dBZ. All in all, a

total of 14,061 cells were identified and analyzed as part of this study.

5.3.1 *Radar and CG Lightning Methodologies*

Using the synoptically conditioned dataset from Chapter 4, over 1,200 daytime

(0900 – 1659 CST) convective volumes of archived WSR-88D Level II data (detailed in

Appendix B) from 15 lightning days over Houston were selected for assimilation into

VDRAS. In addition to the requirement for the occurrence of at least one CG lightning

strike over the Houston area, a nearly equal number of days were chosen from each of the

statistical subsets used in the selective exclusion analysis conducted in the previous

chapter, namely: 4 non-enhanced days, 4 isolated SB days, 4 enhanced UHI days, and

3 enhanced AI days.

Radar data from each of these days were processed using two separate schemes,

one for the VDRAS analysis performed at NCAR, and a second for the area and cell-

scale analyses (conducted locally). In all instances the domain spanned 400 km x 400

km, centered on the location of the League City, TX radar site. For the VDRAS analyses,

the Level II data were shipped to NCAR where they were interpolated to a 1 km

Cartesian grid in the horizontal while an unfolding algorithm was applied to the radial

velocity input data stream. Following gridding, the data underwent an automated quality

control process, and was then further interpolated onto the 4 km model grid in the

horizontal while remaining on the constant elevation angle levels in the vertical. The

vertical resolution of the VDRAS output grids were 0.5 km, extending to an altitude of

7 km. Radar data was also locally gridded so that radar derived precipitation ice mass

quantities could be calculated (as detailed in Appendix B) with horizontal resolutions

matching that of the VDRAS grid; vertical resolution was 1 km, extending 20 km in the

vertical to allow for computation of precipitation ice mass quantities throughout the

domain.

Coincident with each radar volume, ground strike locations (i.e., flashes occurring

from the beginning of one volume scan to the beginning of the subsequent volume scan)

detected by the NLDN were gridded to match the horizontal dimensions of the Cartesian

VDRAS and radar grids; for consistency, positive ground flashes with peak currents less

than 10 kA have been disregarded.

5.3.2 VDRAS Methodology

The assimilation window for VDRAS is 10 minutes, meaning that a total of three

consecutive volumes of radar data (constant elevation levels) were used in each window.

Background wind fields, used to provide a first guess for the cold start cycle and

boundary conditions for subsequent cycles, were generated using a velocity azimuth

display (VAD; [Lhermitte and Atlas, 1961]), coupled with other available observations,

as well as RUC model analyses. Once the background fields had been generated, the radar data were assimilated into the system. Assimilation of the radar data was performed using a continuous cycling procedure [Sun and Crook, 2001, Figure 3]. As previously discussed in Section 5.2, the optimal fit between the model and the data was obtained by minimizing the difference between the model and observations (i.e., minimization of the cost function). This was accomplished by running (cycling) the numerical model forward and the adjoint of the model backward until an optimum solution was obtained. Model results (horizontal convergence at each pixel) were then saved as output grids. Mean BLC values at each horizontal grid-point were taken as the mean convergence within the lowest 1.5 km of the model domain (3 lowest model layers). Due to the length of the assimilation window, the VDRAS analysis resulted in an output grid for every other volume of radar data resulting in a total of 631 VDRAS output grids for use in this study.

5.3.3   *Total Area Convergence (TAC) and Total Cell Convergence (TCC)*

To quantify the overall magnitude of the boundary layer convergence occurring over a given area, the VDRAS convergence fields were used to compute the area-averaged convergence, or total-area convergence (TAC); given as the grid point mean convergence within an enclosed area [Cunning et al., 1982]. Equivalent to the negative of the line integral of the normal component of the wind around the area, this number provides a quantitative measure of the amount of horizontal mass flux into (positive values) or out of (negative values) an area, which can then be used to infer the relative magnitude and sign of compensating vertical motions.

Although TAC proves to be of utility when diagnosing horizontal mass flux in an *Eulerian* sense [e.g., Watson and Blanchard, 1984; Watson et al., 1987], and is an appropriate metric for the quantitative comparisons associated with the spatial climatologies to be presented in Section 5.4.1, this quantity is inappropriate for use in our cell-scale analyses where compensating areas of convergence/divergence within the BL associated with storm-scale up/down drafts routinely coexist; here we are most concerned with sub-cloud forcing that acts to enhance upward vertical motions within the cell. Therefore, a more appropriate method of determining that portion of the flow capable of forcing upward motions within a cell would be to integrate the positive mean BLC values contained within the cell; we call this quantity total cell convergence (TCC) and will use it as our primary metric when discussing differences in VDRAS derived mean BLC between convective cells in Section 5.4.2.

5.4 Results and Discussion

As previously outlined, the data gathered for this investigation were used to construct a spatial climatology of convergence over and around the Houston metropolitan area. Herein, we present results in the form of TI analyses (Section 5.4.1) with the results of the cell-scale analyses presented separately in Section 5.4.2.

5.4.1 Time-Integrated Analysis

Figure 5.1a presents the spatial distribution of VDRAS derived BLC (mean convergence within the lowest 1.5 km of the atmosphere) averaged over all hours contained within the 15-day dataset (note that only positive convergent flow is contoured
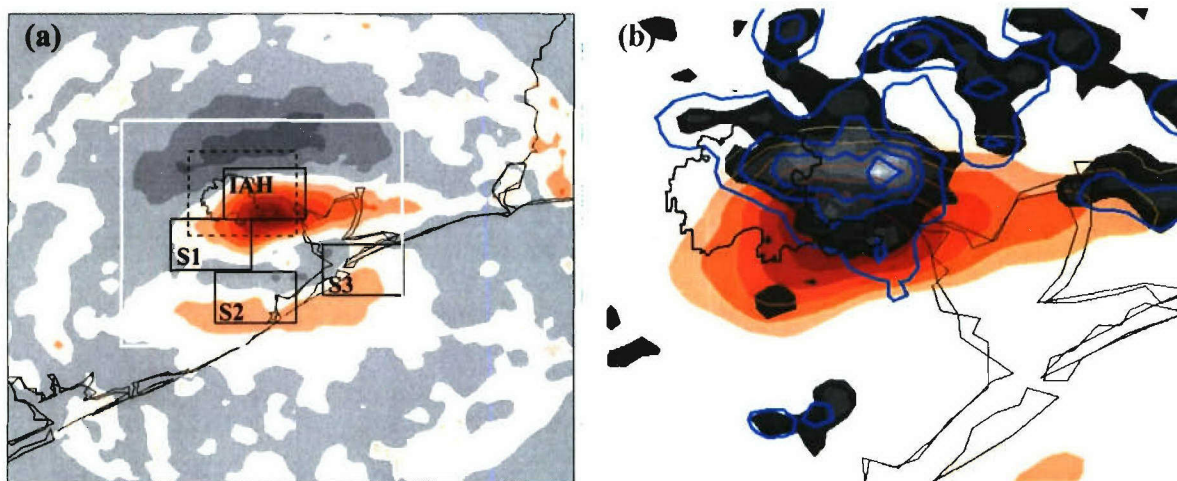
Figure 5.1 Spatial distribution of the 15-day day time integrated mean (a) VDRAS derived boundary layer convergence (BLC) field with darkening shades of maroon associated with increasing positive convergence contoured at intervals of 1×10^{-5} sec^{-1}, relative to the zero value depicted by the white contour. Negative convergence (i.e., divergence) is represented by darkening shades of gray contoured at intervals of -1×10^{-5} sec^{-1}, relative to the same zero value contour, black reference boxes are the same as in Figure 4.16a, white box denotes that portion of the domain presented in Figure 5.1b; and (b) zoomed composite representation of normalized (relative to the domain maximum of each quantity) time integrated BLC (with shades of maroon increasing in darkness every 15%, beginning at 10% of the maximum BLC value within the domain, note divergent flow is not presented), radar derived precipitation ice mass (with shades of gray decreasing in intensity every 10%, beginning at 20%) and ground flash densities contoured in blue at the 20, 40, 60 and 80% levels, relative to the domain maximum flash density value associated with the 15-day mean.

in this figure). Consistent with the wind and convergence climatologies presented in Chapter 4 (see Figure 4.9b), a definite area of localized convergence over the Houston area is apparent in the 15-day mean. Relating the forcing produced by the BLC to the atmospheric response, Figure 5.1b presents a spatial composite with ground flash densities (FDEN; blue contours) and shaded contours of precipitation ice mass (IM) overlaid upon the VDRAS derived BLC presented in Figure 5.1a. From this presentation, a new link in the forcing-response chain begins to emerge. Here, we see that persistently focused, low-level, mesoscale forcing (on the order of 4-5 cm s^{-1}, computed based on continuity) over the Houston area, may give rise to a preferential location of convective initiation (CI), leading to downwind enhancements of radar derived precipitation ice mass within the charging zone (i.e., displaced from peak forcing), and finally enhancements in ground flash densities. Arguably, this sequence of events will in and of itself spawn localized, storm scale, regions of convergent and divergent flow serving to enhance and/or diminish the magnitude of the climatological convergence anomaly; however, the localized persistence of mesoscale BLC in the mean is consistent with the findings, and speculations contained throughout this dissertation. Indeed, the persistent convergence located over the city is consistent with observations presented in Chapter 3, where we found an area of enhanced composite cell merger occurrence located over and downwind of the city. The fact that the locations of enhanced convergence and cell merger activity are in general agreement further highlights the significance that cell mergers have with respect to convective intensity [Simpson, 1980; Simpson et al., 1980; Tao and Simpson, 1984].

Quantifying these spatial observations, Table 5.1 contains summary statistics of the spatial differences between the various sub-domains; statistics include daily mean values of TAC, P35, IM and conditional FDEN (i.e., total flashes in each analysis box normalized by the area encompassing all pixels containing lightning) taken over all 15 days within our VDRAS subset. Clearly, relative to the other sub-domains, the Houston area (IAH) falls victim to enhanced forcing (TAC) leading to enhancements in PIM, P35, and ultimately conditional FDENs. Comparison of the statistics associated with the remaining sub-domains (against one another) indicates that BLC alone, although an important ingredient, is not in and of itself sufficient to spawn deep moist convection and that meteorological conditions (i.e., the presence of sufficient moisture and instability) must be sufficient to allow this to occur. To illustrate this fact, we note that analysis boxes S2 and S3 have nearly equivalent values of TAC; however, the atmosphere responds more vigorously to the climatological forcing over S2 with greater enhancements in precipitation ice mass and resultant ground flash densities. Explanation for the dearth in lightning activity over the mouth of Galveston Bay (S3) can likely be found in the stabilizing effect that the cooler water temperatures have on the atmosphere. Although S2 (a coastal location) is also quite influenced by the Gulf waters, the stronger land-ocean contrasts likely serve to provide the necessary boost in instability enabling the enhanced response, relative to S3. Regardless of the reason for the subtle differences found within the climatological summary just presented, it is clear that the Houston area is more favorable for the development of deep moist convection resulting in enhanced ground flash densities relative to its immediate surroundings.

Table 5.1 VDRAS summary statistics (spatial analysis), see text for full description.

Analysis Box	Mean TAD $[10^{-5}\,\text{s}^{-1}]$	Mean P35 [%]	Mean IM $[10^{7}\,\text{kg km}^{-2}\,\text{day}^{-1}]$	Mean FDEN $[10^{-3}\,\text{flashes km}^{-2}\,\text{day}^{-1}]$
IAH	2.50	0.73	3.70	1.000
S1	0.94	0.28	1.80	0.200
S2	0.46	0.69	1.00	0.100
S3	0.45	0.09	0.51	0.027

As the dataset used in this analysis was comprised of a nearly equal number of days from each of the statistical subsets used in the selective exclusion analysis conducted in Chapter 4 (non-enhanced, isolated SB, etc.) we now examine the statistical differences in BLC found over the larger Houston area (see dashed box in Figure 5.1a) relative to each forcing function. As each of the statistical classifiers used to subset the days into their respective forcing types is focused on the Houston area, spatial distributions outside of this confined area are not shown in this analysis. Instead, we focus our attention on TAC over the Houston area as our primary instrument of measure, summarized in Table 5.2.

Table 5.2 VDRAS summary statistics (by forcing type), see text for full description.

Forcing Function	Mean TAD $[10^{-5}\,\text{s}^{-1}]$	Mean P35 [%]	Mean IM $[10^{7}\,\text{kg km}^{-2}\,\text{day}^{-1}]$	Mean FDEN $[10^{-3}\,\text{flashes km}^{-2}\,\text{day}^{-1}]$
NOF	0.63	0.87	1.27	20.00
SB	0.68	0.44	0.40	8.19
UHI	1.53	0.77	0.75	16.60
AI	0.96	0.54	0.16	13.50

Two caveats must be taken into account when examining these statistics: first, recall that the development of deep moist convection is dependent on the presence of sufficient lift (which may possibly be provided and/or enhanced by BLC), moisture and instability; therefore, enhancements in TAC may not necessarily correlate directly with enhancements in IM and FDEN. Secondly, the statistical size of each of the subsets is out of necessity small; therefore, the statistics presented may be somewhat biased due to a relatively small number events; out of consistency, mean statistics will be presented, note that median values of the compared parameters show similar relative trends. From Table 5.2 it is clear that the net BLC over the Houston area, as measured by TAC, is most notably enhanced on days in which an enhanced UHI exists. This finding is not surprising as the enhanced thermal anomaly over the city would give rise to ascending air capable of enhancing the convergence of air from surrounding areas to replace the resulting mass deficit. The two findings that do stand out, recognizing the aforementioned caveats, are the fact that enhanced aerosol days (AI) have the second greatest measure of TAC of the four statistical subsets, with the weakest atmospheric response in IM (second weakest response in FDEN) and that the non-enhanced days (NOF) rank last in mean TAC, while boasting the greatest atmospheric response in all other areas.

5.4.2   Cell-Scale Analysis

Complementing the time integrated analyses just presented, all 631 convective radar volumes, along with accompanying VDRAS derived BLC fields, radar derived IMs and NLDN detected CG lightning strikes were ingested into the modified cell tracking

algorithm resulting in the identification of 1,928 lightning producing cells and 12,133 non-lightning producing cells throughout the domain; recall that the subjective definition of a cell is that of the area enclosed by the 30 dBZ radar reflectivity contour at 2 km above the ground. Due to the limitations associated with the size of the dataset, discussed in the previous section, we will forgo comparison of mean cell characteristics over the Houston area as a function of forcing type, and instead focus our discussions as follows: first we discuss spatial differences between mean cell characteristics for cells geo-located in each of the sub-domains compared in Section 5.4.1 (IAH, S1, S2 and S3), we then go on to investigate differences between lightning and non-lightning cells in general, throughout the domain.

To that end, Table 5.3 provides a summary of the statistics to be discussed in this section. Focusing first on Table 5.3, columns a-d, we note that the IAH analysis box contained nearly 60% of the CG lightning producing cells (CG) observed in all analysis areas, and relative to the other sub-domains mean TCC associated with these cells were the greatest. Consistent with these findings we also note that the IAH CG cells contained larger quantities of precipitation ice mass located within the charging zone with higher CG flash rates (by a factor of 2, save S2). Comparing CG cells located within analysis boxes S1 and S2 (Table 5.3, columns b and c), we note larger mean TCC values associated with S1 CG cells (mean values over twice that observed in S2); however, CG cells located within S2 contain 1.5 times as much IM and produce nearly 23% more lightning on a per cell basis. As in the previous section, the apparent discontinuity between the low-level forcing and the atmospheric response, lead us to conclude that

relative to S1, analysis area S2 must be more favorable for the formation of deep moist convection, at least during the 15 days on which this analysis was based.

Some insightful findings surrounding the characteristic differences between lightning and non-lightning (noCG) cells surface when comparing the mean statistics associated with all cells identified within the dataset (summarized in Table 5.3, column e). Here we see that, on average, CG cells have TCC values approximately 7 times greater than noCG cells with IM values being an order of magnitude larger. Not included in Table 5.3, we also note that the average peak radar reflectivity at tracking altitude (i.e., peak reflectivity at an altitude of 2 km) is on the order of 10 dBZ greater in the CG cells, nearly 50 dBZ.

The relationship between TCC, cell total IM and FDEN, is shown in Figure 5.2, where we present a three-parameter scatter plot of TCC and cell total IM, with varying pixel colors based on the flash density associated with the each particular cell. We first note a linear correlation (R = 0.7) between TCC and cell total IM with enhanced BL forcing associated with cells containing enhanced quantities of precipitation ice in the charging zone. Consistent with our findings in Appendix B, we further note that cells with more IM generally have larger ground flash densities associated with them (see dark gray and red data points in Figure 5.2). The fact that the most electrically intense storms (from a CG perspective) do not reside in the extreme upper-right hand portion of the parameter space is reassuring, as previous studies have highlighted an apparent anti-correlation between storms with extremely intense updrafts (> 30-35 m s^{-1}) and CG lightning production [e.g., MacGorman et al., 1989, Lang et al., 2000; Lang and Rutledge, 2002]. Hypothesized to be the result of an "elevated charge mechanism," it is

Table 5.3 VDRAS summary statistics associated with 14,061 convective cells.

	(a) IAH		(b) S1		(c) S2		(d) S3		(e) DOMAIN	
	CG	noCG	CG	noCG	CG	noCG	CG	noCG	CG	noCG
COUNT	127	297	40	302	44	176	9	79	1,928	12,133
TCC [10^{-3} sec^{-1}]	1.80	0.29	1.10	0.30	0.50	0.30	0.36	0.12	1.60	0.23
IM [10^5 kg]	161	9	85	10	130	9	47	6	145	9
Flashes per cell	6.55		3.175		3.9		2.1		5.13	
FDEN [flashes km^{-2} cell^{-1}]	0.027		0.02		0.027		0.017		0.02	
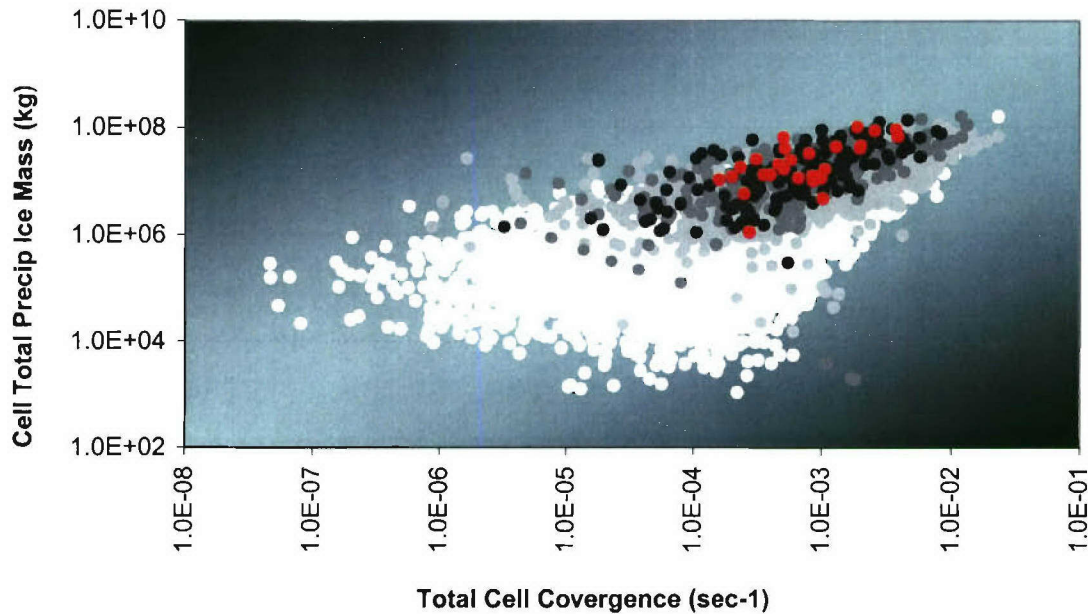
Figure 5.2 A three-parameter scatter plot of cell total precipitation ice mass (IM; ordinate) as a function of total cell convergence (TCC; abscissa) and cell flash density (FDEN; no lightning = white, with increasing shades of gray associated with more intense flash densities, light gray = FDENs in the lower 3 quartiles of the conditional cumulative FDEN distribution, medium gray = FDEN within the 75-90th percentile range, dark gray = FDEN > 90th percentile with cells producing the most intense flash densities plotted in red).

argued that intense updrafts loft the main negative charge layer to greater altitudes than normal, thereby reducing the magnitude of the electric field between the main negative charge center and ground due to the increased spatial separation; this sequence of events would also likely delay the development of the lower positive charge center (LPCC) believed to be important in the development of ground flashes. It follows that this reduction in electric field may then favor intra-cloud (IC) lightning over CG lightning until such time as the storm begins to weaken, allowing the descent of precipitation ice to warmer regions of the cloud. This eventuality may then lead to the possible development of a the LPCC (recall discussions on the development of the electrical tripole, Chapter 2)

reinvigorating the occurrence of CG flashes. Although unable to quantify it, we suspect that this is what we are observing in Figure 5.2, where strong updraft enhancements (on the order of 15-25 m/s, based on convergence alone) are associated with a decrease in ground flash densities of storms that have been electrically "primed" (i.e., storms containing ample precipitation sized ice particles in the mixed-phase region).

5.5 Summary

Utilizing BL convergence fields generated by NCAR's Variational Doppler Radar Assimilation System, we investigated the relationship between VDRAS derived boundary layer convergence, radar derived precipitation ice mass and NLDN detected CG lightning over 15 non-consecutive summer days, independently establishing the presence of an enhanced convergence zone located in the vicinity of the Houston metropolitan area. Coupling *Eulerian* and cell-scale analyses over the Houston area, we clearly link the BL convergence zone with enhancements in radar derived precipitation ice mass and ultimately enhanced ground flash densities. Statistics associated with over 14,000 convective cells occurring throughout the domain highlight distinct differences between lightning and non-lightning producing cells, with the average lightning producing cells having convergence based updraft enhancements nearly 7 times that of non-lightning producing cells, with an order of magnitude increase in precipitation ice mass within the charging zone. Collectively, the findings presented in this chapter firmly establish a physical proportionality between the ability of the cloud ensemble to produce enhanced CG lightning activity, and the amount of low-level convergent flow available to feed the updraft(s).

CHAPTER 6

CONCLUDING REMARKS AND SUGGESTIONS FOR FUTURE RESEARCH

6.1 Concluding Remarks

The work presented in this dissertation has addressed a fundamental question regarding anthropogenic influences on convection as it relates to CG lightning. All tolled, eight independent datasets were utilized throughout this research with five distinct research components, each geared towards determining the primary causative mechanism(s) behind the documented enhancement in summer-season ground flash densities over and around the Houston area. Salient *observations* (conclusions will follow) contained within this body of research include the following:

- Mean temperatures over the industrial portion of the city are on the order of 2° C warmer than surrounding areas giving rise to a diurnally persistent thermal anomaly located over portions of the city. Peak intensities of this UHI occur between 12 – 14L, proceeding peaks in both onshore flow associated with the inland penetration of the sea breeze (1-2 hours), and lightning activity (2-3 hours).

- Independent observational and modeling climatologies corroborate the presence of an enhanced low-level convergence zone located in the vicinity of the Houston

metropolitan area providing a preferential location for convective initiation, under appropriate atmospheric conditions.

- Coincident climatologies of summer-season ground flash densities and radar derived precipitation ice mass support the non-inductive charging theory of thunderstorm electrification, extending the global results of Petersen et al. [2005] to much smaller scales.

- Complementing these observations, we found the convective structure over the Houston area on days in which an enhanced UHI was present to be much more vigorous than the overall mean with the probability of radar reflectivities of 35 dBZ located in the charging zone being 69% greater on enhanced UHI days; similarly, mean total area convergence values on enhanced UHI days were on the order of 35-40% greater than the overall mean values.

- Statistics associated with over 14,000 convective cells highlight distinct differences between lightning and non-lightning producing cells, with the average lightning producing cells having convergence based updraft enhancements nearly 7 times that of non-lightning producing cells, with an order of magnitude increase in precipitation ice mass within the charging zone.

- The magnitude of cell total precipitation ice mass was found to be linearly correlated with the amount of low-level convergence occurring within the convective cell, establishing a physical proportionality between a storms ability to produce enhanced CG lightning activity, and the amount of low-level convergent flow available to feed the storms updraft.

- On average, convective cells located over the Houston area fell victim to enhanced forcing (via BLC), contained larger quantities of precipitation ice, and yielded more lightning, than cells elsewhere.

- Results of the cell merger climatology corroborate past assertions (and observations) that merged cells are more vigorous, and produce more lightning than their unmerged counterparts, lending credible support to the speculations advanced by Changnon [1976] following METROMEX regarding cell merger occurrence relative to the urban domain.

- Findings highlight the importance of cell-mergers on enhancing the magnitude of regional ground flash densities with areas of enhanced flash densities being generally co-located with enhanced merger activity, regardless of geographic location of occurrence.

- Cell mergers occurring over the Houston area result in more vigorous convective cells capable of producing more lightning with larger flash densities relative to mergers elsewhere in the domain.

Throughout this dissertation we have referenced (and documented) several possible climatological forcing-response relationships that appear to provide a consistent explanation of the Houston lightning anomaly. Namely, we have quantified a three-step process by which thunderstorm electrification may become enhanced over the Houston area relative to its surroundings: (1) enhanced convergence within the atmospheric boundary layer over the city leads to the development of a preferential convective initiation point over the city, with individual cells containing more vigorous

(likely broader) updrafts than cells not influenced by the "Houston convergence zone." All else being equal, these intensified updrafts then lead to (2) the development of enhanced quantities of precipitation sized ice particles within the mixed-phase region of these storms, resulting in (3) enhanced ground flash densities, and CG flash rates. It then follows that *hypotheses offered to explain the lightning anomaly must be capable of enhancing precipitation ice mass in the charging zone,* likely through the enhancement of boundary layer convergence.

Findings indicate that the *spatial extent* of the flash density anomaly is primarily the result of "typical" convective activity tied to the presence of a persistent thermal anomaly over the center of the city, giving rise to a preferential location of low-level convergence and convective initiation and/or enhancement, coupled with the land surface heterogeneity of the surrounding area. That is not to say that the magnitudes of these features are not enhanced through the hypotheses investigated in this study, rather that the presence of these *key features cannot be directly attributed to the hypotheses under investigation.* As it pertains to the attribution of causation, we present the following key *conclusions*:

- Although cell mergers occurring over the Houston area result in more vigorous convection, our findings suggest that CG lightning contributions due to mergers are similar throughout the domain. The implication here is that extension of the METROMEX hypotheses to the problem at hand is inappropriate. *Enhanced cell mergers alone are incapable of explaining the existence of the Houston lightning*

anomaly, with the anomaly continuing to persist subsequent to the removal of that portion of the lightning "signal" attributed to mergers.

- From a climatic viewpoint, we conclude the primary causative mechanisms responsible for the *intensity* of the Houston CG lightning anomaly (i.e., *those responsible for the predominant enhancements to the background* features discussed above) to be those associated with a mixture of urban and natural influences, specifically that **UHI thermodynamics** provide a more favorable environment for convective initiation and thunderstorm intensification as well as contributing to an area of preferred convergence over, and to the east-northeast of the city, with associated ***mesoscale enhancements in sea breeze convergence.*** Acting together, these two enhancements cause more frequent convection over the Houston urban area resulting in more lightning activity (and heavier precipitation) over and downwind of the city. The dominant of the two, however, remains uncertain as they are both intimately tied to thermal forcing, a common denominator.

- Regarding the effects of anthropogenic aerosols on enhanced flash densities, from the analyses presented here, it is unclear that enhanced aerosol (CCN) concentrations (in particular, SO_2) have any significant impact on the flash density enhancements under investigation leading us to the conclusion that *enhanced aerosol concentrations are the **least likely** (or at best, secondary) contributor* to the climatological enhancements in ground flash density over and around the Houston metropolitan area during the summer season.

From the above summary, it is clear that the Houston lightning anomaly is a spatially unique feature, relative to its immediate surroundings. Located in an environment primed for the development of summer-season convection, we found that factors serving to enhance updraft intensity were most likely to be associated with an enhanced convective response, ultimately resulting in increased lightning activity.

6.2 Suggestions for Future Research

Past researchers have argued for a detailed field campaign over the Houston area to further investigate the causes behind the Houston lightning anomaly. The conclusions contained within this dissertation, however, suggest that efforts would be better spent examining regional to local scale circulations and the response of convection and subsequent lightning frequencies to those forcing scales. As the research presented in this dissertation is primarily observationally based, additional insights into these scales may be realized through detailed modeling studies.

Although a strong correlation between precipitation ice mass and CG lightning has been established, total lightning data would prove to be a more complete estimate of the electrical strength of a thunderstorm, and of the Houston "lightning anomaly" in general. Given the recent installation of the second generation Lightning Detection and Ranging (LDAR-II) network over the Houston area, similar correlations between radar derived precipitation ice and total lightning and/or source densities should be developed (similar to the approach taken in Appendix B). The robust statistics associated with these complementary datasets (CG and total lightning correlations with precipitation ice) may then be able to be used to develop *operational*, radar-based lightning thresholds. Further,

statistics of this nature open the door for the assimilation of lightning data into mesoscale models. Here one could envision the relationships between precipitation ice and lightning being used to "nudge" the initialization of model ice fields such that the model more accurately represented the observed state of the atmosphere. In addition to a better initial model state, such an endeavor could ultimately lead the generation of forecast products identifying areas favorable for the development of lightning, thereby increasing critical warning lead times and enhancing public safety.

Additionally, such "tuning" of forecast models, would enable researchers to further investigate the impact that urban land use has on the spatial distribution and intensity of CG (and total) lightning activity relative to the urban domain. Past modeling studies have shown that removal of the Houston urban area (through the modification of land-use type in the model) resulted in the elimination of enhanced convergence over the city [Orville et al., 2001]. If model ice fields were more exact, researchers could then adopt a similar methodology to determine the effect that removal of the city has on the redistribution (spatial, temporal and magnitude) of precipitation ice, and therefore lightning. A very preliminary attempt into this was made using the fifth-generation Pennsylvania State University – National Center for Atmospheric Research Mesoscale Model (MM5; [Grell et al., 1994]) coupled with a sophisticated three-class ice microphysics scheme [Tao and Simpson, 1993]. Initial estimates are that removal of the Houston area *may* result in a decrease in precipitation ice mass on the order of 30-40% over the city, relative to the control run for a single 24-hour period. Such a decrease in mixed-phase ice would surely have implications on the redistribution and magnitude of resultant lightning activity; the question would then become, *is the resultant impact*

significant enough to climatologically eliminate the lightning anomaly? Clearly, an area deserving of additional attention.

In closing, we offer the following final comments. Although anthropogenic influences on convection can be quite complex, they none the less appear to exert a positive influence on the initiation, frequency and intensity of resultant storms. To *first-order*, these influences appear to be manifested in mechanisms capable of physically enhancing convective motions within the atmosphere. Although enhanced pollution associated with anthropogenic emissions are indeed important factors in cloud-scale interactions and can have *secondary* and *tertiary* effects on convective activity – the scale of the problem (climatological) prohibits the broad assertion of blame to being primarily one of "pollution." One must therefore exercise caution in the future to avoid potential pitfalls associated with these, and other complexities.

APPENDICES

APPENDIX A

AN INDEPENDENT ANALYSIS OF THE HOUSTON LIGHTNING ANOMALY

A.1 Introduction

A three-fold enhancement of cloud-to-ground lightning flash density over and downwind of the Houston metropolitan area in a twelve-year record (1989 – 2000; [Orville et al., 2001; Steiger et al., 2002]) corroborates results of previous studies [i.e., Westcott, 1995] indicating that observed enhancements in CG flash densities can occur over, and downwind of urban corridors. Westcott, Orville et al. and Steiger et al., each propose explanations for the observed local enhancements that revolve around "urban" effects, specifically (1) enhanced convergence, thermodynamic instability, or dynamical influences associated with the urban heat island; (2) altered microphysical processes associated with anthropogenic pollution; and/or (3) mesoscale enhancements in sea breeze convergence.

The intent of this study is to (1) extend the findings of Orville et al. [2001] and Steiger et al. [2002] by presenting a statistical analysis of the variance associated with daily summertime (June, July and August) CG flash densities observed throughout eastern Texas and Louisiana, (2) scrutinize the underlying uniqueness of the signal in a regional sense, and (3) examine how flash density characteristics change by selectively

135

excluding relevant subsets of the data (days without lightning, large events, etc.) from subsequent calculations.

A.2 Data and Method

Herein we create a regional climatology of total ground flash densities based on 9 years (1995 – 2003) of NLDN CG lightning data [Cummins et al., 1998] for the months of June, July and August for portions of eastern Texas and Louisiana. We have chosen to disregard flashes with positive peak currents less than 10 kA following the recommendations of Cummins et al. [1998] and Wacker and Orville [1999a,b].

A.2.1 Calculation of Flash Density

Ground strikes detected for the period of record within our domain (see Figure A.1a) were interpolated onto a 143 × 139 Cartesian grid with fixed spatial resolution of 5 km. The total flash density (flashes km^{-2} day^{-1}) for each of the 19,877 grid points was then calculated for each of the 828 days analyzed, yielding a dataset containing greater than 1.6×10^7 data points from which various descriptive statistics were calculated.

A.2.2 Mean and Variance Calculations

Daily flash densities for each grid point were used to generate spatial distributions of the nine-year mean summer flash density (flashes km^{-2} $summer^{-1}$) and the variance of the flash density at each pixel. For these calculations, the temporal sample size (N) is equal to 828 days (92 days per summer × 9 summers).

For further comparison, we partitioned the analysis into "Filtered," "Conditional" and "Conditional-Filtered" mean flash densities, and variances thereof. The filtered mean flash density and variance were calculated in the same manner as the seasonal mean (and variance) except that pixels classified as "large event days" were excluded from the dataset thereby creating a variable sample size from pixel to pixel ($\overline{N}$ = 808 days, $\overline{N}$ = mean number of summer days used in the filtered sample across the entire domain). A "large event day" was defined for a pixel as a day having a flash density that fell within the upper quartile of the positively-skewed flash density distribution of the gridded domain (see Section A.2.3 for further discussion). For the case of the conditional mean flash density and variance, rather than eliminating pixels classified as "large event days," we excluded pixels classified as "non-lightning days," or containing no lightning ($\overline{N}$ = 81 days). Finally, the conditional-filtered mean flash density and variance, as their names imply, are a combination of the conditional and filtered partitions, where all pixels classified as "non-lightning" or "large event" were removed from the dataset ($\overline{N}$ = 61 days).

A.2.3 "Large Event" Classification

Using daily flash counts for each pixel, we used statistics of the daily flash count distribution to guide the classification of "large" event days within our dataset. Due to the skewed, non-Gaussian nature of the flash density distribution, we chose thresholds appropriate to the nature of the flash density histograms based on the cumulative conditional flash density distribution (conditioned on the presence of lightning) to identify "large" events. Specifically, we chose lightning days whose flash counts

exceeded the 75th percentile (or fell within the upper quartile) of the cumulative distribution. Using the third quartile (Q3 = 6 flashes) as our threshold allows for an objective classification of the tail of the distribution as "large" events. Therefore, our objective definition of "large" events is any pixel whose flash count is in excess of 6 flashes in a given Julian day (or flash density > 0.24 flashes km^{-2}).

This definition is different than that used by Steiger et al. [2002]; in their analysis, it was suggested that flash density enhancements over the Houston area were due to those days in which the sum of flashes within three separate geographic boxes was greater than, or equal to 100. For the purposes of the analysis herein, using 100 flashes as the defining threshold for "large" events is not appropriate. For example, if we reconstruct the Steiger et al. analysis by summing the summer season flashes in each of the three geographic regions depicted in Figure A.1b (boxes A, B and C) for the period of 1989 – 2003 (Steiger et al. stopped at 2000), we find that during the 1,380 day period there were 1,075 days in which 1 or more flashes occurred in at least one of the three boxes. Of those 1,075 days, 68% (or 733 days) met or exceeded the 100 flash count threshold used in their analysis. This means that only 32% of the summertime lightning days contained less than 100 flashes (total in all 3 boxes). From a statistical standpoint, in this study we did not wish to classify 68% of the lightning distribution as "large" events. Applying the quartile method to the Steiger et al. reanalysis we find that 1,028 flashes day^{-1} (Q3 for this distribution) would produce an objective "large" event classifier comparable to the one utilized in the present analysis.
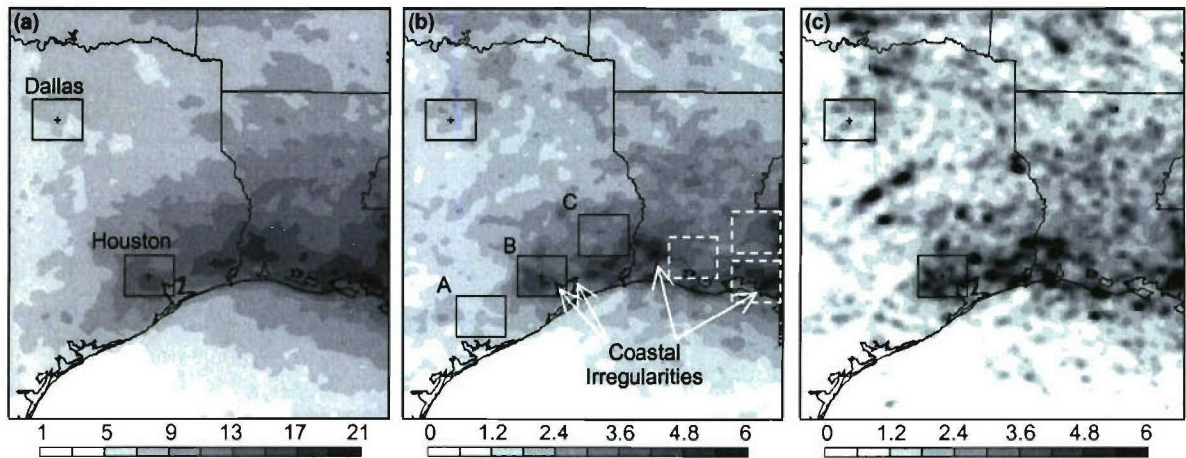
Figure A.1 Nine-year (1995-2003) summer season cloud-to-ground lightning statistics for (a) mean number of lightning days (92 possible); urban areas associated with the Houston and Dallas metropolitan areas are approximated by 0.75° latitude × 0.85° longitude boxes centered on each city. (b) Spatial variations of the 9-year mean summer season ground flash density (flashes km^{-2} $summer^{-1}$). Boxes labeled A, B and C were used in the analysis of Steiger et al. [2002], and are included for reference, with box B being the same as the Houston "urban" box in Figure A.1a; arrows highlight referenced coastal irregularities, while dashed boxes identify the referenced locations in which a student's t-test was applied. (c) Spatial variations of the 9-year summer season variance of the daily mean flash densities presented in Figure A.1b (flashes km^{-2} $summer^{-1}$)^2.

A.3 Results and Discussion

Figure A.1a displays the mean number of lightning days occurring for each pixel within our regional domain throughout the summer season (JJA). Here we clearly see the influence of mesoscale interactions in shaping the location and frequency of lightning events along the Gulf Coast, with a larger number of lightning days occurring in the Houston area and extending eastward along the coastal region. Comparing the lightning days (Figure A.1a) to mean lightning flash density (Figure A.1b), we find flash density enhancements in areas experiencing a greater number of storm days co-located along apparent coastal convergence zones, likely associated with the sea breeze, and evident irregularities in the coastline (see arrows in Figure A.1b). Consistent with

Orville et al. [2001] and Steiger et al. [2002], we also note the occurrence of a definite localized enhancement in flash densities situated over the Houston metropolitan area. The "enhancements" spread eastward from Houston, with similar localized maxima distributed along the coast of southeastern Texas and central portions of Louisiana. Examination of the spatial variance of the mean daily summer flash densities along the Gulf Coast (Figure A.1c) reveals significant variance, often times in excess of the mean, collocated with areas of larger mean flash density, and in particular, in the areas of local "enhancement."

Normalizing the mean flash density of each pixel ($\hat{x}$) by the mean flash density of the entire domain ($\bar{x}$), we can define domain flash density "anomalies" (i.e., $\hat{x}/\bar{x}$). For this parameter, values >1 (<1) are referred to as "positive" ("negative") anomalies. This approach enables a more direct comparison between anomaly patterns of the four sample types. Similarly, the coefficient of variation was computed to allow for inter-comparisons of the variance fields for each of these scenarios. Flash density anomalies shown in Figure A.2a, reveal that absolute flash densities in the vicinity of the Houston area and along the coast, east of Galveston Bay, are on the order of 2.5 times the domain mean, while flash densities in the Dallas area, and throughout north and central Texas, are predominantly centered on the mean. The Dallas area was included for comparison because it is another major urban area within the domain that exists in a different meteorological regime.

The data indicate that 25% of the days in which lightning occurred were classified as "large events days," contributing over 70% of the mean flash density within the domain. To evaluate the influence of large event days on the flash density patterns, we
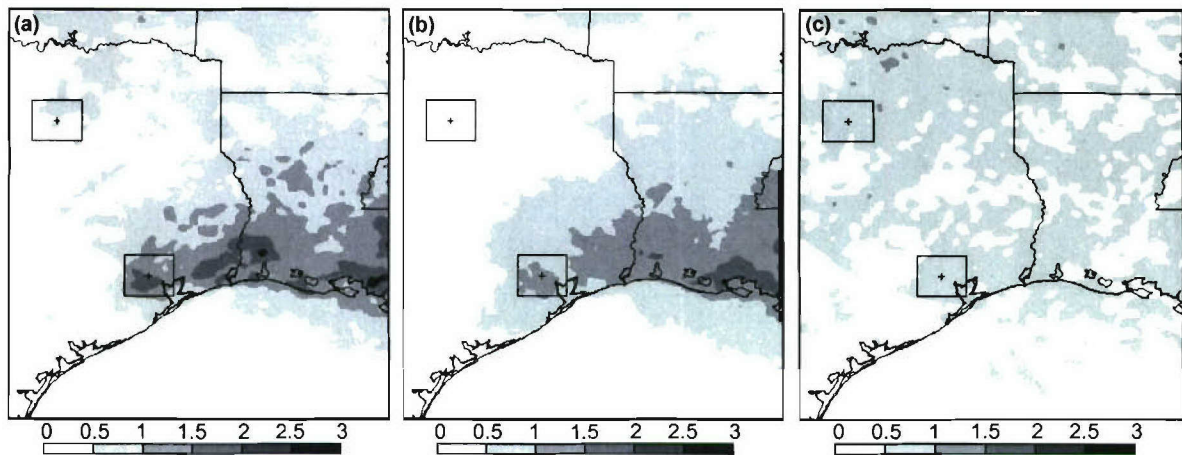
Figure A.2 Nine-year (1995-2003) summer season ground flash density anomalies created by normalization of (a) mean flash densities of each pixel by the domain mean, (b) filtered pixel mean flash densities (i.e., "large" event days excluded from the analysis) and (c) conditional pixel mean flash densities (conditioned on the presence of lightning). In all cases, values > 1 indicate positive anomalies and values < 1 negative anomalies. Reference boxes are the same as in Figure A.1a.

created a spatial distribution of the filtered mean flash density by removing large events from the sample (not shown). As expected, the magnitude of the maximum flash densities decreased across the domain, with the domain mean decreasing to 0.61 flashes km^{-2} summer^{-1}. Normalizing each pixel by the domain-filtered mean, we are able to examine the spatial distribution of the filtered mean flash density anomaly (Figure A.2b). Here we see that flash densities in the vicinity of Houston, and immediately east of Galveston Bay are 1.5 to 2.0 times that of the domain mean, with flash densities increasing eastward along the coast reaching peaks in southeastern Louisiana. While there is some suppression of the local anomaly over Houston, it is important to note that *the enhancement in CG lightning over the Houston area persists even with the removal of these large events.* Further inland, flash densities in the central Texas region have decreased to 0.5 to 1 times the mean. In particular, our analyses show

the mean flash density over the Dallas area to be almost half that observed over the Houston area. These results indicate that the enhanced flash densities present in the Houston area, as well as along the Gulf Coast (Figure A.2b) are not solely due to the occurrence of large events, as proposed by Steiger et al. [2002]; we speculate that *the enhancements are due, in part, to a much greater frequency of occurrence* (Figure A.1a), likely associated with the frequent forcing along coastal mesoscale boundaries.

Although the flash density data presented thus far include non-lightning producing periods, additional insight as to the relative significance of the anomalies and intensity of storms throughout the domain can be gained by examining only days with lightning producing storms. If only lightning days (i.e., one or more CG flashes in a grid box) are considered in our analysis, a marked change in the flash density anomaly pattern becomes evident, relative to that in Figure A.2a. As expected, conditional mean flash densities increase significantly by removing the non-events from our analysis, but more intriguing is the fact that the flash densities become more uniform across the domain, with the positive anomaly previously evident in the Houston area being significantly diminished. In fact, peak conditional mean flash densities within the domain are now located in, and north of, the Dallas area. Further examination of Figure A.2c reveals that the mean conditional flash density anomaly in the Houston area is only *slightly* greater than the domain mean, and more similar to that observed in central Texas. When removing all data points classified as either non-lightning or "large event" days, the conditional-filtered mean flash density converges to the domain mean with only slight spatial variation about this value (not shown), and no sign of an "urban anomaly" over Houston. This indicates that both increased frequency, as well as the occurrence of large

event days contribute to the flash density "enhancements" observed over the Houston area (Figures A.1b and A.2a). Figure A.1a shows that on average, there are twice as many lightning days occurring near Houston, in comparison to the Dallas area; however, the conditional mean flash density in each location is very similar (Houston: 25.3 flashes km^{-2} $summer^{-1}$; Dallas: 25.9 flashes km^{-2} $summer^{-1}$). This suggests that, on average, storms occurring over the Dallas area may produce twice as much lightning as those occurring over the Houston area. Further, these findings are not dependent on the number of "large" event days in the sample.

A.4 Conclusions

The documented enhancement in ground flash densities in and around the Houston metropolitan area was examined using 9 years of NLDN CG lightning data. Collectively, our findings indicate, as in previous studies [i.e., Orville et al., 2000 and Steiger et al., 2002] that the summer season flash density anomaly situated over the Houston area is a robust feature that continues to persist even when large event days associated with the upper quartile of the positively skewed flash density distribution are removed from the analysis. This subset comprises less than 5% of the total daily sample, but produces in excess of 75% of the total lightning in the Houston area.

By comparison, when examining inland regions (e.g., toward Dallas) we found that even fewer large event days (relative to the total daily sample) produced roughly the same contribution to the total flash density over the Dallas area. If only lightning-days were averaged to produce a "conditional mean," we found that the anomaly in the Houston area became almost nonexistent, and that the conditional mean flash density was

actually larger moving into central and northern Texas. The combined results suggest that although the Houston area sees an increased frequency of lightning events (including more large flash density events), storms occurring further inland (e.g., in and north of the Dallas area), actually appear to produce more lightning on an event basis.

Finally, the findings highlight the fact that the local Houston CG lightning anomaly, while being a spatially intriguing and persistent feature, is non-unique along the Gulf Coast. Application of a simple two-sample t-test comparing the means and variances of CG flash density for numerous Gulf Coast locations (see dashed boxes in Figure A.1b), including Houston indicate that although the Houston flash density enhancement clearly exists in a spatial sense, the flash density magnitude compared to other coastal locations is not statistically unique (at p-values < 0.05). Although hypotheses invoking anthropogenic influences have been offered by Orville et al. [2001] and Steiger et al. [2002] to explain the observed increases in flash density over the Houston area (e.g., aerosol influences on storm microphysics, urban heat island, etc.), it seems equally plausible that regular daily mesoscale influences on convective forcing associated with the coastline may also contribute to the observed Houston "anomaly." On the other hand, the mesoscale influence of the coastline and its irregularities do not explain previously documented lightning enhancements observed over and downwind of other inland cities, and therefore may have little to do with the Houston spatial anomaly in flash density. Clearly, the problem is complex and, to the extent possible, requires a comprehensive set of surface and tropospheric measurements (e.g., aerosol, cloud microphysical and precipitation structure, total lightning, thermodynamic, land surface, regional circulation, etc.) that targets each of the most likely forcing mechanisms.

APPENDIX B

CLOUD-TO-GROUND LIGHTNING ACTIVITY AND RADAR DERIVED

PRECIPITATION ICE MASS OVER HOUSTON

B.1 Introduction

Through numerous laboratory, in-situ, remote sensing, and modeling studies

[cf., MacGorman and Rust, 1999], it is generally accepted that clouds become

significantly electrified and produce lightning when sufficient numbers of ice crystals

collide with graupel particles in the presence of super-cooled water via the non-inductive

charging (NIC) mechanism [e.g., Takahashi, 1978; Saunders et al., 1991]. The

particle-cloud scale physics associated with NIC assert *three key requirements for*

thunderstorm electrification and subsequent lightning production: (1) the existence of

convective updrafts, capable of (2) driving robust mixed-phase precipitation ice processes

(i.e., production of graupel/hail and smaller ice crystals/splinters); and the occurrence of

resultant (3) rebounding graupel-ice crystal collisions in the presence of super-cooled

cloud water. Although these three ingredients are critical to the thunderstorm

electrification process, it is clear that (2) and (3) cannot proceed without the presence of a

significant convective updraft. Indeed from an energetics standpoint, stronger updrafts

should be capable of producing more lightning.

Further, there appear to be localized enhancements of ground flash densities in and around various urban areas, specifically the Houston metropolitan area, (see Appendix A). Therefore, we postulate that the unique aspects of the Houston urban area must first generate an anomaly in precipitation ice mass (similar to those observed globally [Petersen et al., 2005]), via localized enhancements in cloud forcing, which then generates the observed anomaly in lightning. Utilizing Weather Surveillance Radar-1988 Doppler (WSR-88D) data collected at the League City, TX (KHGX) radar site, we establish a physical link between the occurrence of cloud-to-ground (CG) lightning and the presence of enhanced precipitation ice mass in the mixed phase region of the atmosphere (-10° C to -40° C, hereafter referred to as the "charging zone") over and around the Houston area.

B.2 Data and Method

Seven years (1997-2003) of archived (Level II) KHGX radar data obtained from the National Climatic Data Center (NCDC) were analyzed for the warm season (June – August) daylight hours (0900 – 1859 CDT). These archived data consist of volumetric measurements of radar reflectivity (Z), radial velocity and spectrum width. To adequately sample the atmosphere, the WSR-88D employs several scanning strategies or Volume Coverage Patterns (VCPs), each having its own utility based on a given weather scenario (i.e. non-precipitating "Clear Air," "Precipitation," "Severe Weather," etc.; details available at http://www.ncdc.noaa.gov/oa/radar/radarresources.html).

To investigate the relationship between precipitation sized ice in the charging zone (approximately 7-11 km above ground level, based on NCEP reanalysis for this

climatological period [Kalnay et al., 1996]) and the location (intensity) of NLDN detected lightning ground strikes (ground flash densities) we desire radar coverage that adequately samples those levels of the atmosphere. The proximity of the Houston area to the radar (approximately 40 km from city center to KHGX) coupled with the climatological altitude of the charging zone dictate the use of radar volumes collected while the radar was scanning to higher elevation angles, thereby sampling the upper portions of the atmosphere at ranges closer to the radar. Of the available VCPs, the scanning strategy employed in VCP-11 ("Severe Weather") mode provides the best vertical sampling, relative to the geometry of the problem at hand, sweeping out a total of 14 elevation scans in 5 minutes. Of the 55,571 available volumes (all VCPs), over 83% were collected in VCP-11 mode, providing a dataset of 46,479 volumes from which our analyses were conducted.

Each of the 46,479 VCP-11 volumes were converted from their native (Level II) format to UF (Universal Format [Barnes, 1980]), and then interpolated onto a 150 x 150 x 20 (x, y, z) Cartesian grid (centered on KHGX) using the National Center for Atmospheric Research (NCAR) REORDER software package [Mohr et al., 1986]. Horizontal (x,y) and vertical (z) grid resolutions were 2 km and 1 km respectively, with the radii of influence for the Cressman filter [Cressman, 1959] employed in the interpolation process being 1.25 km in the horizontal and 1.75 km in the vertical. In order to minimize erroneous data-pairs resulting from missing, and/or poorly sampled data, the radar analysis was only performed for pixels at a range in excess of 15 km from the KHGX radar (i.e. outside of the "cone of silence") and within 150 km of the radar.

Estimations of the precipitation ice mass (M) in each volume were then made by applying the following M-Z relationship to all valid 4 km^3 pixels located between z = 7 and 11 km:

$$M = 1000\pi\rho_i N_0^{3/7}\left(\frac{5.28\times10^{-18}}{720}Z\right)^{4/7} \text{ g m}^{-3}, \qquad (\text{B.1})$$

where Z is in mm^6 m^{-3}, N$_0$ = 4 X 10^6 m^{-4}, and ρ_i = 917 kg m^{-3}. Note this particular M-Z relationship, first presented by Carey and Rutledge [2000], is for tropical convection; however, it has since been applied to more regional [Petersen and Rutledge, 2001] and global [Petersen et al., 2005] lightning studies, with minor density alterations. Additionally, we note that the N$_0$ selected for this relationship is based on comparisons between cloud modeling simulations and observations of both tropical island and oceanic convection [Petersen, 1997]. Although many other Z-M relationships exist in the literature, reflecting variations in continentality, convective regime, and cloud system type [cf., Black, 1990] we feel justified in utilizing Equation B.1 for the following reasons: (1) strong oceanic influences due to the proximity of the KHGX radar (and its domain) to the coast, coupled with prevailing onshore flow during the summer season, as dictated by the climatological presence of the sub-tropical high pressure center, create an environment not overly dissimilar to that of a tropical island, distinctly different than mid-latitude continental conditions, and (2) the spatial and temporal trends in column integrated values of M (IM), as opposed to the computed values are what will be emphasized in this study. Furthermore, the use of Equation B.1 will provide a consistent

basis from which we can *extend the global results of Petersen et al. [2005] to regional and cell scales*.

Coincident with each radar volume, ground strike locations (i.e. flashes occurring from the beginning of one volume scan to the beginning of the subsequent volume scan) detected by the NLDN [Cummins et al., 1998] were gridded to match the horizontal dimensions of the Cartesian radar grid, with flash densities (FDs) calculated in flashes km^{-2} $hour^{-1}$. Note that we have chosen to disregard flashes with positive peak currents less than 10 kA following the recommendations of Cummins et al. [1998]. In this fashion we are able to correlate column integrated values of precipitation ice mass in the charging zone (IM) with the ground strike locations, and flash densities (FDs), observed by the NLDN.

Two separate *Eulerian* methods were used to compare warm-season statistics of precipitation ice mass and CG lightning, both of which mimic the approach taken by Petersen et al. [2005], who performed similar analyses on a global scale utilizing coincident data gathered by the precipitation radar (PR) and lightning imaging sensor (LIS) flown on the TRMM (Tropical Rainfall Mapping Mission) satellite. In the first method (the "ensemble" approach; EN) each individual radar volume was treated as a single data point with spatially integrated values of IM being correlated to observed FDs (each computed relative to the area of the entire domain). This approach yielded an ensemble sample size equal to the number of individual radar volumes processed, 46,479. The second approach compared time-integrated (TI) or cumulative means for each 2 km grid square within the domain by dividing the sum of the normalized IMs and flash counts (each normalized by the pixel area, 4 km^2) by the number of summer seasons used

in the analysis (seven). This method yielded a total of 17,560 data points for comparison (one for each valid 4 km^2 pixel within the horizontal analysis domain).

A third approach utilized an Interactive Data Language (IDL) variant of the Thunderstorm Identification, Tracking, Analysis and Nowcasting cell tracking algorithm (TITAN [Dixon and Wiener, 1993]) to perform a *Lagrangian* analysis, comparing storm total IMs with storm flash counts (FCs) on a cell-by-cell basis. Here, we set the minimum storm size area, and tracking altitude for identifying radar reflectivity cells as 12 km^2 (3 pixels) at Z = 2 km with a threshold reflectivity value of 30 dBZ. Since IMs and FCs had previously been computed for each pixel in the dataset, cell totals of each parameter were taken as the sum of IMs and FCs associated with each pixel comprising the cell. Note this approach effectively treated each cell as a vertical entity, accounting for neither vertical tilt, nor ground flashes coming to ground in regions of reflectivity less than 30 dBZ. Using geometric logic regarding storm cell positions and shapes, the algorithm then tracked identified cells between sequential volume scans. Tracking was accomplished by matching cells at some time (t_1) with their corresponding counterparts in a subsequent timeframe (t_2). Done successively, the cells were tracked for their entire duration. Applied to each day within our radar dataset, the algorithm yielded a total of *676,153 tracked cells for comparison allowing us to test (extend) the global results of Petersen et al. on (to) much smaller scales.*

B.3 Results and Discussion

Similar to the summer season ground flash density anomaly map presented in Appendix A (see Figure A.2a), Figure B.1 presents an anomaly map of TI mean FDs
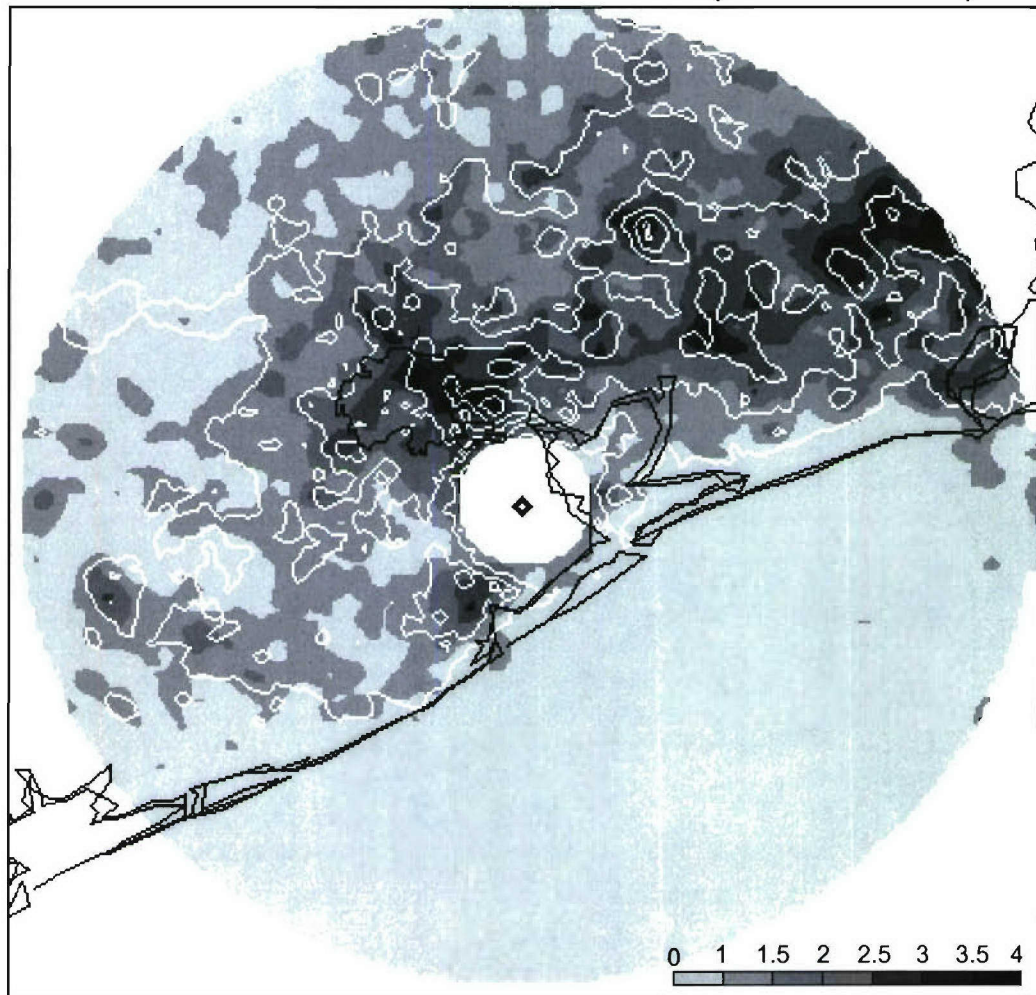
Figure B.1 Seven-year (1997-2003) summer season ground flash density anomalies created by normalization of mean flash densities of each pixel by the domain mean (shaded contours); values > 1 indicate positive anomalies and values < 1 negative anomalies. Corresponding anomalies in radar derived ice mass are overlaid as white contours.

(shaded contours) for ground strikes occurring over all volumes included in this study; here the TI mean FD for each pixel was normalized by the TI mean FD of the entire domain with values >1 (<1) being associated with positive (negative) anomalies. Overall, this seven-year seasonal mean FD anomaly map is similar to that presented in Appendix A, with FDs in the vicinity of the Houston area on the order of 2 to 3 times that of the domain mean. Regarding our IM-FD hypothesis, the white contours in Figure B.1 represent corresponding anomalies in radar derived ice mass (i.e. TI mean IM anomalies). In qualitative agreement with the findings of Petersen et al. (2005), a clear correspondence between the two variables is observed with areas of enhanced mean FDs spatially collocated near enhancements in mean IM indicating that precipitation ice mass in the charging zone and CG lightning are well correlated. To quantify this statement, we present scatter plots relating IM with lightning activity (not anomalies) for each analysis method: EN, TI and CT (Figures B.2a – B.2c, respectively). Consistent with the qualitative relationship identified in Figure B.1, regardless of analysis technique, Figures B.2a – B.2c indicate strong positive correlations between precipitation ice mass and lightning, with $R = 0.72$, 0.91 and 0.80 for the EN, TI and CT methods, respectively. As pointed out by Petersen et al. [2005], the unexplained variances (i.e. discrete bands of noise and scatter) found in these types of analyses are likely the result of sampling issues (both spatial resolution and instrumentation), coupled with the discrete nature of CG discharges. Relative to our analyses, primary deviations from a best fit line most likely arise: (1) when ground flashes initiated in the vicinity of convective cores come to ground several kilometers away from its source region (i.e. generated in one pixel but detected in a different pixel). Although it is not uncommon for ground flashes to propagate several
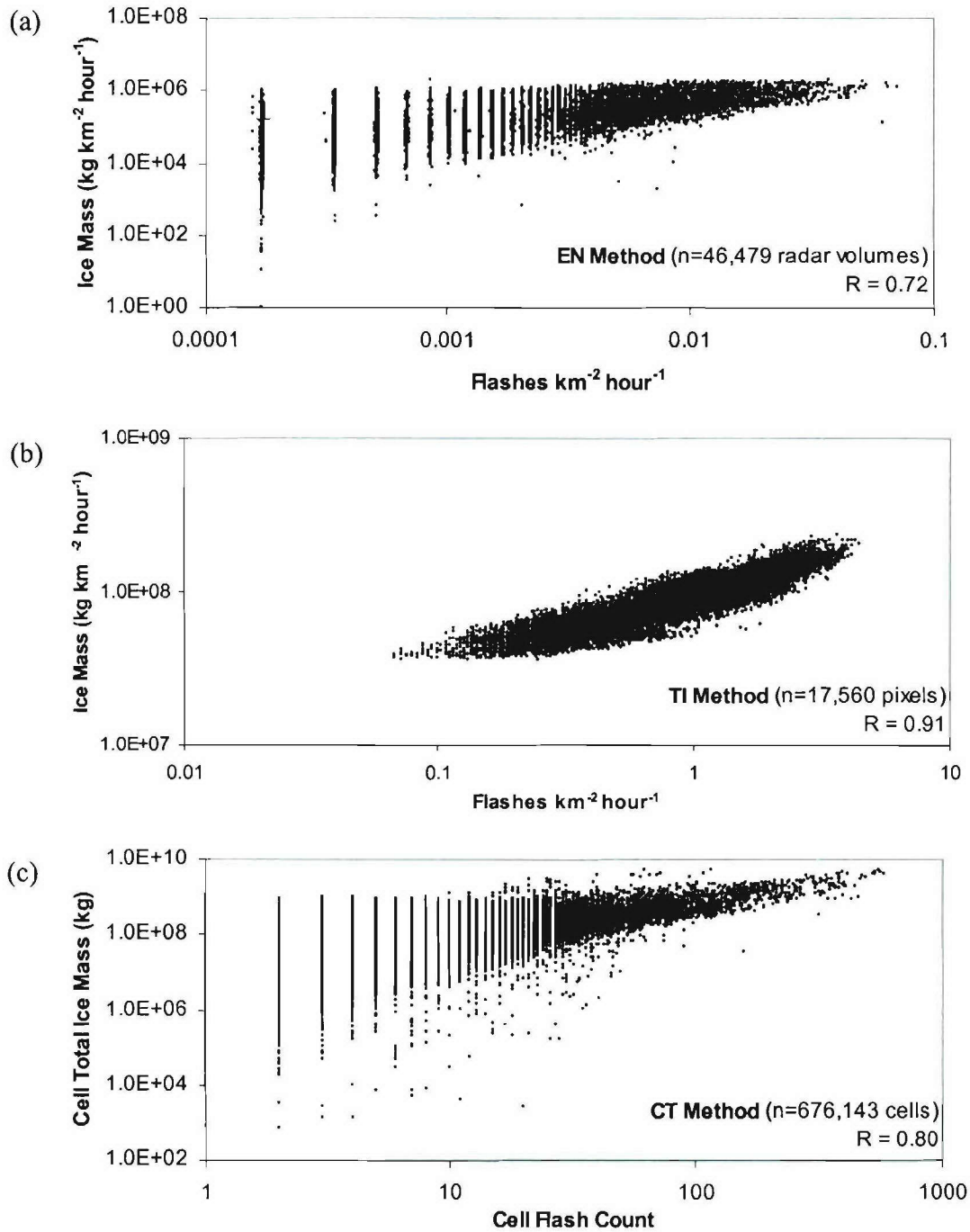
Figure B.2 Scatter plots of the warm-season convective IM as a function of FD for (a) volume total IM – the "ensemble" method [EN] and (b) time-integrated [TI] mean IM for each 2 km pixel. Panel (c) presents similar results for the cell tracker [CT] analysis, with cell total IM (abscissa) presented as a function of cell flash count (FC, ordinate). The number of samples (n) contained in each figure, as well as the linear correlation coefficient (R) are included with their respective panels.

kilometers in the horizontal direction before ultimately terminating at the ground, the horizontal resolution of the analysis grid may add to the observed scatter, and (2) due to the principles of radar operations. Here, aside from the assumptions inherent in the choice of Z-M relationship used in this study (addressed above), radar beam geometry coupled with the interpolation process can result in uneven smoothing of reflectivity data, as pixel sampling degrades with increased range from the radar.

One method of minimizing the effects of this "noise floor" scatter, in a statistically meaningful way, is to present the data in the form of binned scatter plots. Figures B.3a - B.3b examine mean IM values binned as a function of FD for each Eulerian analysis method, while in Figure B.3c the mean cell total IMs are binned as a function of flash counts (FCs) per tracked cell in the CT method. Here, means and standard deviations (error bars) of IM samples falling in each FD/FC bin are plotted relative to the center of each bin interval. For sample sizes similar to those in this study, Wilkes [1995] suggests 20-25 class intervals, as an appropriate number of bins to represent the dataset; caution must be exercised to ensure that an adequate number of samples exist in each of the bins to allow for statistically meaningful calculations. To address this issue, we have elected to use the statistics of the FD and FC distributions to divide the FD and FC bins into 20 variable sized intervals, each specific to the chosen analysis method. In all cases, the first bin is associated with the mean IM for pixels / cells containing no lightning (i.e. FC = FD = 0). The cumulative distribution functions (CDFs) of the conditional FD grid points and FC cells (each conditioned on the occurrence of lightning) were then used to ensure that approximately the same number of data-pairs were present in each of the remaining class intervals. This approach ensured

(a) EN Method (n=46,479 radar volumes)
y = 5E+07x + 118908 (R = 0.978)

(b) TI Method (n=17,560 pixels)
y = 4E+07x + 5E+07 (R = 0.991)

(c) CT Method (n=676,143 cells)
y = 8E+06x + 2E+07 (R = 0.995)
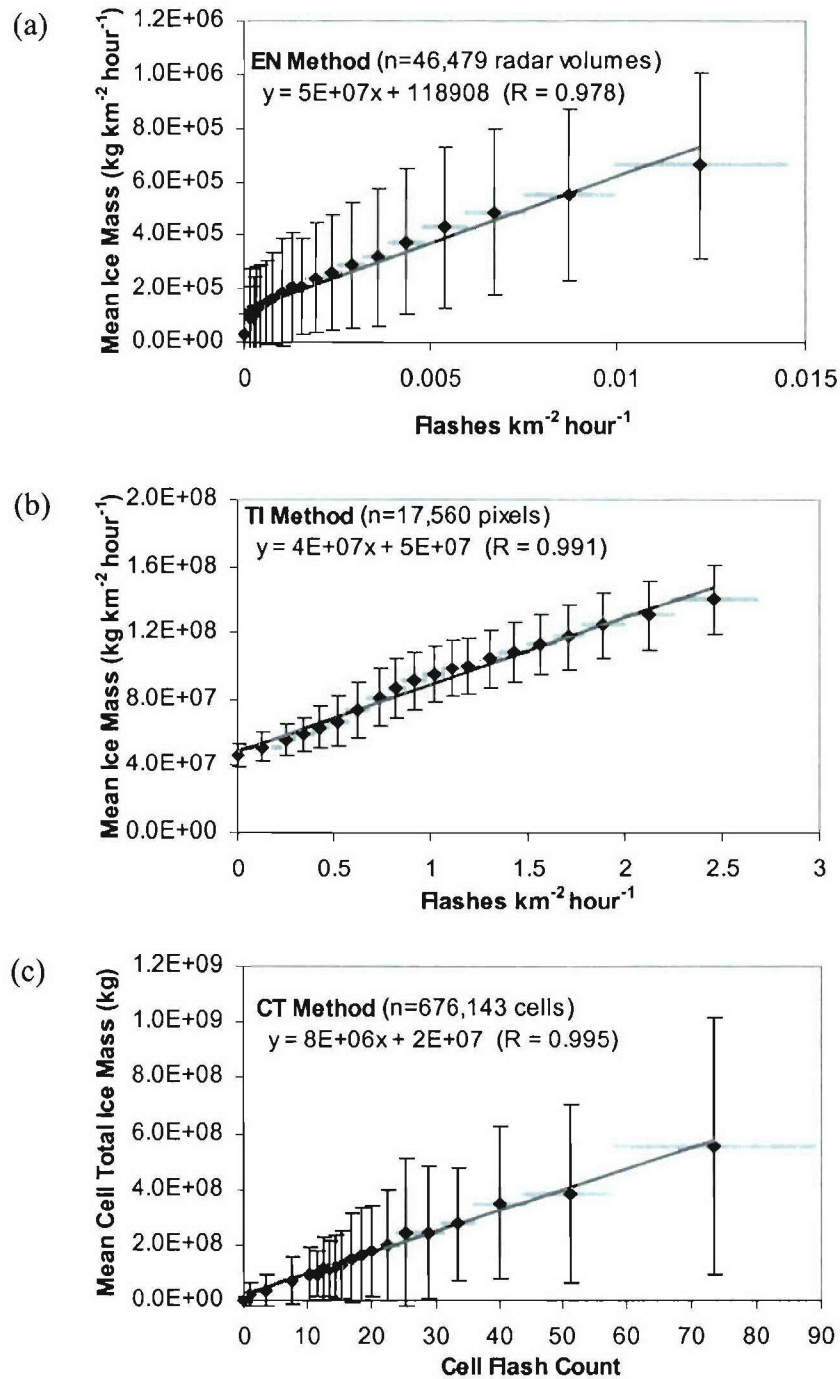
Figure B.3 Average convective IM (ordinate) occurring in each lightning FD bin (abscissa) for (a) EN radar volume samples and (b) TI pixel samples, with (c) average cell total IM occurring in each cell FC bin. In all cases, the first bin interval is associated with non-lightning events (i.e., FD = FC = 0), with remaining variable sized bin intervals each encompassing roughly 5-10% of the remaining data pairs (see text for details); data points are plotted relative to the interval mid-point, horizontal bars represent bin widths, vertical error bars associated with ±1 standard deviation for each data point.

that statistics computed within each bin were done with similar sample sizes, thereby increasing the number of statistically meaningful bins. In the case of the EN and TI methods, non-lightning producing pixels (i.e. pixels in the first bin interval) equated to 55% and 0.1% of the CDF of FD grid points, respectively; the remaining 19 bins each contain roughly 3-8% of the remaining conditional FD grid points based on their respective CDFs (at least 679 and 587 points in each bin, respectively). In the CT method, however, over 90% of the tracked cells had no CG lightning associated with them, thereby requiring a slightly different approach in the division of the remaining 19 bins. Here, the second bin interval represents cells that had exactly one ground flash associated with them, the third and fourth bins being associated with cells producing 2-4 and 5-9 flashes respectively, with the remaining 16 bins each containing approximately 4-9% of the remaining data-pairs associated with lightning producing cells (at least 601 points in each bin). The final bin interval presented in Figures B.3a – B.3c are each associated with the 95th percentile of the CDFs of their respective conditional FD / FC distributions. That is to say that the final class interval is truncated such that the data-pairs associated with the largest 5% of the FDs / FCs were excluded from the analyses. The decision to exclude these extreme events as outliers was based on an examination of the bin interval widths. As seen in Figures B.3a – B.3c, an increase in bin interval (moving right along the abscissa) is typically associated with an increase in interval width (see horizontal bars denoting interval width in each figure), indicating that there are fewer high flash density (count) pixels (cells) as we progress towards larger lightning events. In all cases, the width of the bin interval containing the largest 5% of the FD pixels (FC cells) exceeds the entire interval ranges presented in Figures B.3a –

B.3c (not shown in figures). Although there are ample data-points within each of these final bin intervals to calculate mean IM values for each method, the extended breadth of the bin intervals makes their utility questionable – therefore they were excluded from our analyses.

Clearly, Figures B.3a and B.3b show strong linear relationships between column integrate ice and ground flash densities for our *Eulerian* analyses, with Figure B.3c corroborating these findings from a cell-by-cell perspective. Overall, the slopes of best fit lines through the mean IM values in each bin, presented in Figures B.3a – B.3c, are fairly similar, all with non-zero intercepts suggestive of the presence of a minimum threshold IM value required for the occurrence of CG lightning. For these plots, data are correlated at levels in excess of $R = 0.97$ (0.978, 0.991 and 0.995 for EN, TI and CT methods, respectively).

B.4 Conclusions

Examining over 46,000 daytime volumes of convective WSR-88D radar data, this study investigated the relationship between radar derived precipitation ice mass and NLDN CG lightning over the period of 7 summer seasons (1997 – 2003). Whether examining observations of CG lightning and derived ice mass in a climatological (*Eulerian*) fashion, or doing so on a cell-by-cell basis, our findings corroborate those of previous investigators [e.g., Workman and Reynolds, 1949; Larsen and Stansbury, 1974; Carey and Rutledge, 2000; Petersen et al., 2005], firmly establishing a link between a storms ability to generate enhanced concentrations of precipitation sized ice particles in the mixed-phase region, and its ability to generate lightning.

Cheng, F., D. Byun, and S. Kim (2005), Study the interaction between meteorology and chemistry on the Houston's high ozone problem using CMAQ/MM5, *4th Annual CMAS Models-3 Users' Conf.*, Chapel Hill, NC, 6 pp.

Chisnell, R. F., and J. Latham (1976), Ice particle multiplication in cumulus clouds, *Quart. J. Roy. Meteor. Soc.*, *102*, 133-156.

Cotton, W. R., R. A. Pielke, Sr., R. L. Walko, G. E. Liston, C. J. Tremback, H. Jiang, R. L. McAnelly, J. Y. Harrington, M. E. Nicholls, G. G. Carrio, and J. P. McFadden (2003), RAMS 2001: Current status and future direction, *Meteor. Atmos. Phys.*, *82*, 5-29.

Cressman, G. P. (1959), An operational objective analysis system, *Mon. Wea. Rev.*, *87*, 367-374.

Crook N. A., and J. Sun (2004), Analysis and forecasting of the low-level wind during the Sydney 2000 Forecast Demonstration Project, *Wea. Fcsting.*, *19*, 151-167.

Cummins, K. L., M. J. Murphy, E. A. Bardo, W. L. Hiscox, R. B. Pyle, and A. E. Pifer (1998), A combined TOA/MDF technology upgrade of the U.S. National Lightning Detection Network, *J. Geophys. Res.*, *103*(D8), doi: 10.1029/98JD00153.

Cunning J. B., R. L. Holle, P. T. Gannon, and A. I. Watson (1982), Convective evolution and merger in the FACE experimental area: Mesoscale convection and boundary layer interactions, *J. App. Meteor.*, *21*, 953-977.

Dabberdt, W. F., J. Hales, S. Zubrick, A. Crook, W. Krajewski, J. C. Doran, C. Mueller, C. King, R. N. Keener, R. Bornstein, D. Rodenhuis, P. Kocin, M. A. Rossetti, F. Sharrocks, and E. M. Stanley (2000), Forecast issues in the urban zone: Report of the 10th Prospectus Development Team of the U.S. Weather Research Program, *Bull. Amer. Meteorol. Soc.*, *81*, 2047-2064.

Dash, J. G., B. L. Mason, and J. S. Wettlaufer (2001), Theory of charge and mass transfer in ice-ice collisions, *J. Geophys. Res.*, *106*, 20,395-20,402.

DeMott, C. A., and S. A. Rutledge (1998), The vertical structure of TOGA COARE convection. Part I: Radar echo distributions, *J. Atmos. Sci.*, *55*, 2730-2747.

Dixon, M., and G. Wiener (1993), TITAN: thunderstorm identification, tracking, analysis, and nowcasting—A radar-based methodology, *J. Atmos. Ocn. Tech.*, *10*, 785-797.

Estoque, M. A. (1961), A theoretical investigation of the sea breeze, *Quart. J. Roy. Meteor. Soc.*, *87*, 136-146.

Fan, J., R. Zhang, L. Guohui, and J. Nielsen-Gammon (2005), Simulations of fine particulate matter ($PM_{2.5}$) in Houston, Texas, *J. Geophys. Res., 110*, D16203, doi:10.1029/2005JD005805.

Fovell, R. G. (2005), Convective initiation ahead of the sea-breeze front, *Mon. Wea. Rev., 133*, 264-278.

Fujibe, F., and T. Asai (1980), Some features of the surface wind system associated with the Tokyo heat island, *J. Meteorol. Soc. Japan., 58*, 149-152.

Gauthier, M. L., W. A. Petersen, L. D. Carey, and R. E. Orville (2005), Dissecting the anomaly: A closer look at the documented urban enhancement in summer season ground flash densities in and around the Houston area, *Geophys. Res. Lett., 32*, L10810, doi:10.1029/2005GL022725.

Gentry, R. C., and P. L. Moore (1954), Relation of local and general wind interaction near the sea coast to time and location of air-mass showers, *J. Meteor., 11*, 507-511.

Gibson, H. M., and T. H. Vonder Haar (1990), Cloud and convection frequencies over the southeast United States as related to small-scale geographic features, *Mon. Wea. Rev., 118*, 2215-2227.

Goodman, S. J., D. E. Buechler, P. D. Wright, and W. D. Rust (1988), Lightning and precipitation history of a microburst-producing storm, *Geophys. Res. Lett., 15*, 1185-1188.

Hallett, J., and S. C. Mossop (1974), Production of secondary ice particles during the riming process, *Nature, 249*, 26-28.

Hjelmfelt, M. R. (1982), Numerical simulation of the effects of St. Louis on mesoscale boundary layer airflow and vertical air motion: Simulations of urban vs. nonurban effects, *J. Appl. Meteor., 21*, 1239-1257.

Houze, R.A., Jr., and C. Cheng (1977), Radar characteristics of tropical convection observed during GATE: Mean properties and trends over the summer season. *Mon. Wea. Rev., 105*, 964-980.

Huff, F. A., and S. A. Changnon, Jr. (1973), Precipitation modification by major urban areas, *Bull. Amer. Meteor. Soc., 54*, 1220-1232.

Jauregui, E., and E. Romales (1996), Urban effects on convective precipitation in Mexico City, *Atmos. Environ., 30*, 3383-3389.

Jayaratne, E. R. (1993), The heat balance of a riming graupel pellet and the charge separation during ice-ice collisions, *J. Atmos. Sci., 50*, 3185-3193.

Jayaratne, E. R., C. P. R. Saunders, and J. Hallet (1983), Laboratory studies of the charging of soft hail during ice crystal interactions, *Quart. J. Roy. Meteor. Soc., 109*, 609-630.

Kalnay, E., M. Kanamitsu, R. Kistler, W. Collins, D. Deaven, L. Gandin, M. Iredell, S. Saha, G. White, J. Woollen, Y. Zhu, A. Leetmaa, B. Reynolds, M. Chelliah, W. Ebisuzaki, W. Higgins, J. Janowiak, K.C. Mo, C. Ropelewski, J. Wang, Roy Jenne, and Dennis Joseph (1996), The NCEP/NCAR 40-year reanalysis project, *Bull. Amer. Meteor. Soc., 77*, 437-471.

Karan, H., and K. Knupp (2005), Mobile integrated profiler system (MIPS) observations of low-level convergent boundaries during IHOP, *Mon. Wea. Rev., 134*, 92-112.

Laird, N. F., D. A. R. Kristovich, R. M. Rauber, H. T. Ochs, III, and L. J. Miller (1995), The Cape Canaveral sea and river breezes: Kinematic structure and convective initiation, *Mon. Wea. Rev., 123*, 2942-2956.

Lang, T. J., and S. A. Rutledge (2002), Relationships between convective storm kinematics, precipitation, and lightning, *Mon. Wea. Rev., 130*, 2492-2506.

Lang, T. J., S. A. Rutledge, J. E. Dye, M. Venticinque, P. Laroche, and E. Defer (2000), Anomalously low negative cloud-to-ground lightning flash rates in intense convective storms observed during STERAO-A. *Mon. Wea. Rev., 128*, 160-173

Larson, H. R. and E. J. Stansbury (1974), Association of lightning ashes with precipitation cores extending to height 7 km, *J. Atmos. Terr. Phys., 36*, 1547-1553.

Lhermitte, R. M., and D. Atlas (1961), Precipitation motion by pulse Doppler, *Proc. Ninth Weather Radar Conf.*, Kansas City, MO, Amer. Meteor. Soc., 218–223.

Lopez, R. E. (1978), Internal structure and development processes of C-scale aggregates of cumulus clouds, *Mon. Wea. Rev., 106*, 1488-1494.

Lucas, C., E. J. Zipser, and M. A. LeMone (1994), Convective available potential energy in the environment of oceanic and continental clouds: Correction and comments, *J. Atmos. Sci., 51*, 3829-3830.

MacGorman, D. R., and W. D. Rust (1998), *The Electrical Nature of Storms*, 422 pp., Oxford Univ. Press, New York.

MacGorman, D. R., D. W. Burgess, V. Mazur, W. D. Rust, W. L. Taylor, and B. C. Johnson (1989), Lightning rates relative to tornadic storm evolution on 22 May 1981, *J. Atmos. Sci., 46*, 221-250.

Martilli, A. (2002), Numerical study of urban impact on boundary layer structure: Sensitivity to wind speed, urban morphology, and rural soil moisture, *J. App. Meteor., 41*,1247-1266.

Miller, S. T. K., B. D. Keim, R. W. Talbot, and H. Mao (2003), Sea breeze: Structure, forecasting and impacts, *Rev. Geophys.*, 41, 1-31, doi:10.1029/2003RG000124.

Mohr, C. G., L. J. Miller, R. L. Vaughn, and H. W. Frank (1986), On the merger of mesoscale data sets into a common Cartesian format for efficient and systematic analyses, *J. Atmos. Ocn. Tech., 3,* 143-161.

Mossop, S. C., and J. Hallett (1974), Ice crystal concentrations in cumulus clouds: Influence of the drop spectrum, *Science, 186*, 632-634.

Mossop, S. C., J. L. Brownscombe, and G. J. Collins (1974), The production of secondary ice particles during riming, *Ibid., 98*, 427-436.

McPherson, R. D. (1970), A numerical study of the effect of a coastal irregularity on the sea breeze, *J. Appl. Meteor., 9,* 767-777.

Naccarato K. P., O. Pinto Jr., and I. R. C. A. Pinto (2003), Evidence of thermal and aerosol effects on the cloud-to-ground lightning density and polarity over large urban areas of Southeastern Brazil, *Geophys. Res. Lett., 30* (13), 1674, doi:10.1029/2003GL017496.

Nielsen-Gammon, J. W. (2000), The Houston heat pump: modulation of a land-sea breeze by an urban heat island, Preprints, *11th Joint Conf. on the Applications of Air Pollution Meteorology with the A&WMA*, Long Beach, CA, Amer. Meteor. Soc., 65-69.

Oke, T. R. (1982), The energetic basis of the urban heat island, *Quart. J. Roy. Meteor. Soc., 108,* 1-24.

Orville, R. E., and G. R. Huffines (2001), Cloud-to-Ground lightning in the United States: NLDN results in the first decade, 1989–98, *Mon. Wea. Rev., 129*, 1179-1193.

Orville, R. E., R. W. Henderson, and L. F. Bosart (1983), An east coast lightning detection network, *Bull. Amer. Meteor. Soc., 64*, 1029-1030.

Orville, R. E., G. Huffines, J. Nielsen-Gammon, R. Zhang, B. Ely, S. Steiger, S. Phillips, S. Allen, and W. Read (2001), Enhancement of cloud-to-ground lightning over Houston, Texas, *Geophys. Res. Lett., 28*(13), doi:10.1029/2001GL012990.

Petersen, W. A. (1997), Multi-scale process studies in the tropics: Results from lightning observations, *Ph.D. dissertation, Department of Atmospheric Science, Colorado State University, 632,* 354 pp.

Petersen, W. A., and S. A. Rutledge (2001), Regional variability in tropical convection: Observations from TRMM, *J. Clim., 14,* 3566-3586.

Petersen, W. A., H. J. Christian, and S. A. Rutledge (2005), TRMM observations of the global relationship between ice water content and lightning, *Geophys. Res. Lett., 32,* L14819, doi:10.1029/2005GL023236.

Prupacher, H. R., and R. J. Schlamp (1975), A wind tunnel investigation on ice multiplication by freezing of water drops falling at terminal velocity in air, *J. Geophys. Res., 80,* 380-385.

Reap, R. M. (1986), Evaluation of cloud-to-ground lightning data from the western United States for the 1983–84 summer seasons, *J. Appl. Meteor., 25,* 785-799.

Reap, R. M. (1994), Analysis and prediction of lightning strike distributions associated with synoptic map types over Florida. *Mon. Wea. Rev., 122,* 1698-1715.

Reynolds, S. E., M. Brook, and M. Foulks Gourley (1957), Thunderstorm charge separation, *J. Atm. Sci., 14,* 426-436.

Rosenfeld, D. (1999), TRMM observed first direct evidence of smoke from forest fires inhibiting rainfall, *Geophys. Res. Lett., 26,* 3105-3108.

Rosenfeld, D. (2000), Suppression of rain and snow by urban and industrial air pollution, *Science, 287,* 1793-1796.

Rosenfeld, D., and M. I. Lensky (1998), Space-borne based insights into precipitation formation processes in continental and maritime convective clouds, *Bull. Am. Meteorol. Soc., 79,* 2457-2476.

Rosenfeld, D., and W. L. Woodley (2000), Convective clouds with sustained highly supercooled liquid water down to -37.5°C, *Nature, 405,* 440-442.

Rosenfeld, D., and W. L. Woodley (2003), Spaceborne inferences of cloud microstructure and precipitation processes: Synthesis, insights and implications, *Cloud Systems, Hurricanes, and the Tropical Rainfall Measuring Mission (TRMM) – A tribute to Dr. Joanne Simpson, Eds. W-K Tao and R. Adler, Meteorological Monographs, 29,* Amer. Meteor. Soc., 59-80.

Rozoff, C. M., W. R. Cotton, and J. O. Adegoke (2003), Simulation of St. Louis, Missouri, land use impacts on thunderstorms, *J. App. Meteor., 42,* 716-738.

Saunders, C. P. R., and S. L. Peck (1998), Laboratory studies of the influence of the rime accretion rate on charge transfer during crystal/graupel collisions, *J. Geophys. Res., 103,* 13,949-13,956.

Saunders, C. P. R., W. D. Keith, and R. P. Mitzeva (1991), The effect of liquid water on thunderstorm charging, *J. Geophys. Res., 96,* 11,007-11,017.

Shackford, C. R. (1960), Radar indications of a precipitation-lightning relationship in New England thunderstorms, *J. Meteor., 17,* 15-19.

Shepherd, J. M. (2005), A review of current investigations of urban-induced rainfall and recommendations for the future, *Earth Interactions, 9,* 1-27.

Shepherd, J. M., and S. J. Burian (2003), Detection of urban-induced rainfall anomalies in a major coastal city, *Earth Interactions, 7,* 1-17.

Shepherd J. M., H. F. Pierce, and A. J. Negri (2002), Rainfall modification by major urban areas: Observations from spaceborne radar on the TRMM satellite, *J. Appl. Meteor., 41,* 689-701.

Shreffler, J. H. (1978), Detection of centripetal heat-island circulations from tower data in St. Louis, *Bound. Layer Meteor., 15,* 229-242.

Simpson, J. (1980), Downdrafts as linkages in dynamic cumulus seeding effects, *J. Appl. Meteorol., 19,*477-487.

Simpson, J., and W. L. Woodley (1971), Seeding cumulus in Florida: New 1970 results, *Science, 172,* 117-126.

Simpson, J. N. E. Westcott, R. J. Clerman, and R. A. Pielke (1980), On cumulus mergers, *Arch. Met. Geoph. Biokl., 29,* 1-40.

Smith, J. R., H. E. Fuelberg and A. I. Watson (2005), Warm season lightning distributions over the northern Gulf of Mexico coast and their relation to synoptic-scale and mesoscale environments, *Wea. Fcsting., 20,* 415-438.

Soriano, L. R., and F. Pablo (2002), Effect of small urban areas in central Spain on the enhancement of cloud-to-ground lightning activity, *Atmos. Env., 36*(17), 2809-2816.

Steiger S. M., R. E. Orville, and G. Huffines (2002), Cloud-to-ground lightning characteristics over Houston, Texas: 1989-2000, *J. Geophys. Res., 107*(D11), doi:10.1029/2001JD001142.

Stull, R. B. (1988), *An Introduction to Boundary Layer Meteorology,* 666 pp., Kluwer Academic Publ., Dordrecht, The Netherlands.

Sun J., and N. Andrew Crook (1997), Dynamical and microphysical retrieval from doppler radar observations using a cloud model and its adjoint. Part I: Model development and simulated data experiments, *J. Atmos. Sci., 54(12),* 1642-1661.

Sun J., and N. Andrew Crook (1998), Dynamical and microphysical retrieval from doppler radar observations using a cloud model and its adjoint. Part II: Retrieval experiments of an observed Florida convective storm, *J. Atmos. Sci., 55(5),* 835-852.

Sun, J., and N. A. Crook (2001), Real-time low-level wind and temperature analysis using single WSR-88D data, *Wea. Fcsting., 16(1),* 117-132.

Takahashi, T. (1978), Riming electrification as a charge generation mechanism in thunderstorms, *J. Atmos. Sci., 35,* 1536-1548.

Tao, W.-K., and J. Simpson (1984), Cloud interactions and merging: Numerical simulations, *J. Atmos. Sci., 41,* 2901-2917.

Twomey, S. (1977), *Atmospheric Aerosols. Developments in Atmospheric Science, Vol. 7,* 299 pp., Elsevier Scientific Publishing Co., Amsterdam, The Netherlands.

Ulanski S. L., and M. Garstang (1978), The role of surface divergence and vorticity in the life cycle of convective rainfall. Part I: Observation and analysis, *J. Atmos. Sci., 35,* 1047-1062.

U. S. Bureau of Census (1996), Land area, population, and density for metropolitan areas: 1990, *Population Distribution Branch,* U. S. Bureau of the Census, Washington, D.C. 20233.

Vincent, B. R., L. D. Carey, D. Schneider, K. Keeter, and R. Gonski (2004), Using WSR-88D reflectivity for the prediction of cloud-to-ground lightning: A central North Carolina study, *Nat. Wea. Digest, 27,* 35-44.

Wacker, R. S., and R. E. Orville (1999a), Changes in measured lightning flash count and return stroke peak current after the 1994 U.S. National Lightning Detection Network upgrade: 1. Observations, *J. Geophys. Res., 104*(D2), doi:10.1029/1998JD200060.

Wacker, R. S., and R. E. Orville (1999b), Changes in measured lightning flash count and return stroke peak current after the 1994 U.S. National Lightning Detection Network upgrade: 2. Theory, *J. Geophys. Res., 104*(D2), doi:10.1029/1998JD200059.

Watson A. I., and D. O. Blanchard (1984), The relationship between total area divergence and convective precipitation in South Florida, *Mon. Wea. Rev., 112,* 673-685.

Watson A. I., R. E. López, R. L. Holle, and J. R. Daugherty (1987), The relationship of lightning to surface convergence at Kennedy Space Center: A preliminary study, *Wea. Fcsting., 2,* 140-157.

Watson, A. I., R. L. Holle, R. E. López, and R. Ortiz (1991), Surface wind convergence as a short-term predictor of cloud-to-ground lightning at Kennedy Space Center, *Wea. Fcsting., 6,* 49-64.

Westcott, N. E. (1984), A historical perspective on cloud mergers, *Bull. Amer. Meteor. Soc.*, 65, 219-226.

Westcott, N. E. (1995), Summer-time cloud-to-ground lightning activity around major Midwestern urban areas, *J. App. Meteor., 34*, 133-1642.

Wilde, N. P., R. B. Stull, and E. W. Eloranta (1985), The LCL zone and cumulus onset, *J. App. Meteor., 24,* 640-657.

Wilkes, D. S. (1995), *Statistical Methods in the Atmospheric Sciences*, 465 pp., Academic Press, San Diego, CA.

Williams, E. R. (1989), The tripole structure of thunderstorms., *J. Geophys. Res., 94,* 13,151-13,167.

Williams, E. R. (2001), The electrification of severe storms. *Severe Convective Storms, C. A. D. III, ed., Amer. Meteor. Soc., 50, Meteor. Monogr.,* 527-561.

Williams, E. R., and S. Stanfill (2002), The physical origin of the land-ocean contrast in lightning activity, *C. R. Physique, 3,* 1-16.

Williams, E. R., S. G. Geotis, and A.B. Bhattacharya (1989), A radar study of the plasma and geometry of lightning, *J. Atmos. Sci., 46,* 1173-1185.

Williams, E. R., D. Rosenfeld, N. Madden, J. Gerlach, N. Gears, L. Atkinson, N. Dunnemann, G. Frostrom, M. Antonio, B. Biazon, R. Camargo, H. Franca, A. Gomes, M. Lima, R. Machado, S. Manhaes, L. Nachtigall, H. Piva, W. Quintiliano, L. Machado, P. Artaxo, G. Roberts, N. Renno, R. Blakeslee, J. Bailey, D. Boccippio, A. Betts, D. Wolff, B. Roy, J. Halverson, T. Rickenbach, J. Fuentes, and E. Avelino (2002), Contrasting convective regimes over the Amazon: Implications for cloud electrification, *J. Geophys. Res., 107*, D20, 8082, doi:10.1029/2001JD000380.

Williams, E., V. Mushtak, D. Rosenfedl, S. Goodman, and D. Boccippio (2005), Thermodynamic conditions favorable for the superlative thunderstorm updraft, mixed phase microphysics and lightning flash rate, *Atmos. Res., 76,* 288-306.

Workman, E. J., and S. E. Reynolds (1949), Electrical activity as related to thunderstorm cell growth, *Bull. Amer. Meteor. Soc., 30,* 142-149.

Yoshikado, H. (1992), Numerical study of the daytime urban effect and its interaction with the sea breeze, *J. Appl. Meteor., 31,* 1146-1164.

Yoshikado, H. (1994), Interaction of the sea breeze with urban heat islands of different sizes and locations. *J. Meteor. Soc. Japan., 72,* 139-142.

Yuter, S. E., and R. A. Houze Jr. (1995), Three-dimensional kinematic and microphysical evolution of Florida cumulonimbus. Part III: Vertical mass transport, mass divergence, and synthesis, *Mon. Wea. Rev., 123,* 1964-1983.

Zajac, B. A., and S. A. Rutledge (2001), Cloud-to-ground lightning activity in the contiguous United States from 1995 to 1999, *Mon. Wea. Rev., 129,* 999-1019.

Zhong, S., J. M. Leone, Jr., and E. S. Takle (1991), Interaction of the sea breeze with a river breeze in an area of complex coastal heating, *Bound.-Layer Meteor., 56,* 101-139.